F I N A L

IN 24.-12
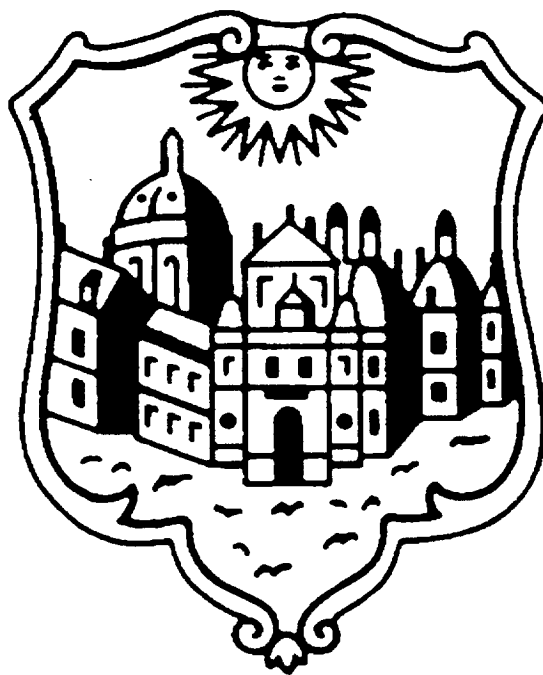
A FINAL TECHNICAL REPORT ENTITLED:

Trans-Laminar-Reinforced (TLR) Composites

BY

Prof. Mark Hinders and Dr. Larry Dickinson
Department of Applied Science
The College of William and Mary in Virginia
Williamsburg, VA 23187

April 22, 1997

WILLIAM &MARY

TRANS-LAMINAR-REINFORCED
(TLR)
COMPOSITES

TABLE OF CONTENTS

LIST OF TABLES

LIST OF FIGURES

LIST OF SYMBOLS

BC   boundary condition

CAI   compression after impact

C_{ij} stiffness matrix

DCB   double cantilever beam

DHM   drilled hole model

E_f longitudinal extensional modulus of fiber

E_l longitudinal extensional modulus of unidirectional composite

E_m extensional modulus of matrix

E_t transverse extensional modulus of unidirectional composite

E_x x direction extensional modulus of elasticity

E_y y direction extensional modulus of elasticity

E_z z direction extensional modulus of elasticity

ENF   end notch flexure

FEA   finite element analysis

G_{IC} mode I critical strain energy release rate, fracture toughness

G_{xy} in-plane shear modulus, xy plane

G_{xz} out-of-plane shear modulus, xz plane

G_{yz} out-of-plane shear modulus, yz plane

Gr-Ep   graphite-epoxy

hwx   half dimensions of the unit cell in the X direction

hwy   half dimensions of the unit cell in the Y direction

hwz   half dimensions of the unit cell in the Z direction

K-Ep   Kevlar®-Epoxy

MPC   multi-point constraint

$P1^{xz}$ maximum transverse tensile stress due to inter-laminar shear loading

$P1^z$ maximum transverse tensile stress due to inter-laminar normal loading

SFM   straight fiber model

S_{ij}	compliance matrix
TLR	trans-laminar reinforcement or trans-laminar-reinforced
u_i	i direction displacement
V_f,	fiber volume fraction
V_m	matrix volume fraction
wx	dimensions of the unit cell in the X direction
wy	dimensions of the unit cell in the Y direction
wz	dimensions of the unit cell in the Z direction
UC	unit cell
v_{ij}	Poisson ratio
ε_i	normal strain
γ_{ij}	shear strain
σ_i	normal stress
τ_{ij}	shear stress
ψ	TLR through-thickness angle
θ	angle of curvature of the in-plane curved fibers

ABSTRACT

A Trans-Laminar-Reinforced (TLR) composite is defined as composite laminate with up to five percent volume of fibrous reinforcement oriented in a "trans-laminar" fashion in the through-thickness direction. The TLR can be continuous threads as in "stitched laminates", or it can be discontinuous rods or pins as in "Z-Fiber™" materials. It has been repeatedly documented in the literature that adding TLR to an otherwise two dimensional laminate results in the following advantages: substantially improved compression-after-impact response; considerably increased fracture toughness in mode I (double cantilever beam) and mode II (end notch flexure); and severely restricted size and growth of impact damage and edge delamination. TLR has also been used to eliminate catastrophic stiffener disbonding in stiffened structures. TLR directly supports the "Achilles' heel" of laminated composites, that is delamination. As little as one percent volume of TLR significantly alters the mechanical response of laminates.

The objective of this work was to characterize the effects of TLR on the in-plane and inter-laminar mechanical response of undamaged composite laminates. Detailed finite element models of "unit cells," or representative volumes, were used to study the effects of adding TLR on the elastic constants; the in-plane strength; and the initiation of delamination. Parameters investigated included TLR material, TLR volume fraction, TLR diameter, TLR through-thickness angle, ply stacking sequence, and the microstructural features of pure resin regions and curved in-plane fibers. The work was limited to the linear response of undamaged material with at least one ply interface. An inter-laminar dominated problem of practical interest, a flanged skin in bending, was also modeled.

Adding a few percent TLR had a small negative effect on the in-plane extensional and shear moduli, E_x, E_y and G_{xy}, but had a large positive effect (up to 60 percent) on the thickness direction extensional modulus, E_z. The volume fraction and the axial modulus of the TLR were the controlling parameters affecting E_z. The out-of-plane shear moduli, G_{xz} and G_{yz}, were significantly affected only with the use of a TLR with a shear modulus an order of magnitude greater than that of the composite lamina. A simple stiffness averaging method for calculating the elastic constants was found to compare closely with the finite element results, with the greatest difference being found in the inter-laminar shear moduli, G_{xz} and G_{yz}. The unit cell analyses results were used to conclude that in-plane loads are concentrated next to the TLR inclusion and that the microstructural features of pure resin regions and curved in-plane fibers slightly lessen this stress concentration. Delamination initiation was studied with a strength of materials approach in the unit cell models and the flanged skin models. It was concluded that if the formation of a transverse crack is included as a source of delamination initiation, the addition of TLR will not be effective at preventing or delaying the onset of delamination. The many benefits of TLR may be accounted for by an increased resistance to delamination growth by crack bridging phenomenon, which is best studied with a fracture mechanics approach.

CHAPTER 1
INTRODUCTION AND LITERATURE REVIEW

This chapter contains an overview and comprehensive literature review. Important terms are defined and a brief history and general state of the art are discussed. The chapter closes with a section stating the purpose and scope of this research, and how it fits within the general realm of trans-laminar-reinforced composites.

1. 1. MOTIVATION

"Composite materials," are materials composed of two or more constituents distinguishable on the macroscopic scale. Composite materials have a wide range of tailorable properties. When modern polymers or plastics are combined with high performance fibers such as carbon or glass, strong, stiff and lightweight materials result. These composites have demonstrated tremendous advantage in applications where weight and performance are critical factors. However, in applications where cost is a limiting factor, composites have been slow to make inroads against traditional engineering materials such as steel and aluminum. There is no question that composite materials offer tremendous potential in an almost unlimited variety of applications. However, to realize that potential, much work needs to be done in the areas of design, failure and cost.

1. 2. OVERVIEW

Advanced polymeric matrix composites have a long and successful history in applications where performance and weight are overriding factors. Their wide spread use

in structural applications has not been achieved due to limiting factors such as high cost, low damage resistance and low damage tolerance*. The most common form of advanced composite in structural applications is layers of fibrous reinforcement in a surrounding matrix. These composite "laminates" are plagued by a well documented inter-laminar weakness. The mechanical response of the region between the plies of a laminate is controlled by the relatively weak matrix. This weakness results in a low damage resistance and low damage tolerance, and is demonstrated by large impact damage areas, low compression-after-impact strength, low fracture toughness, etc. Damage tolerance and damage resistance are very important considerations in aerostructures such as commercial aircraft. General discussions/overviews of damage tolerance, delamination, and concepts for their improvement may be found in [1-3].

In general, there are two approaches for strengthening the inter-laminar region. The mechanical response of the matrix can be changed by using different matrix materials and/or adding particles or films between the plies (e.g. interleaving). Stronger and tougher resins are generally difficult to process and/or are prohibitively expensive. Alternatively, fibrous reinforcement may be included across lamina interfaces in a trans-laminar fashion. Stitching through-the-thickness is an example of trans-laminar reinforcement (TLR). However, the use of TLR is increasing. Only small amounts of out-of-plane reinforcement (volume fractions less than five percent) are required to significantly change the mechanical response of the laminate. Established and developed processes such as

---

* Damage resistance is measured by the size or amount of damage for a given event and damage tolerance is measured by the performance of the material or part for a given damage size.

industrial sewing/stitching and new processes/materials such as Z-Fiber™ offer economic means of achieving TLR, or through-thickness reinforcement.

The concept of three-dimensional (3-D) fibrous reinforcement has been around a long time. Three-dimensionally reinforced carbon-carbon composites have been studied and manufactured since the 1960's. More recently, research efforts have increased in the area of 3-D polymeric matrix composites. Many composites utilizing fibrous reinforcements in the form of 3-D weaving, 3-D knitting and 3-D braiding, do not have the same inter-laminar problems as laminates. Such true 3-D textile composites generally have significant volume fractions of fiber in all three directions, and hence do not have a simple layered structure. The following discussion will focus on the topic of trans-laminar reinforcement (TLR) of an otherwise 2-D laminated composite. The important distinction is that only small amounts of TLR modify an otherwise laminated structure. TLR composites in this work are defined as laminated fiber-matrix composites with thickness direction fibrous reinforcement totaling five percent or less of the total volume of the laminate. The number five percent is somewhat arbitrary, and may be redefined as research in this field continues.

Trans-laminar reinforcement[*] (TLR) has two general forms: continuous and discontinuous (see Figure 1-1). Continuous rovings, threads, yarns or tows can be inserted into the lamina with the use of industrial sewing/stitching technology. Discontinuous trans-laminar reinforcement (in the form of short fibers, whiskers, pins,

---

[*] "Trans-laminar-reinforcement" is used here as a general term encompassing several different phrases commonly used in the literature. Some examples include "through-thickness", "through-the-thickness", "Z-direction", and "inter-laminar".

etc.) can also be used to bridge the inter-lamina region. When compared to similar unreinforced (2-D) laminates, both continuous and discontinuous trans-laminar reinforcement have been shown to significantly improve inter-laminar dominated responses such as compression-after-impact strength, fracture toughness, and inter-laminar shear strength.

The following sections are intended to present a general overview and comprehensive literature citation of trans-laminar-reinforced (TLR) composites. Although a few references can be found where TLR has been applied to ceramic matrix composites [4, 5] and carbon-carbon composites [6], this work and the vast majority of published TLR research has dealt with polymeric matrix composites. Stitched laminates will be discussed first and in greater detail, as the vast majority of published research and available data deals with stitched materials. Discontinuous TLR composites are discussed in section 1.4 while section 1.5 provides a general review of analysis and modeling. Section 1.6 closes the chapter with summary comments and a discussion of the objective, approach and scope of this research.

1. 3.   STITCHED COMPOSITES

Previously published reviews of stitching can be found in the papers of Dransfield, Baillie and Mai [7, 8]. While they cover many of the important concepts, there is a vast amount of stitching research documented in U.S. government reports (e.g. NASA, DoD, Army, etc.) that is not cited in these two papers[*]. This review includes many such

---

[*] Access to government reports included personal contacts with various authors and the grateful use of both facilities and services of the NASA Langley Technical Library.

documents. While some of these documents may not be readily accessible to the general public, this work is intended to be as comprehensive a bibliography of TLR research as possible.

Low density stitching (small threads and few stitches per unit area) is finding increasing use as a means of stabilizing dry fabric preforms. Stitched preforms are made into composites by liquid molding processes such as resin transfer molding (RTM) and resin film infusion (RFI). Such use of stitching technology aids the automation of composite processing. When used in conjunction with RTM or RFI, stitching offers great potential for cost effective composite manufacturing (see for example [9-15]). The "multiaxial stitching" described in [15] is actually a multiaxial warp knitting process. Both knitting and stitching can produce some of the same textile looped-knotted-stitched structures. In general, knitting refers to the formation of fabric from yarns or tows and is an integral part of the initial fabric forming process. Stitching (which can be multi-needle) describes the process of tying together layers of previously formed fabric. High density stitching (larger threads and more stitches per unit area) can be used to enhance the properties of composite materials and structures. Of course both benefits, economical manufacturing and improved mechanical properties, can be achieved at the same time.

References [16-22] document some of the earliest published stitched composites research. The author's results varied, but one consistent conclusion was that significant in-plane fiber damage occurred when stitching prepreg. The in-plane fibers of prepregs, held in place by the matrix, were severely damaged by the needle and thread of the stitching process. This realization that significant damage occurs when prepreg is stitched

has been echoed by several authors, with [17] being the earliest citation found. The majority of recent development work found in the literature has dealt with stitching the fiber preform before impregnation with the matrix, followed by consolidation by liquid molding. Less fiber damage results since the in-plane fibers are free to move slightly and allow the stitching needle and thread to penetrate the preform.

1. 3.1.   SELECTIVE STITCHING

Selective stitching, that is stitching in a localized area only, has been investigated for joining applications and as a means of handling the inter-laminar stresses near a free edge. In references [23-26], the study of stitched and unstitched lap joints is discussed. A single row of stitching near the end of a single lap joint improved tension strength up to 38 percent [23]. References [25-31] studied the attachment of stiffeners to flat panels with stitching. In [21] and [22], several trans-laminar reinforcement concepts including mechanical fasteners and stitching were studied for use in stiffener attachment. Reference [21] refers to carbon fiber laminates for aerospace applications while reference [22] refers to fiberglass laminates for marine applications. Compared to bonding/co-curing alone, stitching completely eliminated stiffener separation as a failure mode in compression [29, 30] and improved the stiffener pull-off strength by factors of two to ten [28]. In general, attachment by stitching has been shown to consistently offer significant improvements over simple bonding/co-curing or mechanical fastening.

The use of stitching to suppress edge delamination in tension was experimentally evaluated in [32-35]. In references [26] and [34] stitching was tried around an open hole. Finite element analysis was used in [36] and [33] to stitched laminates, with the results of

the analyses leading to the conclusion that the stitches must be very near the free edge to be effective. Although results varied somewhat, in practical terms, these research efforts suggest that it is unlikely that stitches can be close enough together and near enough to the free edge to effectively counter the free edge inter-laminar stresses that lead to delamination. However, stitching consistently and significantly restricted delamination growth once initiated.

1. 3.2.   COMPREHENSIVE STITCHING

In addition to stitching in targeted areas only, a great deal of research has been done on comprehensive stitching, or stitching in a particular pattern across an entire part or panel. The terms "selective" and "comprehensive" stitching are somewhat arbitrary, but can provide helpful classification. Comprehensive stitching may be used in reference to material issues (e.g. material properties) while selective stitching refers to structural issues (e.g. joints). Most early comprehensive stitching research was done with woven or uniwoven fabric composites. Reference [37] appears to be the sole published work concerning the stitching together of 2-D braided fabrics. Early data for stitched multi-axial warp knits can be found in [38-41]. The stitched multi-axial warp knit became the material of choice for the development of a stitched wing for commercial aircraft documented in [42-47]. The vast majority of stitching research efforts have been experimental with many different exploratory and often similar investigations.

These efforts have shown that when compared to similar unstitched materials, stitched laminates have increased damage tolerance (e.g. higher strength for a given damage size) and damage resistance (e.g. smaller damage areas for a given impact

energy). Compared to unstitched materials, stitching has been shown to improve compression-after-impact (CAI) strength by more than 50 percent and ultimate compressive strain up to 80 percent [10, 16, 17, 30, 32, 37-41, 48-69]. In sublaminate buckling tests of laminates with artificial delaminations, stitching improved the compression strength up to 400 percent [68]. For CAI, stitching with first generation fibers and matrix (AS4 carbon and 3501-6 epoxy) was equally effective as using "state of the art" toughened material systems [53, 54]. Similar results were found in Tension-after-impact testing [67, 69]. Compared to unstitched, stitching only slightly affected or did not affect the impact force required to initiate damage in low velocity impact [70]. Stitching did raise the peak impact force for a given impact energy [17, 59, 67-69]. Stitching has also been shown to improve ballistic impact performance [27, 71].

Stitching has also been shown to significantly increase inter-laminar fracture toughness [48-51, 55, 68, 72-79]. In double-cantilever-beam (DCB) testing, stitching increased mode I critical strain energy release rate (G_{Ic}) by as much as a factor of 30. This finding is not surprising because stitching directly reinforces the inter-laminar region in a mode I fashion. Stitching has also been shown to improve the mode II behavior [48, 68, 72, 73, 75]. While 2-D laminates fail catastrophically in end notch flexure testing (ENF), stitched laminates exhibited a stable crack growth. Stitching has been shown to increase the mode II critical strain energy release rate by as much as a factor of 15 [68, 75].

These improvements in inter-laminar dominated properties were achieved at a cost to the in-plane properties. Compared to unstitched materials, high density stitching has

been shown to reduce in-plane tension and compression strengths by amounts ranging from almost nothing up to 50 percent (see for example [17, 30, 31, 52, 53, 55, 65, 66, 80-84]. Stiffness was also degraded in most cases, although to a much lesser extent . However, in [85], stitching was reported to have improved the ultimate strain under compression loading at high strain rates, and both stitched and unstitched materials experienced an increase in the dynamic modulus as the strain rate was raised.

Charpy type impact and flexural test data for stitched and unstitched materials was reported in [34, 48, 72, 86-91]. For comprehensive stitching, the impact resistance was increased while in-plane flexural properties were decreased.

The inter-laminar shear strengths of TLR composites were investigated using short-beam-shear tests [48, 87, 91] and double-notch-shear tests [92, 93]. The results reported are somewhat contradictory for cases with small amounts of stitching, but in general, sufficient amounts of comprehensive stitching was found to improve inter-laminar shear strength as measured by these tests. In-plane shear properties, as measured by isopescue [92] and by a "modified rail shear" test, [94] were not significantly affected by stitching.

While it is important to consider that stitching may reduce undamaged in-plane tension and compression strength, notched (open hole) properties are often critical design drivers for structural applications. Open hole tension and compression strengths were not adversely affected by stitching [54, 61-63, 94, 95]. Independent analysis efforts in [96] and [97] were used to conclude that 3-D composites can be notch insensitive. Data in [95] support the idea that stitching may reduce the notch sensitivity in tension.

Other important structural design considerations are fatigue and environmental degradation. Compared to unstitched materials, undamaged fatigue behavior is relatively unaffected by stitching and stitching helped retard damage growth in fatigue testing of damaged and notched materials [51, 56, 61, 62, 64, 95, 97-101]. The environmental effects of moisture and/or heat were investigated and reported in [83, 84, 100, 102-110]. Due to the complicated states of stress near stitches and the unavoidable resin rich areas around the stitches, microcracks were found to be common. Stitched materials were also found to absorb moisture at a faster rate than unstitched materials. However, compared to similar 2-D laminates, stitched materials did not experience any worse environmental degradation of static or fatigue compression properties.

In addition to affecting mechanical properties, stitching has been shown to significantly affect the quality and accuracy of standard ultrasonic nondestructive evaluation (NDE) techniques. Various NDE techniques including ultrasound, photoelasticity and acoustic emission have been used on stitched and 3-D materials [111-116].

1. 3.3.   STITCHING VARIABLES

The extent that stitching affects mechanical performance is a function of many stitching variables (see Table 1-1) as well as the quality and proficiency of the stitching process. It is intuitive that increasing the amount of trans-laminar reinforcement will increases fracture toughness, reduce impact delamination size and increase the critical load for sublaminate buckling. All researchers who studied the effect of the amount of stitching found this to be the case, that is larger stitching threads and higher stitch densities (stitches

per unit area) resulted in higher fracture toughness and greater compression-after-impact

strength (see for example [17, 30, 49, 51, 52, 55, 56, 65, 66, 68, 72, 76, 79, 117]).

Table 1-1 Stitching variables.

Stitch Thread	Stitch Pattern	Stitching Process
material	stitch density	stitch type
size (linear density)	stitch direction	thread tension
finish	stitch pitch (step)	needle size/type
twist	stitch row density (spacing)	stitching machine
	stitch angle	

While "more stitching" has been shown to consistently improve inter-laminar

dominated properties, it is not clear what stitch thread property is most important.

Experimental results in [30, 117] lead to the conclusion that for a constant impact energy,

CAI strength is a function of effective stitch strength (total contribution of stitch thread

strength per unit area of laminate) and is not dependent on stitch thread material or

modulus. Based on the results of an analytical model of sublaminate buckling in [77, 118],

it was concluded that the TLR or stitch modulus "strongly" affected sublaminate buckling

strength. Based upon the results of finite element modeling of a double-cantilever-beam

(DCB) specimen, the authors of [79] came to the conclusion that stitch thread strength is

more important than stitch thread modulus in determining an effective critical strain energy

release rate, G_c. However, computer modeling efforts described in [119] indicated that

the ability to suppress delamination depends strongly on the effective axial stiffness of the

stitches. Experimental comparisons have shown no conclusive advantage for either Kevlar®, carbon or glass stitching threads. The only clear, consistent guideline is that large threads that are both strong and stiff need to be used to achieve the desired inter-laminar performance. Sufficient stiffness may be necessary to structurally carry load between plies and sufficient strength may be necessary for survival of the TLR.

High intrinsic stiffness and strength may be necessary, but only small amounts are required to significantly change inter-laminar response. A closed-form sublaminate buckling model described in [96, 120, 121] was used to conclude that most 3-D composites (including stitched) were "over designed" in terms of resisting sublaminate buckling. TLR volume fractions on the order of 0.1 percent are sufficient to suppress sublaminate buckling.

Unfortunately, while more stitching with larger threads improves the inter-laminar or out-of-plane performance, larger threads and higher stitch densities lower the in-plane tension and compression properties (see for example [17, 49, 52, 53, 55, 65, 66, 94]). More and larger threads lead to greater amounts of damaged and curved in-plane fibers. This subject of the mechanisms involved in the reduction of certain properties will be expanded upon in the next section. However, it is clear from the literature that there is a tradeoff of lowered in-plane tension and compression properties versus inter-laminar improvement.

This tradeoff was not evident for in-plane shear properties. Limited data for the in-plane shear testing of stitched laminates can be found in [92, 94]. Shear modulus (G_{xy}) and strength were not significantly affected by stitch density or thread size.

Stitch density and thread material are only two of the many variables that should be considered when stitching laminates (see Table 1-1). Reference [122] presents a good discussion of the various types of stitches and stitching machines available in the textile industry. The modified lock stitch (with the knot at the surface of the preform/fabric) and the chain stitch are the stitch types most commonly used for laminated composites (see Figure 1-1). References [31, 52] discuss a direct comparison of chain and modified lock stitch types used to reinforce graphite-epoxy laminates. Although the chain stitched materials had marginally better mechanical properties, the modified lock stitch was selected for continued development because of a better capability to stitch large and complex preforms.

While the amount and type of stitching appear to be the most important considerations, a given stitch density and stitch type can be implemented in a variety of patterns. Different zigzag, diagonal, horizontal and square patterns, investigated in [56, 57], only changed the shape, and not the size of delaminations caused by impact. The fracture mechanics model developed in [51] was used to conclude that a repeating pattern was more effective at resisting delamination than randomly located stitches. Parallel rows of stitching in the 0° (loading) direction were found to be equally effective for compression-after-impact performance as stitching in both the 0° and 90° directions or both the +45 and -45° directions [31, 53, 100]. While stitch pattern seems to have little affect on out-of-plane performance, this is not the case for in-plane properties. References [17, 31, 60] discuss how stitching perpendicular to load carrying fibers degraded in-plane properties more so than stitching parallel to the primary load direction. For fibers near the

surface, greater crimping takes place if the plies are oriented perpendicular to the stitching direction (that is perpendicular to a row of stitching).

1. 3.4. FAILURE MODES AND MECHANISMS

In addition to displacing the in-plane fibers and thus creating waviness or crimp, stitching also damages or breaks in-plane filaments and creates resin rich regions next to the stitches (see Figure 1-2). Many authors have suggested that these microstructural changes are responsible for the in-plane property reduction (see for example [80, 82, 83, 123]). The technology of stitching fabrics made from high performance fibers has advanced to the point where stitched laminates can be manufactured with minimal in-plane fiber breakage. As discussed above, cracks in and around the pure resin regions did not seem to affect mechanical properties. Hence, fiber waviness appears to be the driving factor for in-plane property reduction, particularly in compression [31, 82, 83, 123].

As expected with significant changes in mechanical properties, failure modes are altered by the addition of TLR. In failure under compressive loading, delamination, brooming and sub-laminate buckling are suppressed, allowing the laminate to fail in a "transverse shear" mode (see for example [16, 50, 54, 99]). Detailed observations of compression failure in stitched laminates [123-125] revealed the key damage sequence to be the micro-buckling of load bearing fiber bundles followed by the formation and unstable propagation of kink bands. While stitching played "no obvious part in initiating or moderating failure," failure was sudden and catastrophic making detailed observations of the failure sequence difficult [125]. High speed video was used to observe the compressive failure of stitched laminates [83].

Figure 1-3 shows some of the captured video images. These findings support the hypothesis that stitching caused local misalignment of the load bearing plies and hence lowered the strength as compared to unstitched material . As others have also observed, post failure inspection of compression loaded stitched laminates implied failure in a 45° shear band. Considered as a whole, a laminate that has failed in a "transverse shear" mode bears a close resemblance to the small kink bands discussed in [123-125]. It is possible that the TLR holds the individual plies of a laminate to together during failure and does not allow formation of "kink bands" at the ply level. In effect, a single large kink band may be formed at the laminate level. This idea is consistent with the observations of the various researchers, especially considering the great difficulty in detailed observations of rapid catastrophic failure.

Under tensile loading, stitching suppressed delamination and longitudinal splitting at failure [49, 50]. According to the authors of [123], systems of microcracks that develop in tensile-loaded TLR composites are periodic cracks normal to the applied load in transverse plies and shear cracks in off-axis plies. These cracks are very similar to those found in traditional tape laminates. Although the TLR minimizes delamination at large strains, ultimate failure accompanies rupture of the aligned plies in a similar manner to laminates without TLR [123].

In tension-tension, compression-compression, and tension-compression fatigue, stitching retarded existing delamination growth and changed the sequence of damage accumulation [95, 97, 98, 100].

Under flexural loading, failure changed from a catastrophic, matrix-dominated, delamination predominate failure in the unstitched case, to a more gradual, fiber-dominated failure with fiber breakage, fiber buckling, debonding and fiber pullout in the stitched materials [87-89].

1. 4. DISCONTINUOUS TLR

Trans-laminar reinforcement does not have to be a continuous thread that traverses the laminate thickness and then loops back into the laminate. The TLR can be a discontinuous pin or rod traversing the lamina at some arbitrary angle through-the-thickness (see Figure 1-1).

Short steel wires were used as TLR in two independent investigations discussed in References [126] and [127]. Compared to similar 2-D control laminates, inter-laminar shear strength was improved as much as 50 percent while less catastrophic and more gradual failures resulted. Inserting the discontinuous TLR at an angle 45° to the laminate plane (rather than normal to the plane) was found to effect the greatest improvement in inter-laminar shear strength. These improvements were brought about by TLR volume fractions on the order of only one percent [126, 127].

The fabrication and testing of another form of discontinuous TLR is discussed in [128-132]. The described "Z-fiber™ " materials consisted of composite laminates with TLR in the form of discontinuous pins with a diameter ranging from 0.010 to 0.020 inches, and TLR volume fractions ranging from 0.5-5.0 percent. The addition of these pins through-the-thickness resulted in the same kind of inter-laminar property

improvements as stitching. In a stiffener attachment study documented in [132], a comparison was made between Z-fiber™ TLR, mechanical fasteners and simple co-curing without TLR. As was found for stitching, Z-Fiber™ out performed simple co-curing and mechancial fasteners. Z-Fiber™ materials were also compared to similar materials without TLR in [130, 131]. Compression-after-impact strength was improved up to 50 percent, impact damage areas were reduced up 55 percent, and critical strain energy release rates (G_{Ic}) were increased by a factor of 18. As was the case with stitching, in-plane tension strength decreased with increasing TLR diameter. However, these TLR materials retained 91-98 percent of the tension strength of the 2-D materials. Up to 100 percent of the unreinforced compression strength was retained. The addition of the Z-fiber™ pins resulted in a 70 percent increase in the load required for the onset of edge delamination in tension. The edge delamination resistance was also a function of the density of the Z-fiber™ pins [130, 131].

These data support the conclusion that the surface loop found in stitching is not necessary to achieve the desired performance improvements. While the surface loops and knots of continuous stitching may be useful in holding a debulked state in a dry fiber preform, it may be a liability in the final composite. These loops and knots result in the kinking of the in-plane fibers near the surface [80-82]. In these investigations, the surface loop was removed from already fabricated materials (stitched and 3-D woven) by machining away part of the outer layer of material. Undamaged compression strength was improved up to 35 percent, CAI strength was increased by 11 percent, while impact damage size was unaffected. There was no apparent change in failure modes and

mechanisms [80-82]. Continuous and discontinuous TLR have also been compared by using separate fracture mechanics models. The superiority in mode I fracture toughness of continuous or discontinuous TLR structure was dependent on the TLR length, stiffness and strength, as these parameters would affect the load transfer into and by the TLR [78].

While discontinuous TLR offers similar or perhaps superior performance characteristics compared to stitching, technology for manufacturing discontinuous TLR materials is much less mature. Industrial sewing technology is well established and used in many industrial textile applications. Little if any modifications are required to stitch fabrics of advanced fibers. For discontinuous TLR, such readily adaptable methods are not available and new technologies are necessary. The Russian development of automated methods of inserting short fibers into laminates is discussed in [127, 133, 134].*

References [128-132] describe the "Z-fiber™ process" mentioned above (see Figure 1-4). The Z fiber process uses foam in the form of a sheet or tape. The foam contains short pins oriented perpendicular to the XY plane of the sheet. This foam layer is stacked within a standard prepreg bagging sequence used for curing. A release film is placed between the foam and the laminate. A steel shim or backing is placed over the foam. This entire assembly is autoclaved, where the pressure collapses the foam and inserts the fibers into the laminate which is softened by the heat needed for curing. The foam provides lateral support as the rods or fibers start into the laminate. After curing, the collapsed foam is simply peeled away leaving a trans-laminar reinforced laminate. Z direction

---

* A thorough review of Russian literature was not included in this work.

reinforcement (TLR) is thus obtained in a conventional prepreg-autoclave process. The in-plane fibers are minimally affected, resulting in little fiber damage [128, 129, 131].

Another method of inserting pins utilizes ultrasonic vibration. Based upon experimental findings discussed in [134], it was concluded that ultrasonic vibration significantly increases the ease with which pins are inserted into a laminate. An ultrasonically assisted insertion process has been developed and made commercially available [132]. The Ultrasonically Assisted Z-Fiber™ (UAZ) process uses the same foam preforms containing the TLR pins. An ultrasonic horn, rather than autoclave pressure, is used for the insertion step. Using this technique allows insertion of Z-Fiber™ into cured laminates as well as prepreg and preform materials. Thus, in addition to the already discussed applications, UAZ has tremendous potential for repair of composite structures [132].

As with stitching, these discontinuous trans-laminar reinforcement methods may be used in selective areas for structural bonding, stiffener attachment or as reinforcement near holes or other stress concentrations. Unlike stitching, a discontinuous TLR process offers the potential of being utilized in many of the conventional 2-D composite manufacturing process (e.g. tape layup, vacuum bag-autoclave, compression molding, pultrusion, filament winding and automated tow placement) [130]. However, discontinuous TLR may or may not be suitable for the debulking and stabilization of dry fiber preforms for use in subsequent resin transfer molding.

1. 5. ANALYSIS AND MODELING

The manufacture and testing of composite structure is often prohibitively expensive, especially given the wide range of material parameters that may be varied. Hence, if TLR materials are to be extensively used in structural applications, effective and accurate analysis/modeling techniques must be available. This section discusses modeling efforts reported in the literature. Empirical modeling is discussed first, followed by a general review/overview of analytical modeling, and ending with a focus on fracture mechanics type approaches. The discussions herein are kept fairly brief with the reader being referred to the appropriate references for pertinent details.

1. 5.1. EMPIRICAL MODELING

A large majority of the TLR literature has focused on exploratory investigations (often repetitive) with fewer efforts aimed at prediction of material behavior. Several experimental studies have been conducted to examine the tradeoffs of in-plane properties vs. inter-laminar (out-of-plane) dominated properties in stitched materials. Two separate experimental programs resulted in empirical formulations in [55] and [65, 66]. These relations predicted tension, compression and compression after impact fairly well over the limited range of parameters and materials studied. Two separate experimental studies, documented in [17] and [13, 30, 31, 52, 117], arrived at very similar sets of optimum stitching parameters. Reference [17] describes the development of stitched composites for turbine fan blade applications. The resulting optimum stitching was selected to be 40

stitches/in^2 with a 1000 denier* Kevlar® 29 thread. References [13, 30, 31, 52, 117] summarize the ongoing development of stitched composites for use in the primary wing structure of transport aircraft. Balancing increased CAI strength with lower tension and compression strength resulted in a similar selection of stitching variables.

Laminate theory has been applied to stitched laminates using experimentally determined stitched lamina properties [30, 31]. In-plane stiffness was predicted fairly well for the one set of stitching parameters studied, but the modified laminate theory under predicted compression and tension strengths by 30 percent and 15 percent respectively.

An empirical approach was also used in [97] to model the post impact fatigue of stitched laminates. The experimental fatigue lives were predicted to within one or two factors.

1. 5.2.   ANALYTICAL MODELING

TLR composites are distinguished from laminates by the addition of fibrous reinforcement through-the-thickness. The lamina of TLR materials may be derived from textile fabrics or traditional unidirectional tape. No matter the lamina form, TLR materials may be considered a subset of "textile composites" due to their 3-D nature. TLR laminates are distinguished from other 3-D textile composites (e.g. 3-D weaves, 3-D braids, etc.) due to the small amounts of fibrous reinforcement in the thickness direction (on the order of one percent volume). True 3-D textile composites contain significant volume fractions of fiber in many directions, and may or may not have a simple layered

---

* "denier" is unit of measure for linear density. One denier is equivalent to one gram per 9000 meters.

structure. Development, analysis and modeling of textile composites is currently an active research area. In so far as the same or similar techniques and assumptions apply to both TLR and the more general "textile composites," the discussion in the following paragraphs will be broadened to include analysis methods for textile composites. Independent reviews of analytical methods for textile composites can be found in [123, 135-139]. Only a general discussion will be given here. For specific models and their references, the reader is referred to these excellent review articles.

In the mechanics of composites field there is a large variety of analysis methods and analysis products available. Compared to homogeneous metallic materials, composite laminates have inherent material inhomgeneity and complex microstructures that make them difficult to analyze and model, particularly with regard to material and structural failure. The microstructure of textile composites involves yet another level of complexity, as the basic structural blocks are individual yarns or tows rather than simple sheets or layers. These yarns or tows are oriented in, and interact in all three dimensions. Thus, analysis problems are compounded when it comes to textile composites. Given the degree of difficulty involved, it is very important to consider the objective when selecting an analysis method for textile composites. If engineering elastic constants (stiffnesses) are all that are required, relatively quick and simple analyses are available with adequate accuracy. If the objective is predictions of strength, damage tolerance, etc., an entirely different level of analysis is necessary. The models reviewed in [135-138] deal primarily with predictions of elastic constants. The reviews found in [123, 139] also include more recent efforts at strength predictions. In addition to reviewing publicly available models

and their codes, reference [123] also provides an in-depth discussion of the concepts

underlying the simplifying assumptions necessary for textile modeling.

As proposed in [135], textile analysis methods may be placed into three broad

categories; 1) Elementary Models, 2) Laminate Theory Models, and 3) Numerical

Models. A brief discussion of these three groups and how they apply to TLR composites

follows.

1. 5.2.1. Elementary Models

The authors of [135] briefly discusses a variety of fiber-matrix models based on

strength of materials approaches. They state that few of these elementary models "have

achieved broad acceptance beyond their limited range of applicability". In [123] the

authors also distinguished fairly simple and elementary models and methods. They include

"orientation averaging" methods among theses simple modeling approaches.

Orientation averaging is based on the assumption that the textile can be

represented by a periodic configuration known as a "unit cell." The unit cell is composed

of individual segments of unidirectional composite. Curved tows are broken into short

segments of straight fibers. Isostrain, isostress or a combination of both is assumed. The

spatial orientation and volume fractions of the segments are known, allowing stiffnesses or

compliances to be transformed to the global coordinate system using tensor

transformation. The transformed stiffnesses or compliances are then averaged over the

volume of the unit cell*. Applying this methodology with the isostrain assumption is

known as stiffness averaging. In a one dimensional consideration stiffness averaging

follows the derivation of the familiar rule of mixtures equation for longitudinal stiffness of a unidirectional composite:

$$E_l = E_f V_f + E_m V_m$$

Equation 1-1.

Orientation averaging with the isostress assumption is known as compliance averaging. In a one dimensional consideration it follows the derivation of the familiar rule of mixtures equation for transverse stiffness of a unidirectional composite:

$$\frac{1}{E_t} = \frac{V_f}{E_f} + \frac{V_m}{E_m}$$

Equation 1-2.

Here E is the Young's modulus and V is the volume fraction. The subscripts l and t refer to the longitudinal and transverse directions of the unidirectional composite while m and f refer to the matrix and fiber constituents, respectively.

Properly applied orientation averaging will predict the fiber dominated material elastic constants with adequate accuracy, even for fairly complex textile geometries. From energy considerations, stiffness averaging (isostrain) will always provide a lower bound, while compliance averaging (isostress) provides the upper bound [123]. However, even under simple loading, neither isostrain nor isostress conditions actually occur throughout the internal microstructure of even a fairly simple unit cell. In addition, real textile composites contain sufficient geometrical irregularities to raise serious questions as to the

---

* For more detail, see [123], and section 3.3.

validity of modeling with a unit cell of "ideal geometry." These errors are usually not significant in the determination of global-macroscopic elastic constants. However, detailed and accurate stress-strain information is necessary for failure analysis. Hence, orientation averaging is not suitable for the analysis of strength, damage initiation, damage progression, etc.

1. 5.2.2.   Laminate Theory Models

Classical Laminate Theory (CLT) has long been used to model conventional 2-D (tape) laminates. The history and development of applying the principles of plate/laminate theory to textile composites is discussed in [135]. As suggested, "most of these plate bending/stretching models have two-dimensional (2-D) applications in mind, and so do not address the out-of-plane composite properties." As is noted in [123], for a 2-D laminate, orientation averaging with isostrain conditions is equivalent to standard laminate theory for in-plane deformations. Hence, these two methods yield similar results for "quasi-laminar" textile composites (e.g. 2-D woven laminates and 2-D braids). TLR composites may be considered quasi-laminar, and some of these type models could be adapted for use with TLR. However, as just noted, models based on laminate theory do not address thickness direction or trans-laminar properties and behavior. Hence, they are not suitable for most of the applications for which TLR is required, that is joining, damage resistance, etc. In addition, laminate theory approaches do not allow accurate and detailed representation of stress and strain within the modeled microstructures. Hence they have the same limitations that orientation averaging methods have. As noted in the previous section, the direct application of laminate theory to TLR with the use of experimentally

determined stitched lamina properties resulted in fairly accurate estimates of in-plane stiffnesses, but inaccurate predictions of strength. Such methods are also limited to the one set of TLR parameters used to generate the lamina properties.

1. 5.2.3. Numerical Models

Numerical methods such as finite element analysis (FEA) provide the most general and adaptable modeling method. There are many different general purpose FEA codes commercially available. As discussed in [123], the macroscopic stiffnesses of textile composites can be calculated with FEA. Typically this involves building the macroscopic stiffness matrix by applying six independent sets of homogeneous boundary conditions (displacements). For each case a global, or macro average stress is obtained by integrating either the internal stresses or the boundary tractions. The elastic constants are calculated by relating the applied displacements (that is strains) to the average macrostress.

Since full field displacement, strain and stress results are available throughout a FEA model, failure analyses are possible. However, due to the level of detail required for 3-D textile microstructures, this type modeling is both computationally and labor intensive. Even considering recent and continuing advances in computational hardware and software, general purpose FEA codes may not be suitable for use in the general design of textile composites and their structures for the next decade.

To alleviate some of these drawbacks, materials researchers using FEA to study textile composites have often employed simplifying assumptions and approximate modeling methods. These modeling short cuts can be classified into two categories: 2-D approximations and improvements in meshing. Although 2-D approximations are often

used, plane strain or plane stress assumptions are not applicable in most cases due to the inherent 3-D geometry of 3-D textiles. Detailed meshing of 3-D structures is becoming easier with advances in 'state of the art' solid modelers and automatic meshers. Another meshing shortcut that has been employed in the modeling of textile composites is the use of heterogeneous elements. In a heterogeneous element, different regions of the element are assigned different material properties. During the generation of the element stiffness matrix, the local material stiffness is determined at each Gaussian integration point. When these heterogeneous elements are used, the FEA mesh is not required to map directly to the microstructural geometry. With different material properties allowed within the same element, larger elements may be used. However, the stresses in heterogeneous elements may converge slowly with respect to mesh density [123].

Another problem with the traditional finite element approach is that the modeling is restricted to a representative and idealized unit cell. In real textile composites the microstructure will vary significantly from unit cell to unit cell. Unavoidable and irregular features such as fiber waviness, crimping, changing yarn cross-sections, etc. play a very important role in failure mechanisms [123, 140]. While giving detailed information, unit cell modeling does not account for the significant geometrical irregularity commonly found in even the best textile composites. In fact, this observation led the authors of [140] to "infer that detailed analysis of local stress distributions based on finite element simulations using highly refined grids to represent *geometrically ideal* unit cells are of questionable value in predicting strength." Although the calculation of average stress and

elastic constants is not sensitive to these typical geometrical irregularities, accurate calculation of elastic constants can be done with much simpler methods.

The authors of [140] did not discount FEA methods in general, only the supposition that "ideal" unit cells are useful in modeling strength and failure. In fact they proposed a new modeling technique based on the numerical finite element method. In their "Binary Model" the textile composite is simulated by only two types of element; 1) tow elements, representing the reinforcing fibers and 2) effective medium elements representing everything else. This simplification along with the inclusion of a method allowing for the statistical variation in geometry, enabled the modeling of a more realistic textile composite microstructure. This model may be particularly useful for analysis of complicated macrostructure (e.g. stiffener attachment, thickness changes, etc.) where "ideal" periodic unit cells can not be identified. For details, see [101, 123, 141, 142]. This binary model has been thus far developed primarily for the study 3-D woven composites. Although a more general application is possible, the published literature only shows its use with the 3-D weaves. Although its originators also performed some experimental studies of stitched composites, their analytical work on TLR composites has taken the direction of the study of bridged crack phenomenon (see next section).

Another specially developed numerical model was reported in [119, 143]. This 2-D model was based on a higher order plate theory with the TLR modeled as springs. It was intended to help designers determine the "optimum" stitching for stiffener/structure attachment. Model details are given in [119] while correlation with experiment and parametric studies are discussed in [143].

Other researchers have also applied general purpose FEA modeling to TLR materials [33, 36, 79, 106-108, 110, 144]. Two dimensional approximations were made with plane strain assumptions in [36, 79] and axisymetric assumptions in [108, 110]. Three dimensional FEA models were used and the results reported in [33, 106, 107, 110, 144]. The TLR (stitches) were modeled with spring, rod or beam elements in [33, 36, 79]. These approaches did not capture many of the important microstructural features (e.g. induced in-plane fiber curvature and pure resin regions) that are known to exist. In [106-108] the TLR and other microstructural features were modeled in detail, but the investigations were limited to thermal effects. The results of a limited investigation of extensional moduli and Poisson's ratios (3-D) is reported in [144], but the models were limited to one layer with no inter-laminar interface. To date, there have been no detailed investigations using general purpose 3-D FEA to study the mechanical response of TLR composites. Particularly lacking are considerations of macroscopic shear behavior.

Numerical modeling is not limited to the finite element method. The development of a one dimensional micromechanical model is described in [145]. The model consists of homogeneous, transversely isotropic and axisymmetric nested cylinders. Governing equations were formulated and a general solution procedure was under development. The author suggests that the model will be useful for mechanical and thermal analysis and design of Z-Fiber™ materials.

1.5.3.   ANALYSIS OF BRIDGED CRACKS

As has been discussed in the preceding sections, many researchers have shown that sufficient TLR will prevent the growth of delamination. TLR that bridge delamination

cracks can both prevent sublaminate buckling and retard crack growth. The structural

performance of the material or part is thereby significantly improved, as shown by the

significantly higher loads required to sustain catastrophic failure. The important question

is then, how much TLR is sufficient. Concepts developed for the analysis of bridged

cracks (see for example [146]) can be very useful in addressing this question.

Several different authors have applied sublaminate buckling and/or crack bridging

concepts to the TLR problem. In terms of sublaminate buckling, two different one

dimensional sublaminate buckling models (based on beam on elastic foundation

assumptions) are described in [96, 120, 121] and [77, 118]. Several different mode I

fracture mechanics models are reported in [51, 76, 78]. Both sublaminate buckling and

delamination extension were combined in a model discussed in [77]. Cracks bridged with

TLR in curved structures are addressed in [4, 123, 147, 148]. Mode II delamination with

bridged cracks is discussed in [123, 149]. Such modeling approaches offer great promise

for determining guidelines of how much TLR is required to prevent premature structural

failure due to the existence of delaminations. However, it is important to understand that

these approaches assume that delaminations already exist. While useful for determining

the critical size of delaminations, they do not address the onset or initiation of

delamination.

1. 6.   OBJECTIVE AND SCOPE

As discussed above, most of the variables and principles associated with TLR

composites apply to both "stitched" (continuous TLR) and "pinned" (discontinuous TLR)

laminates. Many researchers have shown that small amounts of TLR can significantly

delay damage progression. Both analytical and experimental work has consistently demonstrated that the load required for sublaminate buckling is increased; fracture toughness in mode I (double cantilever beam) and mode II (end notch flexure) are significantly improved; and the size and growth of impact damage and edge delamination are severely restricted. These benefits are found in both static and fatigue loading. TLR directly supports the "Achilles' heel" of laminated composite, that is delamination. By directly bridging cracks between lamina, even small amounts (order of one percent volume) of TLR significantly alter the mechanical response of the laminate.

While the restriction of damage progression has been demonstrated many times, there is little or no data supporting the supposition that TLR increases the load or energy required to initiate damage/delamination. In fact, as discussed in section 1.2.2, research on low velocity impact has shown that the addition of stitching did not alter the force at which damage initiates. Of course not all practical values and combinations of values of the many different TLR parameters have been investigated. At commonly investigated values of TLR parameters, it is likely that there is sufficient unreinforced space between the discrete through-thickness reinforcements for damage to initiate in the same fashion and at the same values as in the traditional unstitched 2-D laminate. After the delamination is initiated however, even in the dynamic event of low velocity impact, delamination growth is restricted by TLR and the resultant overall damage areas are smaller.

The question of whether TLR does or does not improve damage initiation has not been specifically addressed in detail. Where it has been discussed, the definition of

"damage initiation" or "failure initiation" has not been clearly articulated. A great deal of research has been and is currently being conducted on sublaminate buckling, crack bridging, damage progression, etc. However, little or no work has addressed how the addition of TLR alters the stress states in pristine material, and how these changes might affect damage initiation. It is important to understand that failure in composite materials almost always involves a sequence or progression of different but related mechanisms. Only very small amounts of TLR are required to change dominant failure mechanisms, alter their sequence, and revise their relative importance. The question of the effect of TLR on delamination initiation has important implications regarding different philosophies that can be used to design composite structures: design to prevent the initiation of delamination, or design to prevent the growth of potential existing delaminations

With these ideas in mind, it was the general objective of this work to characterize the effects of TLR on the in-plane and inter-laminar mechanical response of *undamaged* composite laminates. Primary goals included the determination and understanding of TLR effects on the elastic constants and delamination initiation. A unit cell approach was utilized with 3-D finite element modeling of TLR laminates. Such modeling is necessary to investigate the complicated 3-D states of stress in and around the microstructural details of TLR as it bridges lamina interfaces. Various TLR parameters were studied, including; TLR material, TLR diameter, TLR volume fraction, TLR through-thickness angle, laminate ply stacking sequence (layup), and the microstructural features of pure resin regions and curved fibers. These investigations were performed with current 'state of the art' analysis tools and commercially available general purpose finite element

software. The work was limited to the study of the linear response (undamaged) of a unit cell with a ply interface. The unit cell results are presented in terms of the effects of TLR on 1) elastic constants, 2) strength implications and 3) delamination initiation. In addition to the unit cell models, a simplified model of the stiffener pull-off test was created and used to investigate the application of TLR to a practical, "real life," inter-laminar dominated problem..
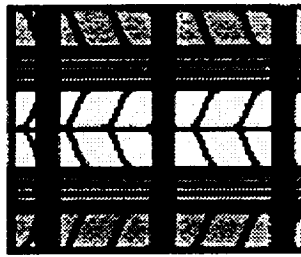
Discontinuous TLR
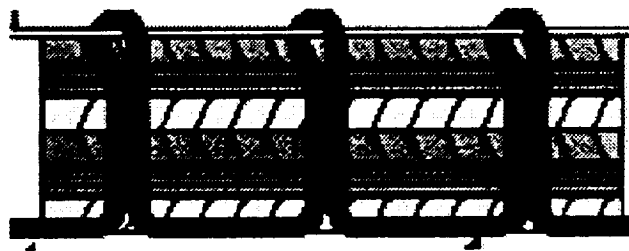
Lock Stitch
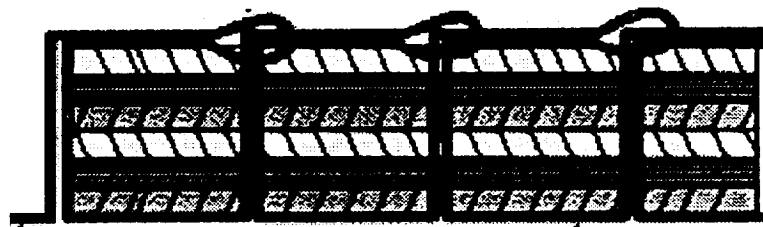
Chain Stitch

Figure 1-1 Trans-Laminar Reinforcement (TLR) types.
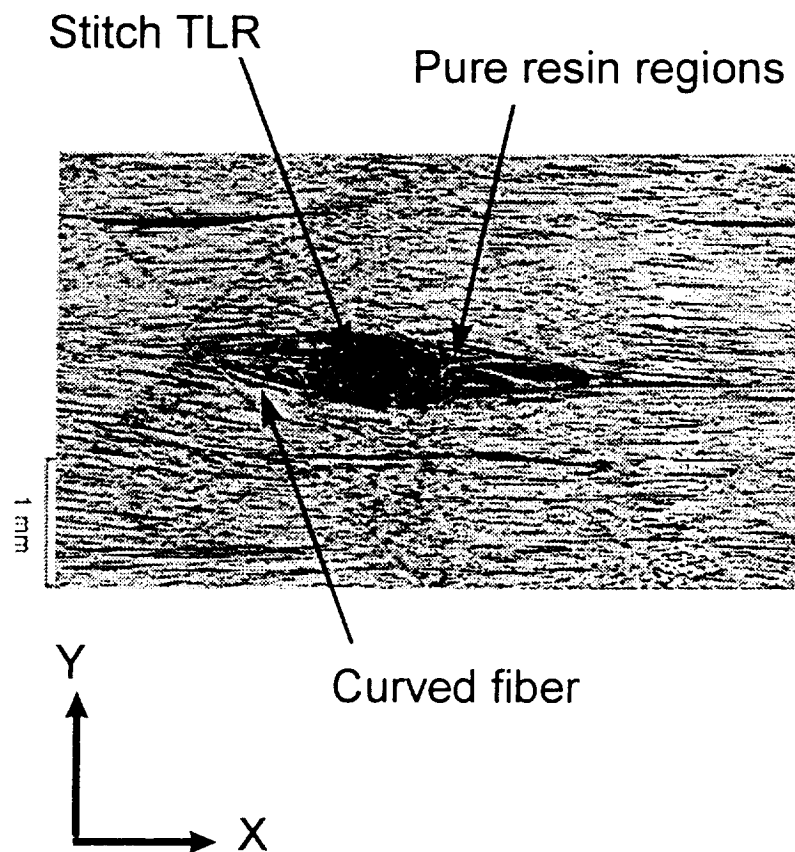
Figure 1-2 a) Micrographs of stitched graphite-epoxy laminates showing curved in-plane fibers, courtesy of James Reeder, Mechanics of Materials Branch, NASA Langley Research Center.
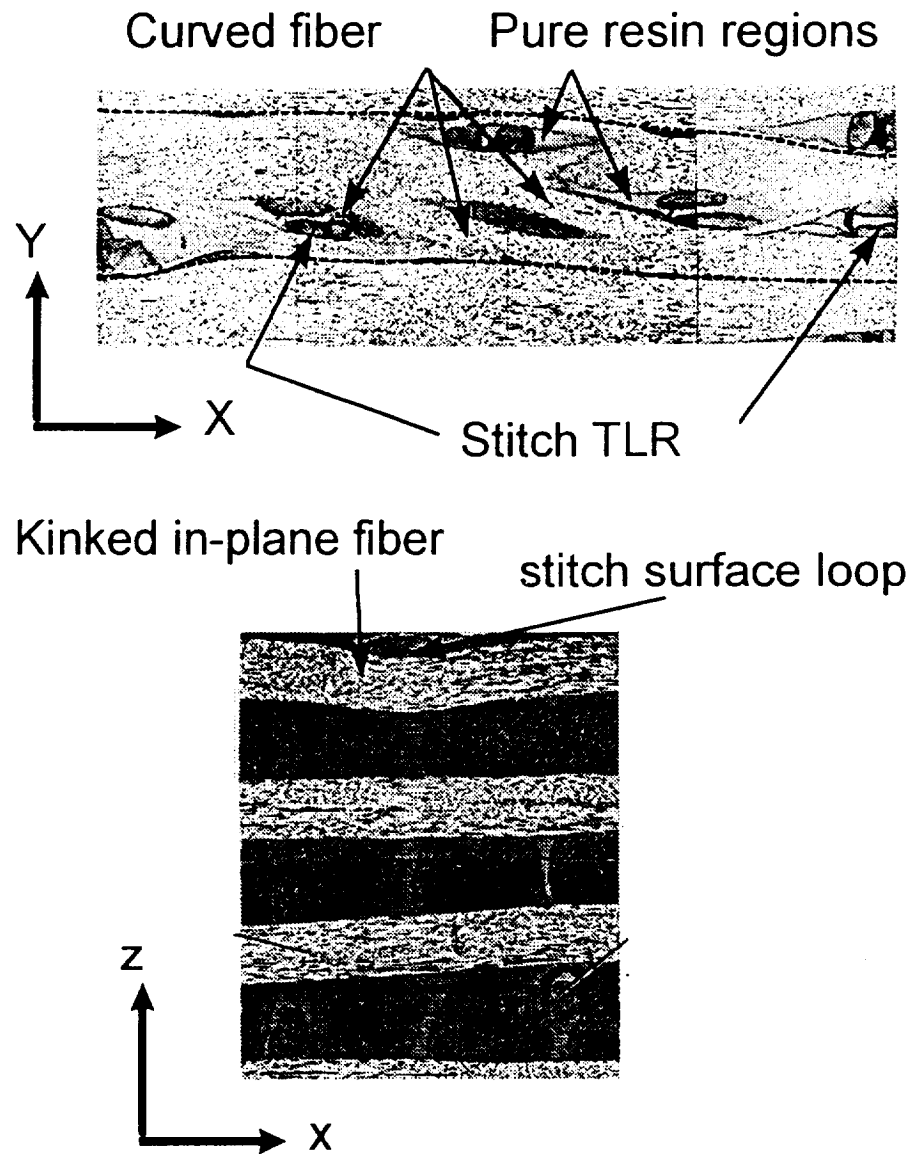
Figure 1-2 b) Micrographs of stitched graphite-epoxy laminates showing curved in-plane fibers, courtesy of Dr. Gary Farley, Army Research Laboratory Vehicle Technology Center.

Initial   1.8 sec   1.2 sec   0.001 sec   Failure
Prior to Failure   Prior to Failure   Prior to Failure
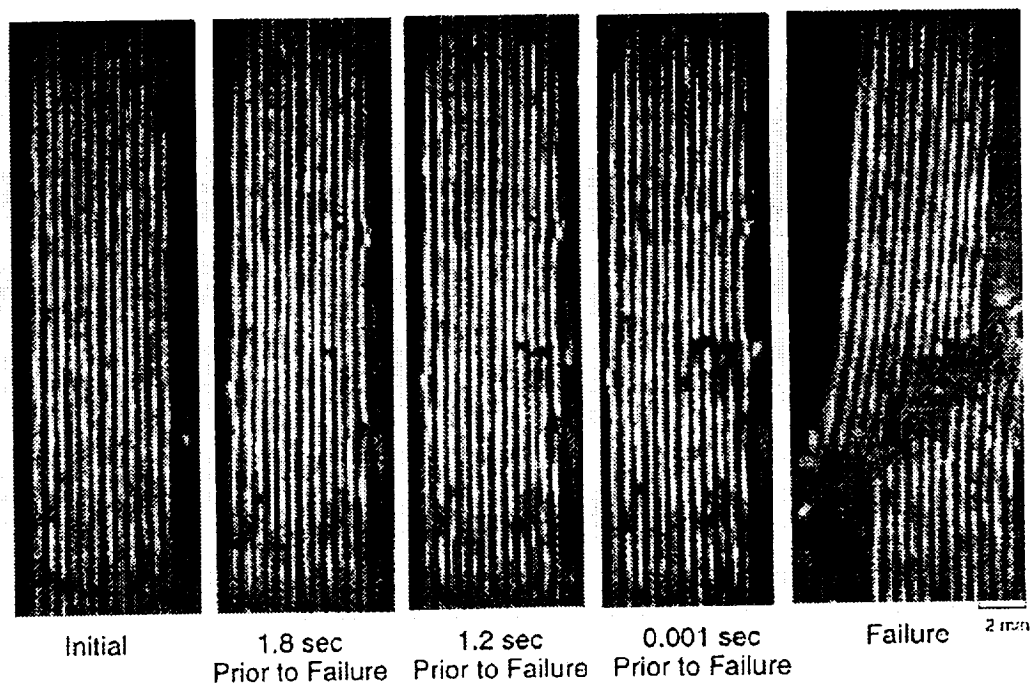
Figure 1-3 Compression failure sequence of stitched laminate. Photo courtesy of James Reeder, Mechanics of Materials Branch, NASA Langley Research Center.
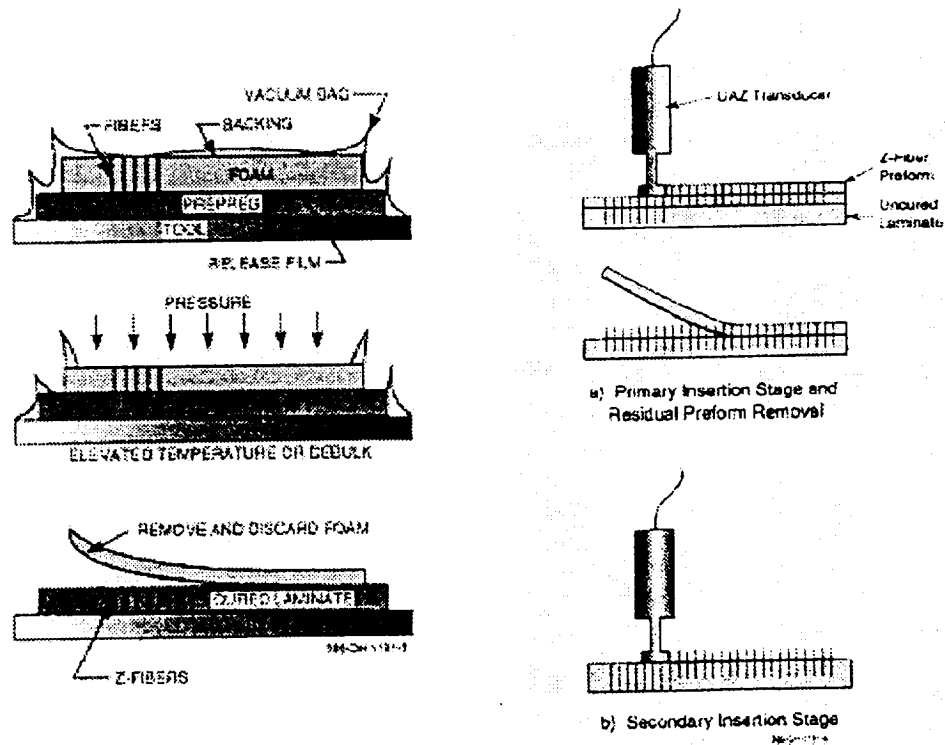
Figure 1-4 Process schematics for "Z-Fiber™" (above) and Ultrasonically Assisted Z-Fiber™, UAZ (below).

CHAPTER 2
UNIT CELL ANALYSIS, BOUNDARY CONDITIONS, AND CALCULATION OF ELASTIC CONSTANTS

In all forms of numerical modeling, including finite element analysis (FEA), assumptions are necessary to define both the general scope and particular details of the models. Since it is most often impractical to model universal conditions, modeling assumptions must be made that restrict the size of the actual model. Typically only a portion of the structure to be analyzed is actually modeled with detail. At times, certain limiting assumptions about behavior are made. Appropriate boundary conditions (BC's) are required to insure that the modeled part relates properly to the rest of the structure. In addition, certain BC's may be required to make a problem numerically tractable*. This chapter begins with a discussion of the "unit cell" (UC) modeling approach and the boundary constraints that it requires. Calculation of material elastic constants using a unit cell analysis is then described. These discussions are then followed by a summary of the actual BC's applied to the UC.

2. 1.   UNIT CELL APPROACH

Many different researchers have used the concept of the "representative volume element" (RVE), or "unit cell" (UC) for the modeling of textiles. Although the basic concept is simple, particulars vary and many definitions of the "unit cell" may be found in

---

* An example of this type BC for FEA is the requirement of enough boundary displacement constraints to prevent rigid body translation and rotation. For details, the reader is referred to any general text on FEA.

the literature. The term "unit cell" has been used for many years in the traditional textile industry and reference [123] suggests that the term "unit cell" is borrowed from crystallography. In all cases, the concept is that an entire material can be represented by simply modeling a representative volume. In the same manner that a sine wave can be represented by one cycle or period, a material with a periodic structure can be represented by one unit cell. Under uniform external loads, a material with a periodic structure will have stress and strain distributions that are periodic. The material "response to external loads can be computed by analyzing the behavior of a single unit cell with suitable boundary conditions" [123]. This statement implies that the entire material structure, before and after deformation, can be generated by simply replicating the unit cell. This concept is shown schematically in Figure 2-1.

Just as a single period of a sine wave can begin at any point and end at the corresponding point one wavelength later, there are an infinite number of possible unit cells in any periodic material. For this discussion the definition of a unit cell will be restricted to an orthogonal hexahedral shaped volume that can be used to generate the entire material structure by replication and translation. A 2-D analogy can be used by saying that an entire puzzle is made up of a single repeated piece. This puzzle can be put together by copying the one piece and fitting the copies around the original without rotation.

Although the use of unit cell modeling with periodic boundary conditions has been shown repeatedly in the literature, most authors simply state that "periodic boundary conditions" are used and then list those conditions. Adequate discussions of exactly what

the unit cell assumption requires in terms of boundary conditions have been sorely lacking. For a hexahedron with three sets of opposing faces, the UC requirement can be stated as follows: the relative spatial relationship between points of one face must also apply to its opposing face, both before and after deformation. These opposing faces (e.g. opposite sides of a cube) must be symmetrical with respect to each other. During deformation, it is not sufficient that the overall shape of these opposing sides be maintained, but distances between internal points must also match up for both sides.

To illustrate this important point, consider a 2-D example. Figure 2-2 shows the unit cell of the material in Figure 2-1. Let one fourth of this representative piece of material (the shaded area) be much stiffer than the rest. Let a uniform loading be applied to the entire piece as shown in Figure 2-2 a. Without the constraints imposed by neighboring unit cells, the piece would want to deform as in Figure 2-2 b. In this free deformation, the right and left hand sides do not stretch the same amount. Not only are they different lengths after deformation, but the internal points do not have the same relative displacement. Requiring the two sides to have the same length is not sufficient, as the right and left side would not match up internally. For this example to meet unit cell requirements, each point on the right side must have the same vertical displacement as its corresponding point on the left side. Deformation with unit cell constraints is shown in Figure 2-2 c. This constraint is the same as would be imposed by the neighboring unit cell in the real structure. Displacement continuity (and hence strain continuity) is thus maintained across the boundaries of the unit cell. While strain must be continuous in a continuous structure, all stress components are not. In the 2-D example of Figure 2-2, the vertical component of stress at point R2 in the stiff material would not be the same as

the vertical component of stress at point L2 in the flexible material. Of course the horizontal components of stress must be the same at R2 and L2.

Although the unit cell approach is general and very useful, it does have its limitation. The assumption of uniform loading does not always apply. Macrostructural discontinuities typically give rise to stress gradients that are significant at the scale of the smallest identifiable unit cell. Strict unit cell assumptions only apply to internal structure under uniform stress, far away from free edges and other geometrical discontinuities. In addition, the unit cell represents an "ideal" structure. Textiles composites contain unavoidable geometrical and material irregularities that are not periodic. Such irregularities (e.g. fiber waviness) and the variation in those irregularities typically play an important role in the material response. This fact is particularly true for damage progression and failure. Such limitations aside, a great deal of understanding can be gained about the basic mechanical response of a material using simple unit cell assumptions. Given the magnitude of the computational effort required, a 'unit cell' or 'representative volume element' approach is the only way to get detailed stress-strain information for complicated microstructure.

2. 2.   CALCULATION OF ELASTIC CONSTANTS

A unit cell analysis as described in section 2.1 was used to calculate elastic constants for TLR materials. The technique involved applying a known macrostress to a finite element model that is constrained in its deformation to meet both unit cell requirements and basic definitions of strain. Macrostrain is calculated from the displacement output of the FEA analysis. The macrostrains are then used in simple

constitutive relations to determine the engineering elastic constants. This procedure is detailed in the following three subsections.

2.2.1.   EQUATIONS AND DEFINITIONS

Discussions and derivations of stress, strain and their constitutive relations can be found in many texts. The following equations are taken largely from [150] and [151]. Small displacement formulation is assumed and only engineering strains are used. The reader is referred to these or other texts for detailed derivations of these basic concepts of elasticity.

The 3-D strain displacement relations of elasticity are given as:

$$\varepsilon_x = \frac{\partial u}{\partial x} \qquad \varepsilon_y = \frac{\partial v}{\partial y} \qquad \varepsilon_z = \frac{\partial w}{\partial z}$$

$$\gamma_{xy} = \frac{\partial u}{\partial y} + \frac{\partial v}{\partial x} \qquad \gamma_{yz} = \frac{\partial v}{\partial z} + \frac{\partial w}{\partial y} \qquad \gamma_{zx} = \frac{\partial u}{\partial z} + \frac{\partial w}{\partial x}$$

Equation 2-1.

Figure 2-3 graphically shows the basic concept of one dimensional normal strain, ε. If the deformation is distributed uniformly over the original length, the normal strain is defined as the change in length, Δl, divided by the original length, l_0. If the deformation is not uniform, the aforementioned is the average strain. Shear strain, γ, is defined as the total change in the right angle DAB shown in Figure 2-4a. γ is the sum of the two angles α. For small deformations, α is approximated by $\tan(\alpha)$. The shear strain can also be

shown graphically with the schematic in Figure 2-4b. Figure 2-4b is the same as Figure 2-4a with an arbitrary rotation applied. Applying these simple graphical definitions in three dimensions and taking the limit results in the above definitions of strain[*].

Strains can be written in contracted form:

$$\varepsilon_i = \begin{bmatrix} \varepsilon_x \\ \varepsilon_y \\ \varepsilon_y \\ \gamma_{yz} \\ \gamma_{xz} \\ \gamma_{xy} \end{bmatrix} = \begin{bmatrix} \varepsilon_1 \\ \varepsilon_2 \\ \varepsilon_3 \\ \varepsilon_4 \\ \varepsilon_5 \\ \varepsilon_6 \end{bmatrix} \qquad (i = 1,2...6)$$

Equation 2-2.

Similarly, the contracted notation for stress is:

$$\sigma_i = \begin{bmatrix} \sigma_x \\ \sigma_y \\ \sigma_z \\ \tau_{yz} \\ \tau_{xz} \\ \tau_{xy} \end{bmatrix} = \begin{bmatrix} \sigma_1 \\ \sigma_2 \\ \sigma_3 \\ \sigma_4 \\ \sigma_5 \\ \sigma_6 \end{bmatrix} \qquad (i = 1,2...6)$$

Equation 2-3.

The constitutive relations or generalized Hooke's can be written:

---

[*] For a more rigorous derivation/definition of strain, the reader is referred to any basic text on elasticity.

$$
\begin{bmatrix} \sigma_1 \\ \sigma_2 \\ \sigma_3 \\ \sigma_4 \\ \sigma_5 \\ \sigma_6 \end{bmatrix} = \begin{bmatrix} C_{11} & C_{12} & C_{13} & C_{14} & C_{15} & C_{16} \\ C_{12} & C_{22} & C_{23} & C_{24} & C_{25} & C_{26} \\ C_{13} & C_{23} & C_{33} & C_{34} & C_{35} & C_{36} \\ C_{14} & C_{24} & C_{34} & C_{44} & C_{45} & C_{46} \\ C_{15} & C_{25} & C_{35} & C_{45} & C_{55} & C_{56} \\ C_{16} & C_{26} & C_{36} & C_{46} & C_{56} & C_{66} \end{bmatrix} \begin{bmatrix} \varepsilon_1 \\ \varepsilon_2 \\ \varepsilon_3 \\ \varepsilon_4 \\ \varepsilon_5 \\ \varepsilon_6 \end{bmatrix}
$$

Equation 2-4.

where C_{ij} is the stiffness matrix.

Equation 2-4 can also be written in the inverted form:

$$
\begin{bmatrix} \varepsilon_1 \\ \varepsilon_2 \\ \varepsilon_3 \\ \varepsilon_4 \\ \varepsilon_5 \\ \varepsilon_6 \end{bmatrix} = \begin{bmatrix} S_{11} & S_{12} & S_{13} & S_{14} & S_{15} & S_{16} \\ S_{12} & S_{22} & S_{23} & S_{24} & S_{25} & S_{26} \\ S_{13} & S_{23} & S_{33} & S_{34} & S_{35} & S_{36} \\ S_{14} & S_{24} & S_{34} & S_{44} & S_{45} & S_{46} \\ S_{15} & S_{25} & S_{35} & S_{45} & S_{55} & S_{56} \\ S_{16} & S_{26} & S_{36} & S_{46} & S_{56} & S_{66} \end{bmatrix} \begin{bmatrix} \sigma_1 \\ \sigma_2 \\ \sigma_3 \\ \sigma_4 \\ \sigma_5 \\ \sigma_6 \end{bmatrix}
$$

Equation 2-5.

where S_{ij} is the compliance matrix.

For an orthotropic material (3 planes of symmetry), Equation 2-5 simplifies to:

$$
\begin{bmatrix} \varepsilon_1 \\ \varepsilon_2 \\ \varepsilon_3 \\ \varepsilon_4 \\ \varepsilon_5 \\ \varepsilon_6 \end{bmatrix} = \begin{bmatrix} S_{11} & S_{12} & S_{13} & 0 & 0 & 0 \\ S_{12} & S_{22} & S_{23} & 0 & 0 & 0 \\ S_{13} & S_{23} & S_{33} & 0 & 0 & 0 \\ 0 & 0 & 0 & S_{44} & 0 & 0 \\ 0 & 0 & 0 & 0 & S_{55} & 0 \\ 0 & 0 & 0 & 0 & 0 & S_{66} \end{bmatrix} \begin{bmatrix} \sigma_1 \\ \sigma_2 \\ \sigma_3 \\ \sigma_4 \\ \sigma_5 \\ \sigma_6 \end{bmatrix}
$$

Equation 2-6.

In terms of engineering constants, the above equation becomes:

$$
\begin{bmatrix} \varepsilon_1 \\ \varepsilon_2 \\ \varepsilon_3 \\ \varepsilon_4 \\ \varepsilon_5 \\ \varepsilon_6 \end{bmatrix} = \begin{bmatrix} \dfrac{1}{E_{11}} & \dfrac{-\nu_{12}}{E_{11}} & \dfrac{-\nu_{13}}{E_{11}} & 0 & 0 & 0 \\[6pt] \dfrac{-\nu_{12}}{E_{11}} & \dfrac{1}{E_{22}} & \dfrac{-\nu_{23}}{E_{22}} & 0 & 0 & 0 \\[6pt] \dfrac{-\nu_{13}}{E_{11}} & \dfrac{-\nu_{23}}{E_{22}} & \dfrac{1}{E_{33}} & 0 & 0 & 0 \\[6pt] 0 & 0 & 0 & \dfrac{1}{G_{23}} & 0 & 0 \\[6pt] 0 & 0 & 0 & 0 & \dfrac{1}{G_{13}} & 0 \\[6pt] 0 & 0 & 0 & 0 & 0 & \dfrac{1}{G_{12}} \end{bmatrix} \begin{bmatrix} \sigma_1 \\ \sigma_2 \\ \sigma_3 \\ \sigma_4 \\ \sigma_5 \\ \sigma_6 \end{bmatrix}
$$

Equation 2-7.

The engineering constants are used for a physical interpretation of the elastic behavior of materials and structures. Extensional modulus, E, relates the normal strain to normal stress and is the "stiffness" of a material undergoing elongation. Shear modulus, G, relates the shear strain to shear stress. The subscripts refer to the coordinate directions and relate each stiffness with its corresponding stress and strain component.

2.2.2.   ASSUMPTIONS AND METHOD OF APPLICATION

TLR materials may be considered homogeneous and orthotropic on the "macro" scale. However, at the "micro" level, there is considerable material variation[*]. While a large number of unit cells may collectively be assumed homogeneous, a single unit cell is not homogeneous. As discussed in section 1.5.2.3, consideration of only macrostresses and macrostrains should be sufficient for the determination of elastic stiffnesses (that is

engineering constants). However, the variation in the microstresses and microstrains within the unit cell must be considered when failure is to be modeled.

The basic approach used in this work was to apply a known macrostress to a finite element model of the unit cell. The deformations of the unit cell boundaries were constrained to meet both unit cell requirements (see section 2.1) and the basic definitions of strain as shown in Figures

Figure 2-3 and Figure 2-4b. The displacements of the unit cell boundaries, or overall change in unit cell dimensions, were then used to determine a macro strain by way of Equation 2-7. Equation 2-7 can thus be written as:

$$\varepsilon_x = \frac{\Delta w_x}{w_x} \qquad \varepsilon_x = \frac{\Delta w_y}{w_y} \qquad \varepsilon_x = \frac{\Delta w_z}{w_z}$$

$$\gamma_{xy} = \frac{\Delta w_x}{w_y} + \frac{\Delta w_y}{w_x} \qquad \gamma_{xz} = \frac{\Delta w_x}{w_z} + \frac{\Delta w_z}{w_x} \qquad \gamma_{yz} = \frac{\Delta w_y}{w_z} + \frac{\Delta w_z}{w_y}$$

Equation 2-8.

where w_x, w_y, and w_z are the dimensions of the unit cell in the x, Y and Z directions respectively. Δw_x, Δw_y, and Δw_z represent the change in those dimensions.

The constitutive relations (Equation 2-7) reduce to one equation and one unknown when only one stress component is non-zero. Hence, by applying six independent cases of loading and respective BC's, each with only one non-zero applied stress component, Equation 2-7 reduces to six equations each with one unknown.

---

* "Macro" and "micro" are relative terms. For the materials in this study, order of magnitude estimates refer to scales of about 1.0 inches and 0.010 inches, respectively.

These same six independent equations can be derived conceptually by applying

Hooke's law (1D) to the unit cell six different times, for the six stress components. These

equations are shown here using the conventional notation associated with engineering

constants.

$$\varepsilon_x = \frac{1}{E_x}\sigma_x \qquad \gamma_{yz} = \frac{1}{G_{yz}}\tau_{yz}$$

$$\varepsilon_y = \frac{1}{E_y}\sigma_y \qquad \gamma_{xz} = \frac{1}{G_{xz}}\tau_{xz}$$

$$\varepsilon_z = \frac{1}{E_z}\sigma_z \qquad \gamma_{xy} = \frac{1}{G_{xy}}\tau_{xy}$$

Equation 2-9.

By applying a known macrostress and calculating the macrostrain from the FEA results,

E_x, E_y, E_z, G_{xy}, G_{xz}, and G_{yz} are determined with the above equations in a straight forward

manner.

For the cases of extensional loading and ensuing boundary conditions, a Poisson

effect is allowed. The Poisson ratios, v_{ij}, are then calculated using:

$$v_{xy} = -\frac{\varepsilon_y}{\varepsilon_x} \qquad v_{xz} = -\frac{\varepsilon_z}{\varepsilon_x} \qquad v_{yz} = -\frac{\varepsilon_z}{\varepsilon_y}$$

Equation 2-10.

Thus, the nine engineering constants of an orthotropic material may be calculated

by applying six separate cases of loads/BC's to a finite element model of a unit cell. These

six cases will hereafter be referred to as the ε_x, ε_y, ε_z, γ_{xy}, γ_{xz}, and γ_{yz} load cases. The

global coordinate system used throughout this work is defined such that the xy plane

corresponds to the plane of the laminate and the Z direction corresponds to the through-thickness or TLR direction.

Even though advantage can be made of some limited commonality among these six load cases, building large detailed FEA models of TLR composite unit cells involves a significant amount of tedious work. As already discussed in section 1.5, when compared to experimental data, simpler techniques can result in reasonable estimations of engineering constants. However, the shear moduli G_{xz} and G_{yz}, are very difficult to obtain experimentally, making verification of any technique questionable for G_{xz} and G_{yz}. In addition to providing predictions of engineering constants, these large FEA models result in complete stress-strain information at the detailed microstructure level. Such information is used to investigate the failure mechanisms of these materials. While it is impractical to use large FEA models to calculate these properties for design purposes, they can be used to gain a fundamental understanding of how the addition of TLR affects laminate mechanical response.

This method of using FEA unit cell models to calculate engineering constants is similar to that described in [152] and [123]. However, in those works a known macrostrain is applied to the unit cell by applying prescribed displacements to the unit cell boundaries. The macrostress is numerically integrated over certain faces, or throughout the unit cell volume. In the method used in this work, a known macrostress is applied, the unit cell is constrained to deform to a certain shape, and the displacements of the unit cell boundaries are used to calculate macrostrains. In effect, this method applies periodic boundary displacements of an unknown value. This method avoids some potential error

arising from the use of the finite element method. In displacement based finite element formulation, the problem is set up such that the displacements are the unknowns. Stress and strain results are then calculated from the displacement results. By measuring the macrostrain by way of the unit cell displacements, rather than the macrostress by way of the unit cell stress results, the added difficulty and inaccuracy of an additional numerical integration are avoided. Since the unit cell is constrained to deform to a certain shape at the boundaries, the difficult problem of how to introduce load is not an issue.

The constraining of the unit cell boundaries was done with the use of multi-point constraints (MPC's). It is assumed that in actual material, the neighboring unit cell would be imposing similar constraints. However, it is reasonable to suspect potential problems with reactions at these heavily constrained boundaries, particularly when the material and geometrical variations of the microstructure are large near the unit cell borders. It is likely that error due to artificial boundary reactions would not play an important role in determination of engineering constants, since these calculations are based only on macrostress and macrostrain. However, if microstress and microstrain distributions internal to the unit cell are to used to draw conclusions about material failure, potential boundary effects must be considered.

2. 3. UNIT CELL BOUNDARY CONDITIONS AND MULTIPOINT CONSTRAINTS

The BC's discussed in this section are for a full unit cell buried inside of the laminate. That is, none of faces of the unit cell are "free." This set of boundary conditions is referred to as [bc-uc], and serves as the baseline set of boundary constraints. Only

translational degrees of freedom are considered, as the element types used in this work

did not have rotational degrees of freedom. In addition to the specific details of BC's and

their application, the limitations of the FEA software and modeling assumptions are

discussed. Section 2.4 discusses variations on this baseline set of BC's.

2. 3.1. GENERAL OVERIVEW

Displacement constraints at the boundaries of the unit cell were carefully selected

in order to 1) satisfy requirements of the unit cell assumption, 2) create unit cell

deformations that conform to basic definitions of strain, and 3) result in a numerically

solvable problem. These three objectives were accomplished by selectively utilizing large

numbers of multi-point constraints (MPC's) and prescribed zero displacements.

Limitations of the commercial FEA analysis software used in this research did not allow

for perfect application of general unit cell assumptions in all cases. However, reasonable

approximations were made, and discussions of the minor exceptions are included in the

following sections. Although some 2-D problems were formulated during the

development of the unit cell procedure and BC's, the following discussions will be

restricted to the full 3-D case, as this is the problem of interest.

The orthogonal hexagonal volume (rectangular parallelepiped) of the 3-D unit cell

has dimensions of wx, wy, and wz, in the X, Y, and Z directions, respectively. The origin

of the global coordinate system is at the center of the unit cell. Each face of the

parallelepiped is perpendicular to the X, Y, or Z axis, and located at a distance of hwx,

hwy, or hwz from the origin (see Figure 2-5). The term hwx refers to the half width of the

unit cell in the X direction and is one half of wx. The terms hwy and hwz are similarly

related to wy and wz. The six faces of the unit cell are labeled 1 through 6, with odd numbers (1,3,5) representing faces at positive axis coordinates, and even numbers (2,4,6) representing faces at negative axis coordinates. Faces 1 and 2 are X axis faces (yz plane). Faces 3 and 4 are Y axis faces (xz pane). Faces 5 and 6 are Z axis faces (xy plane). Laminate orientation relates to the global coordinate system as follows: the Z axis is in the thickness direction, and the X axis is the 0° direction. This nomenclature is used throughout the following discussions.

To analyze the TLR unit cell, detailed 3-D FEA models were required. Creating new FEA analysis code was not within the scope of this work. The objective was to use existing general purpose codes to build and solve the large FEA models. The general purpose commercial FEA package COSMOS/M™, by Structural Research and Analysis Corporation, was utilized for this research. COSMOS/M™ was selected based on several criteria: cost, functionality, ability to run on both personal computers and engineering workstations, and use (acceptance) by other research institutions and industry.

While COSMOS/M™ was a very capable package, certain limitations were encountered. Most popular general purpose codes would likely have similar limitations. For example, only displacement multi-point constraints were available. Boundary nodes could not be constrained to have the same unknown force (stress). As discussed in section 2.1, certain stress components, such as normal surface tractions, would be expected to be continuous across opposite borders of a true unit cell. This type of multi-point constraint was not available in COSMOS/M™.

The general requirement of the unit cell assumption is that the spatial relationship between nodes on a face also apply to the nodes on the opposing face, both before and after deformation. This requirement could not be programmed directly, but was met by careful selection and application of MPC's within the limitations and command structure of COSMOS/M™. COSMOS/M™ command language was used extensively to write programs that would automatically apply the MPC's and other boundary conditions to the unit cell models. As the borders of these large FEA models contained thousands of nodes, the use of such programming capability was the only practical means of applying the BC's described herein.

2. 3.2. NORMAL STRAIN CASES

All three normal strain cases, ε_x, ε_y, and ε_z, shared the same boundary conditions. There were two general requirements for these cases:

1) all nodes on a given face must have the same out-of-plane displacement (that is same displacement perpendicular to the face). The "box" can grow or shrink, but it must maintain its rectangular box shape.

2) each node on a given face, and the corresponding node on the opposing face must have the same in-plane displacements. These two conditions satisfy both unit cell assumptions and the basic definitions of normal strain. To prevent rigid body motion and a singular stiffness matrix, additional prescribed zero displacements were added, as shown Figure 2-6.

The combination of requirement 1 above and the prescribed zero displacements at the corner of faces 1, 4, and 6; results in all nodes on faces 1, 4 and 6 having prescribed

zero displacements perpendicular to their face. Although not intended, faces 1, 4, and 6, thus have BC's that suggest that the faces are each a plane of symmetry. The planes associated with faces 1, 4, and 6 are indeed planes of symmetry for 0° or 90° plies. However, a +45° or - 45° ply is in reality not symmetric, but anti-symmetric at the border of the unit cell. This compromise was necessary and was kept in mind during interpretation of the results. A brief summary of the final BC's are listed in Table 2-1.

Table 2-1 Full unit cell boundary conditions for normal strain load cases.

[bc-uc]	$\varepsilon_X, \varepsilon_Y, \varepsilon_Z$ LOAD CASES	
Displacement Constraint	Boundary Coordinates	Unit Cell Face
$u_x = 0$	$x = +h_{wx}$	face 1
$u_x = $ constant	$x = -h_{wx}$	face 2
$u_y = $ constant	$y = +h_{wy}$	face 3
$u_y = 0$	$y = -h_{wy}$	face 4
$u_z = $ constant	$z = +h_{wz}$	face 5
$u_z = 0$	$z = -h_{wz}$	face 6
$u_y^i = u_y^j, \quad u_z^i = u_z^j$ *	$x = +h_{wx}, \quad x = -h_{wx}$	faces 1, 2
$u_x^k = u_x^l, \quad u_z^k = u_z^l$ **	$y = +h_{wy}, \quad y = -h_{wy}$	faces 3, 4
$u_x^m = u_x^n, \quad u_y^m = u_y^n$ ***	$z = +h_{wz}, \quad z = -h_{wz}$	faces 5, 6

* i and j refer to matching nodes on opposing faces (corresponding y and z coordinates)
** k and l refer to matching nodes on opposing faces (corresponding x and z coordinates)
*** m and n refer to matching nodes on opposing faces (corresponding x and y coordinates)

Since the shape of the unit cell is forced to remain a rectangular box, and one corner is tied or fixed at zero displacement, the displacements of corner node A (see Figure 2-6) represent the overall change in unit cell dimensions, that is the X direction displacement at A corresponds with Δw_x of Equation 2-8. Similarly, the Y and Z direction displacements of node A correspond to Δw_y, and Δw_z. The constraints as just described also make the introduction of a macrostress very simple. Since face 2 is

constrained to have the same X displacement everywhere, an X direction force applied to node A will give the same results as a uniform σ_x applied to face 2. σ_y, and σ_z loads are accomplished similarly by simply applying a force to node A in the appropriate direction.

2.3.3.   XY SHEAR STRAIN

Figure 2-6 shows the basic method of applying the shear strain γ_{xy}. One face was constrained while the opposite face was displaced parallel with its plane, resulting in a shear strain on the unit cell. Prescribed zero displacements were assigned to all nodes on face 4 (fixed in space). All the face 3 nodes were constrained to have the same x, Y and Z displacement (like a rigid plate). Each pair of corresponding nodes on opposing faces 1 and 2 were constrained to have the same x, Y and Z displacements. Each pair of corresponding nodes on opposing faces 5 and 6 were also constrained to have the same X and Y displacements. All nodes on face 5 and 6 were constrained to have the same Z direction displacement. These constraints allowed the box to skew in the X direction while maintaining proper nodal relationships across opposing faces. Careful consideration of these constraints reveals that all nodes at the boundaries are required to have zero Z direction displacement. This fact is consistent with the intent of applying pure xy shear in the macroscopic sense. These BC's are summarized in Table 2-2.

Table 2-2 Full unit cell boundary conditions for xy shear load case.

[bc-uc]	γ_{xy} LOAD CASE	
Displacement Constraint	Boundary Coordinates	Unit Cell Face
$u_z = 0$	$x = \pm hwx, \ y = \pm hwy, \ z = \pm hwz$	faces 1- 6
$u_x = u_y = 0$	$y = -hwy$	face 4
$u_x = $ constant, $u_y = $ constant	$y = +hwy$	face 3
$u_x^{\ i} = u_x^{\ j}, \quad u_y^{\ i} = u_y^{\ j}$ *	$x = +hwx, \quad x = -hwx$	faces 1, 2
$u_x^{\ m} = u_x^{\ n}, \quad u_y^{\ m} = u_y^{\ n}$ **	$z = +hwz, \quad z = -hwz$	faces 5, 6

* i and j refer to matching nodes on opposing faces (corresponding y and z coordinates)
** m and n refer to matching nodes on opposing faces (corresponding x and y coordinates)

As with the normal strain cases, the constraints resulted in the equivalence of the X displacement of node A with Δw_x of Equation 2-8. Similarly, the Y direction displacement corresponded to Δw_y. The shear strain γ_{xy} was then calculated using the displacements of node A. The macro shear stress was accomplished by applying an X direction force to node A. Due to the constraints, application of this single force was equivalent to applying a uniform τ_{xy} on face 3.

2.3.4.   XZ SHEAR STRAIN

Figure 2-6 shows the basic method of applying the shear strain γ_{xz}. One face was constrained while the opposite face was displaced parallel with its plane, resulting in a shear strain on the unit cell. Prescribed zero displacements were assigned to all nodes on face 6 (fixed in space). All the face 5 nodes were constrained to have the same x, Y and Z displacement (like a rigid plate). Each pair of corresponding nodes on opposing faces 1 and 2 were constrained to have the same x, Y and Z displacements. Each pair of corresponding nodes on opposing faces 3 and 4 were also constrained to have the same X and Z displacements. All nodes on face 1 and 2 were constrained to have the same Y

direction displacement. These constraints allowed the box to skew in the X direction while maintaining proper nodal relationships across opposing faces. Careful consideration of these constraints reveals that all nodes at the boundaries are required to have zero Y direction displacement. This fact is consistent with the intent of applying pure xz shear in the macroscopic sense. These BC's are summarized in Table 2-3.

Table 2-3 Full unit cell boundary conditions for xz shear load case.

[bc-uc]	γ_{xz} LOAD CASE	
Displacement Constraint	Boundary Coordinates	Unit Cell Face
$u_y = 0$	$x = \pm hwx,\ y = \pm hwy,\ z = \pm hwz$	faces 1- 6
$u_x = u_z = 0$	$z = -hwz$	face 6
$u_x = $ constant, $u_z = $ constant	$z = +hwz$	face 5
$u_x^i = u_x^j,\quad u_z^i = u_z^j$ *	$x = +hwx,\quad x = -hwx$	faces 1, 2
$u_x^k = u_x^l,\quad u_z^k = u_z^l$ **	$y = +hwy,\quad y = -hwy$	faces 3, 4

* i and j refer to matching nodes on opposing faces (corresponding y and z coordinates)
** k and l refer to matching nodes on opposing faces (corresponding x and z coordinates)

As with the normal strain cases, the constraints resulted in the equivalence of the X displacement of node A with Δw_x of Equation 2-8. Similarly, the Z direction displacement corresponded to Δw_z. The shear strain γ_{xz} was then calculated using the displacements of node A. The macro shear stress was accomplished by applying a Y direction force to node A. Due to the constraints, application of this single force was equivalent to applying a uniform τ_{xz}.

2.3.5. YZ SHEAR STRAIN

Figure 2-6 shows the basic method of applying the shear strain γ_{yz}. One face was constrained while the opposite face was displaced parallel with its plane, resulting in a shear strain on the unit cell. Prescribed zero displacements were assigned to all nodes on

face 6 (fixed in space). All the face 5 nodes were constrained to have the same x, Y and Z

displacement (like a rigid plate). Each pair of corresponding nodes on opposing faces 3

and 4 were constrained to have the same x, Y and Z displacements. Each pair of

corresponding nodes on opposing faces 1 and 2 were also constrained to have the same Y

and Z displacements. All nodes on face 1 and 2 were constrained to have the same X

direction displacement. These constraints allowed the box to skew in the Y direction

while maintaining proper nodal relationships across opposing faces. Careful consideration

of these constraints reveals that all nodes at the boundaries are required to have zero X

direction displacement. This fact is consistent with the intent of applying pure yz shear in

the macroscopic sense. These BC's are summarized in Table 2-4.

Table 2-4 Full unit cell boundary conditions for yz shear load case.

[bc-uc]	γ_{yz} LOAD CASE	
Displacement Constraint	Boundary Coordinates	Unit Cell Face
$u_x = 0$	x = ±hwx, y = ±hwy, z = ±hwz	faces 1- 6
$u_y = u_z = 0$	z = -hwz	face 6
u_y = constant, u_z = constant	z = +hwz	face 5
$u_y^i = u_y^j, \quad u_z^i = u_z^j$ [*]	x = +hwx, x = -hwx	faces 1, 2
$u_y^k = u_y^l, \quad u_z^k = u_z^l$ [**]	y = +hwy, y = -hwy	faces 3, 4

[*] i and j refer to matching nodes on opposing faces (corresponding y and z coordinates)

[**] k and l refer to matching nodes on opposing faces (corresponding x and z coordinates)

As with the normal strain cases, the constraints resulted in the equivalence of the X

displacement of node A with Δw_y of Equation 2-8. Similarly, the Z direction displacement

corresponded to Δw_z. The shear strain γ_{yz} was then calculated using the displacements of

node A. The macro shear stress was accomplished by applying a Y direction force to

node A. Due to the constraints, application of this single force was equivalent to applying a uniform τ_{yz}.

2. 4.   OTHER SETS OF BOUNDARY CONDITIONS

Large numbers of MPC's were utilized to meet the requirements. COSMOS/M™ 1.75a has a limit of 3000 MPC's, which restricted the size and mesh density of the unit cell models. In order to get around this restriction, and to examine cases where full unit cell assumptions did not apply, two other sets of boundary conditions were applied to the "unit cell" models.

"Laminate" boundary conditions [bc-lam] were developed which did not enforce unit cell requirements across the top and bottom (faces 5 and 6). These bc's were the same as [bc-uc] described in section 2.3, with the exception that corresponding opposing nodes on faces 5 and 6 were not required to have the same in-plane displacements. Hence faces 5 and 6 were not required to match up internally, relaxing the unit cell requirement in the thickness direction. A unit cell with these conditions simulates a full laminate with the top and bottom faces free, rather than a unit cell buried internal to the laminate. To insure adherence to the definitions of strain, faces 5 and 6 were required to remain flat, that is all Z displacements the same. Only the ε_x, ε_y, ε_z and γ_{xy} load cases were affected by these changes. The γ_{xz} and γ_{yz} load cases were exactly the same as [bc-uc]. The [bc-lam] BC's are summarized in Table 2-5.

A third set of boundary conditions, [bc-noopp], were developed with the idea of possible further relaxation of unit cell requirements. Pairs of corresponding and opposing nodes were not required to match up on any set of opposing faces. These conditions only

enforced the overall shape of the model to conform to the strain definitions, and did not meet the unit cell criteria. These [bc-noopp] were the least stringent of the three sets. The [bc-noopp] boundary conditions are summarized in Table 2-6.

The different boundary conditions, [bc-uc], [bc-lam] and [bc-noopp], were evaluated by application to a set of representative models[*]. These evaluation models were control models without TLR. Both [0/90] and [+45/-45] layups were included in the evaluation. Based on maximum stress values and calculated properties, there was no practical difference between the results of models with [bc-uc] and [bc-lam] BC's. There was also no practical difference between the results of models with [bc-uc] and [bc-noopp] BC's, in the ε_x, ε_y and ε_z load cases. However, in the γ_{xy}, γ_{xz} and γ_{yz} load cases, there were significant differences between the output of models with the baseline [bc-uc] BC's, and models with the [bc-noopp] BC's. In the models with [bc-noopp] BC's and γ_{xy}, γ_{xz} and γ_{yz} load cases, large stress concentrations at the boundaries dominated the results. Once these comparisons were made, it was determined that there were no important differences between [bc-uc] and [bc-lam] BC's. Hence, [bc-lam] BC's were used in all subsequent unit cell models[†].

---

[*] Model details will be discussed in the next chapter.
[†] A master list of all models and their BC's is given in the next chapter.

Table 2-5 "Laminate" boundary conditions.

[bc-lam]	$\varepsilon_X, \varepsilon_Y, \varepsilon_Z$ LOAD CASES	
Displacement Constraint	Boundary Coordinates	Unit Cell Face
$u_x = 0$	$x = +hwx$	face 1
$u_x = $ constant	$x = -hwx$	face 2
$u_y = $ constant	$y = +hwy$	face 3
$u_y = 0$	$y = -hwy$	face 4
$u_z = $ constant	$z = +hwz$	face 5
$u_z = 0$	$z = -hwz$	face 6
$u_y^i = u_y^j, \quad u_z^i = u_z^j$ *	$x = +hwx, \quad x = -hwx$	faces 1, 2
$u_x^k = u_x^l, \quad u_z^k = u_z^l$ **	$y = +hwy, \quad y = -hwy$	faces 3, 4

[bc-lam]	γ_{xy} LOAD CASE	
Displacement Constraint	Boundary Coordinates	Unit Cell Face
$u_z = 0$	$x = \pm hwx, y = \pm hwy, z = \pm hwz$	faces 1- 6
$u_x = u_y = 0$	$y = -hwy$	face 4
$u_x = $ constant, $u_y = $ constant	$y = +hwy$	face 3
$u_x^i = u_x^j, \quad u_y^i = u_y^j$ *	$x = +hwx, \quad x = -hwx$	faces 1, 2

[bc-lam]	γ_{xz} LOAD CASE	
Displacement Constraint	Boundary Coordinates	Unit Cell Face
$u_y = 0$	$x = \pm hwx, y = \pm hwy, z = \pm hwz$	faces 1- 6
$u_x = u_z = 0$	$z = -hwz$	face 6
$u_x = $ constant, $u_z = $ constant	$z = +hwz$	face 5
$u_x^i = u_x^j, \quad u_z^i = u_z^j$ *	$x = +hwx, \quad x = -hwx$	faces 1, 2
$u_x^k = u_x^l, \quad u_z^k = u_z^l$ **	$y = +hwy, \quad y = -hwy$	faces 3, 4

[bc-lam]	γ_{yz} LOAD CASE	
Displacement Constraint	Boundary Coordinates	Unit Cell Face
$u_x = 0$	$x = \pm hwx, y = \pm hwy, z = \pm hwz$	faces 1- 6
$u_y = u_z = 0$	$z = -hwz$	face 6
$u_y = $ constant, $u_z = $ constant	$z = +hwz$	face 5
$u_y^i = u_y^j, \quad u_z^i = u_z^j$ *	$x = +hwx, \quad x = -hwx$	faces 1, 2
$u_y^k = u_y^l, \quad u_z^k = u_z^l$ **	$y = +hwy, \quad y = -hwy$	faces 3, 4

* i and j refer to matching nodes on opposing faces (corresponding y and z coordinates)

** k and l refer to matching nodes on opposing faces (corresponding x and z coordinates)

Table 2-6 "No opposing node constraint" boundary conditions.

[bc-noopp]	$\varepsilon_X, \varepsilon_Y, \varepsilon_Z$ LOAD CASES	
Displacement Constraint	Boundary Coordinates	Unit Cell Face
$u_x = 0$	$x = +hwx$	face 1
$u_x = $ constant	$x = -hwx$	face 2
$u_y = $ constant	$y = +hwy$	face 3
$u_y = 0$	$y = -hwy$	face 4
$u_z = $ constant	$z = +hwz$	face 5
$u_z = 0$	$z = -hwz$	face 6

[bc- noopp]	γ_{xy} LOAD CASE	
Displacement Constraint	Boundary Coordinates	Unit Cell Face
$u_z = 0$	$y = \pm hwy, z = \pm hwz$	faces 3- 6
$u_x = u_y = 0$	$y = -hwy$	face 4
$u_x = $ constant, $u_y = $ constant	$y = +hwy$	face 3

[bc- noopp]	γ_{xz} LOAD CASE	
Displacement Constraint	Boundary Coordinates	Unit Cell Face
$u_y = 0$	$y = \pm hwy, z = \pm hwz$	faces 3- 6
$u_x = u_z = 0$	$z = -hwz$	face 6
$u_x = $ constant, $u_z = $ constant	$z = +hwz$	face 5

[bc- noopp]	γ_{yz} LOAD CASE	
Displacement Constraint	Boundary Coordinates	Unit Cell Face
$u_x = 0$	$x = \pm hwx, z = \pm hwz$	faces 1,2,5, 6
$u_y = u_z = 0$	$z = -hwz$	face 6
$u_y = $ constant, $u_z = $ constant	$z = +hwz$	face 5
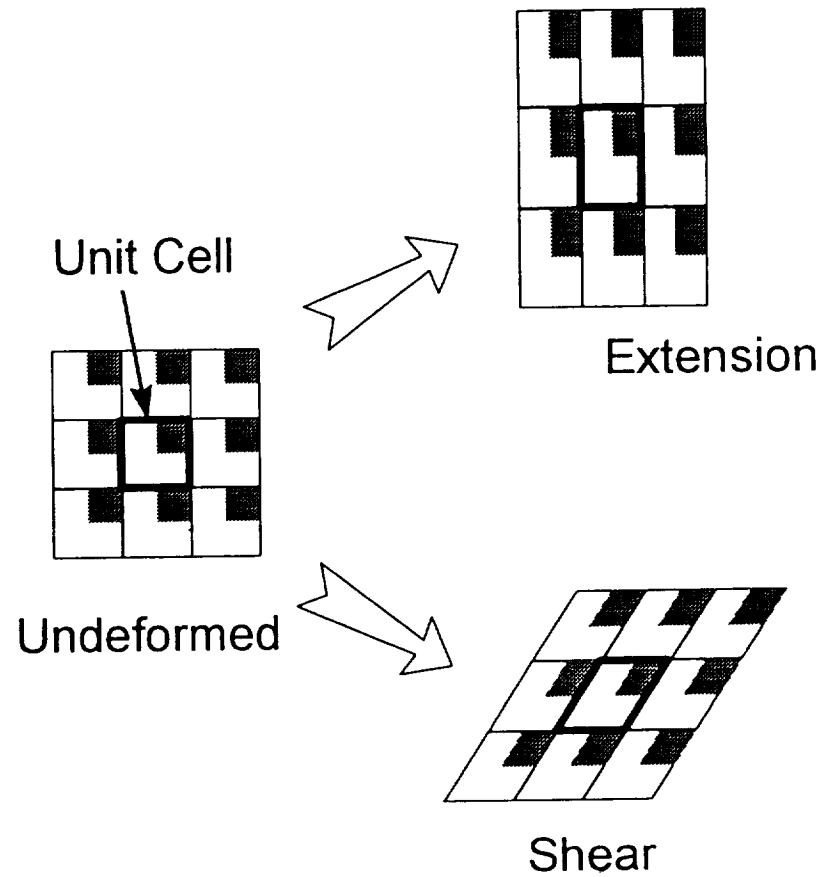
Figure 2-1 Schematic of "Unit Cell" concept showing deformation due to extension and due to shear.
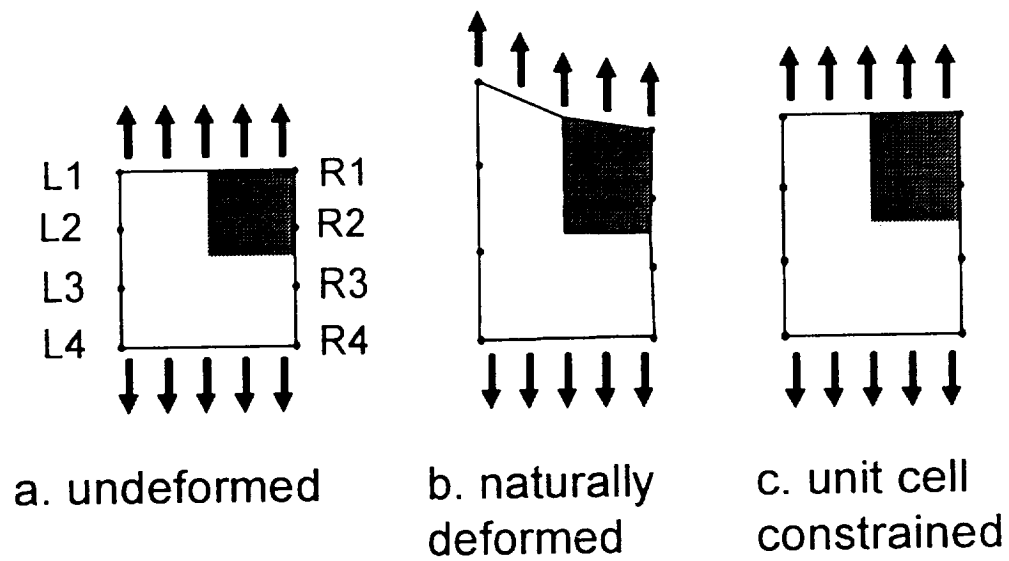
Figure 2-2 Schematic of a unit cell in uniform tension showing the concept of proper unit cell constraints.
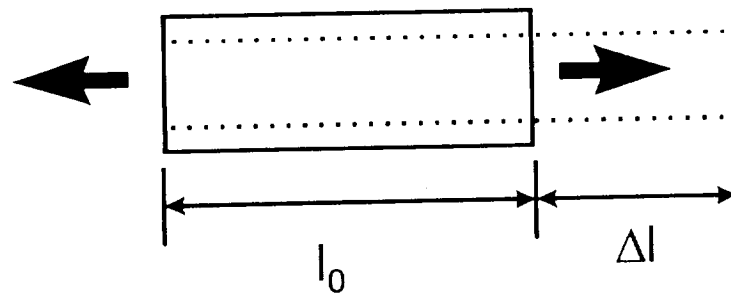
$$\varepsilon = \frac{\Delta l}{l_0}$$

Figure 2-3 Graphical definition of normal strain.

$\gamma = 2\alpha$
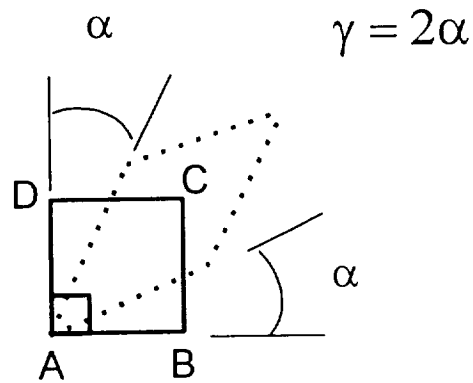
a. Classical definition of shear strain.

$\gamma \sim \tan(\gamma) = \dfrac{\Delta}{w}$
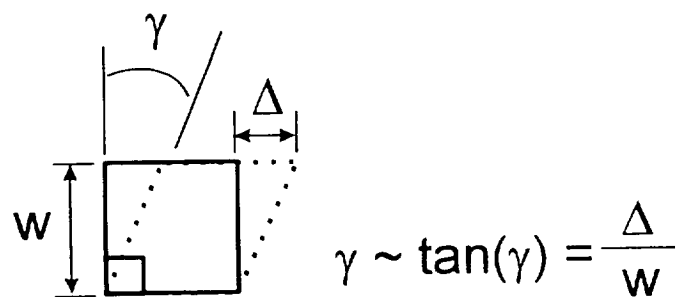
b. Shear strain as applied in this work.

Figure 2-4 Graphical definition of shear strain.
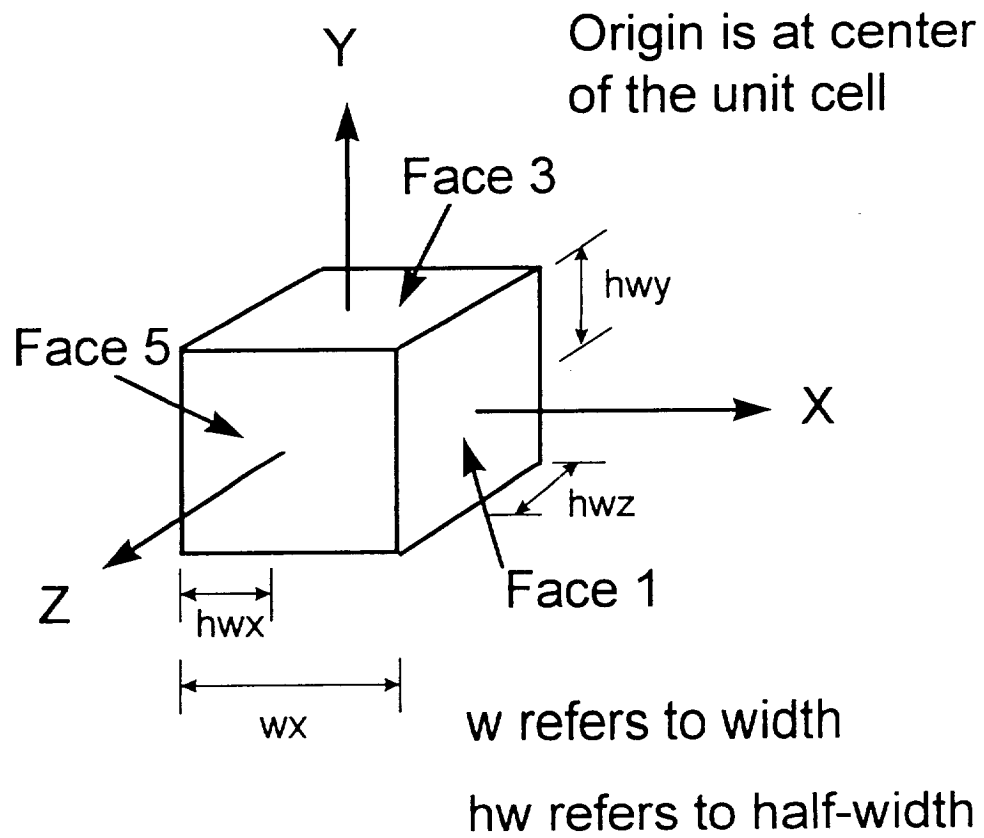
Figure 2-5 Schematic of the unit cell with labeled faces and dimensions.
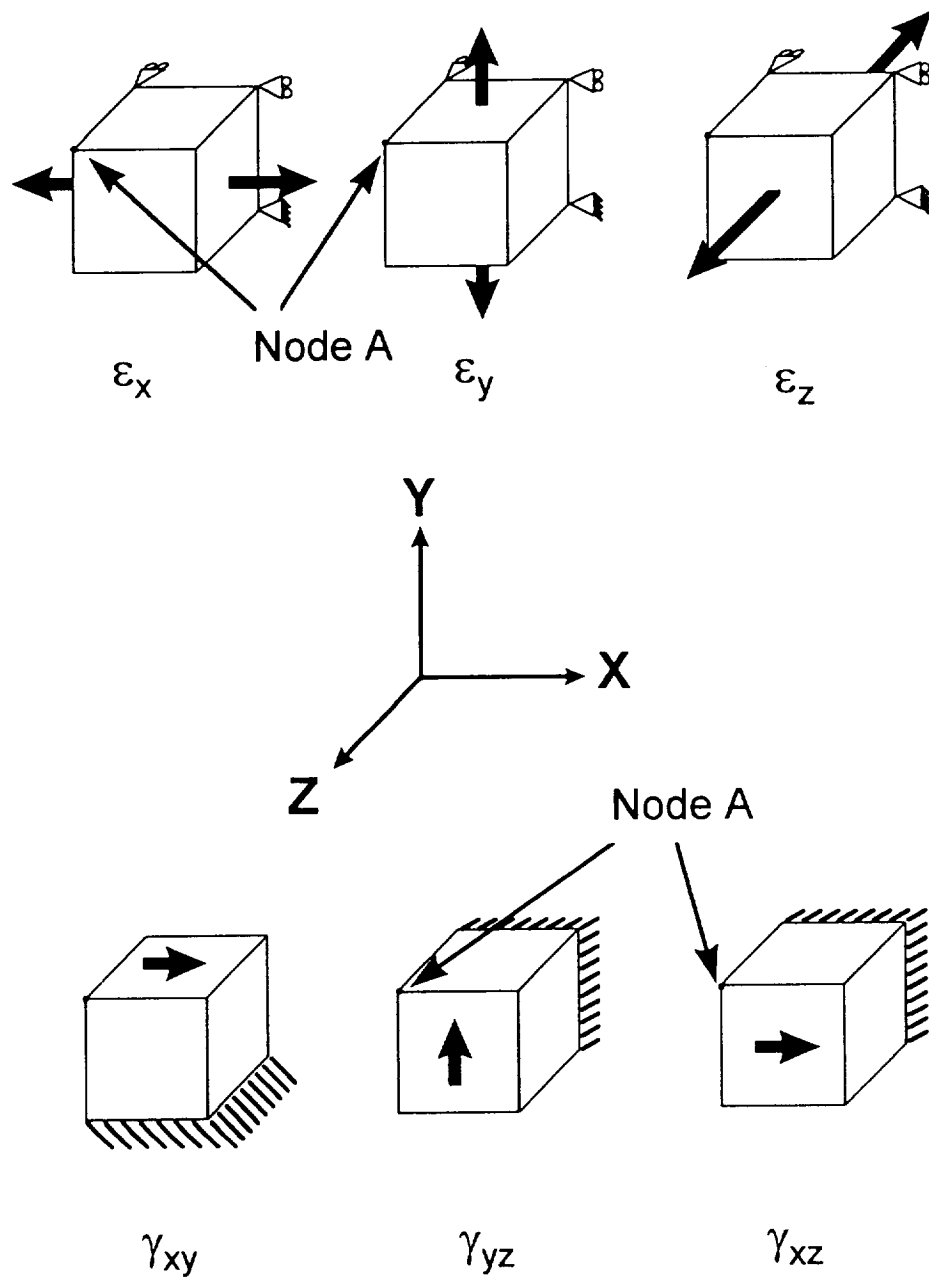
Figure 2-6 Unit cells showing the six load cases corresponding to the six components of strain.

CHAPTER 3
MODELING DETAILS

This chapter describes the various models used for this research. Model geometry and numerical details are discussed for the finite element models. Stiffness averaging and its application by way of the TEXCAD analysis software is also briefly discussed. The final section of this chapter describes the models used for the application of TLR principles to a practical problem.

3. 1. TLR MODEL GEOMETRY

A typical microstructure of TLR materials is shown in Figure 3-1. Shown in the figure points are important microstructural details such as the unavoidable pure resin regions and curved in-plane fibers. A schematic of this microstructure is shown in Figure 3-2. Based on the features shown in Figure 3-2, the fairly simple 2-D model shown in Figure 3-3 was developed.

Here R and d refer to the radius and diameter of the TLR and hW_x and hW_y are the half lengths of the unit cell. The inclusion length and half length, I and hI, refer to the sum of the lengths of the matrix regions and TLR. The TLR was assumed to be cylindrical (circular in the xy plane). The boundary of the resin region was created by drawing a line from the tip of the TLR inclusion to a point tangent to the TLR. The angle θ is the angle made by the intersection of this line with the X axis. When the TLR is inserted into a lamina, the otherwise straight in-plane fibers are pushed aside, creating a region of curved

fibers. This curved fiber region was modeled as shown in Figure 3-2 and Figure 3-3. The width of the curved fiber region was defined by the parameter L1. The material in this curved fiber region was assumed to have fiber oriented in the θ direction. The ratio of the TLR inclusion length to the TLR diameter (l/d) was used as another parameter. Hence, using elementary geometry, both θ and the coordinates of the tangent point can be defined in terms of d and l/d ratio. The parameter L2 was used to define a region of fine mesh in the FEA models (discussed in the next section). Another important variable is the TLR angle through the thickness of the laminate, ψ. The through-thickness angle, ψ, was defined as the angle of the TLR as referenced to a line normal to the laminate plane as shown in Figure 3-4. As can be seen in the schematics in these figures, the entire unit cell can be defined by setting the values for a few simple parameters.

This model does not include the knots or surface loops associated with stitched laminates. For Z-Fiber™ materials, in-plane fiber displacement in the thickness direction were also neglected. Some "fiber-wash" in the Z direction is typically found in Z-Fiber™ materials, and is a result of the insertion process. These simplifications aside, the described model is a reasonable approximation and does capture important microstructural details neglected in other published research. Specifically, the resin regions, curved fiber regions and the TLR through-thickness angle have not previously been modeled at this level of detail, if at all.

3. 2. UNIT CELL FINITE ELEMENT MODELS

The general purpose finite element software, "COSMOS/M™," was used for the FEA analysis performed for this research. The accompanying pre- and post-processor

"Geostar" was used to build and post-process the FEA models. An incremental approach was used, with early efforts involving 2-D plane strain models. The 2-D models were only used to develop the unit cell strategy within COSMOS/M™ since full 3-D models were the objective from the beginning. Only the fully developed 3-D unit cell models are discussed in this report. Model building and analysis was automated as much as possible by writing "scripts," or programs, using the COSMOS/M™ command language.

3.2.1. MODEL GENERATION

The FEA unit cell models were based on the model described in section 3.1. Table 3-1 is a master list of all FEA unit cell models. The unit cell models utilized the eight node "SOLID" element of COSMOS/M™. The SOLID element is a three dimensional "brick" element with three translational degrees of freedom per node. "Prism" or "wedge" shaped elements were judiciously utilized by collapsing one side of the brick. The unit cell models ranged in size from 20,000 to 75,000 degrees of freedom. Typical two ply unit cell models were on the order of 25,000 degrees of freedom. All results reported here in were obtained using a "PC" with a single Intel 200 Mhz Pentium-Pro™ processor and Microsoft Windows NT 4.0. Typical models are shown in Figure 3-5.

Table 3-1 Master list of finite element models and their variable values.

Series Name	TLR Variables					Unit Cell Variables							FE Information		
	Material	d (in.)	Vf (%)	ψ deg	n (/in.²)	Wx (in.)	Wy (in.)	Wz (in.)	l/d	L1	L2	Layup	Nodes	Elements	BC's
c2a	gr/ep	0.025	1.9%	0	38	0.162	0.162	0.012	5	(1/4)d	(1/4)d	[0/90]	7539	8160	[bc-uc]
c2p7a	gr/ep	0.025	1.9%	45	38	0.162	0.162	0.012	5	(1/4)d	(1/4)d	[0/90]	6899	6264	[bc-lam]
c2ap15	gr/ep	0.025	1.9%	15	38	0.162	0.162	0.012	5	(1/4)d	(1/4)d	[0/90]	6899	6264	[bc-lam]
c3a	gr/ep	0.010	1.9%	0	242	0.064	0.064	0.012	5	(1/4)d	(1/4)d	[0/90]	6419	6996	[bc-lam]
c2abig	gr/ep	0.025	1.9%	0	38	0.162	0.162	0.108	5	(1/4)d	(1/4)d	[0/90]9	24975	30576	[bc-lam]
c4a	gr/ep	0.010	0.3%	0	38	0.162	0.162	0.012	5	(1/4)d	(1/4)d	[0/90]	9051	9390	[bc-lam]
c5a	gr/ep	0.025	4.9%	0	100	0.100	0.100	0.012	3.5	(1/4)d	(1/8)d	[0/90]	10136	10332	[bc-lam]
c2b	gr/ep	0.025	1.9%	0	38	0.162	0.162	0.012	5	(1/4)d	(1/4)d	[+45/-45]	7539	8160	[bc-uc]
c2c	gr/ep	0.025	1.9%	0	38	0.162	0.162	0.012	5	(1/4)d	(1/4)d	[0/0]	7539	8160	[bc-uc]
c2quasi	gr/ep	0.025	1.9%	0	38	0.162	0.162	0.024	5	(1/4)d	(1/4)d	[+45/0/-45/90]	12025	14112	[bc-lam]
c2a-kev	kevlar	0.025	1.9%	0	38	0.162	0.162	0.012	5	(1/4)d	(1/4)d	[0/90]	7539	8160	[bc-lam]
c2a-ti	titanium	0.025	1.9%	0	38	0.162	0.162	0.012	5	(1/4)d	(1/4)d	[0/90]	7539	8160	[bc-lam]
c2a-steel	steel	0.025	1.9%	0	38	0.162	0.162	0.012	5	(1/4)d	(1/4)d	[0/90]	7539	8160	[bc-lam]
c2a-sfm	gr/ep	0.025	1.9%	0	38	0.162	0.162	0.012	5	(1/4)d	(1/4)d	[0/90]	7539	8160	[bc-lam]
c2a-dhm	gr/ep	0.025	1.9%	0	38	0.162	0.162	0.012	5	(1/4)d	(1/4)d	[0/90]	7539	8160	[bc-lam]
c2a-lam	gr/ep	0.025	1.9%	0	38	0.162	0.162	0.012	5	(1/4)d	(1/4)d	[0/90]	7539	8160	[bc-lam]
c2a-noop	gr/ep	0.025	1.9%	0	38	0.162	0.162	0.012	5	(1/4)d	(1/4)d	[0/90]	7539	8160	[bc-noop]
c2b-noop	gr/ep	0.025	1.9%	0	38	0.162	0.162	0.012	5	(1/4)d	(1/4)d	[+45/-45]	7539	8160	[bc-noop]

One of the greatest difficulties in building the 3-D multi-ply FEA models was maintaining mesh compatibility across the interface between plies of different orientation. The first step in the model building procedure was to create a 2-D geometric model of the schematic shown in Figure 3-2. This unidirectional geometry was then duplicated and rotated to produce a star-like geometry that could be utilized for a 0°, 90°, +45° or -45° oriented ply (see Figure 3-6). This "star" model approach is very similar to the "flower pedal" model originally proposed by Dr. Gary Farley, and utilized in a limited fashion in [144]. A less detailed but similar approach was also used and reported in [106] and [107].

Utilizing symmetry, 1/8th of the geometry shown in Figure 3-6 was meshed using a combination of automatic meshing and manual mesh manipulation. This 1/8th pie slice was then replicated and rotated to produce a meshed version of Figure 3-6. Scripts were written to keep track of and apply the correct material properties and material directions for each of the 209 different regions shown in Figure 3-6. A different script was developed for each ply orientation; 0°, 90°, +45° and -45°. Three different materials (unidirectional lamina, TLR and pure matrix) and 13 different material directions (z direction, 0°, 90°, +45°, -45°, and a ±θ for each 0°, 90°, +45°, -45°) were necessary to characterize the four ply orientations. Typical graphite-epoxy and neat epoxy resin properties were used. Graphite-epoxy, Kevlar®-epoxy, titanium and steel were used as TLR materials. The material properties are listed in Table 3-2. A micro-mechanics analysis described in [153, 154] was used to generate the properties for composites listed in the table. The inputs for the micro-mechanics analysis were taken from manufacturers product information sheets and from references [153, 155]. The properties for titanium

and steel were obtained from a built in material library within the COSMOS/M™

software.

Table 3-2 Material input properties for unit cell models.

	LAMINA	TLR	TLR	TLR	TLR	PURE RESIN
	AS4/3501-6	Kevlar/3501-6	T300/9310	Titanium	STEEL	3501-6
E_1 (Msi)	19.4	5.6	20.5	16.0	30.0	0.632
E_2 (Msi)	1.26	1.30	1.04	-	-	-
E_3 (Msi)	1.26	1.30	1.04	-	-	-
G_{12} (Msi)	0.847	0.790	0.634	6.3	12.0	0.235
G_{23} (Msi)	0.457	0.765	0.378	-	-	-
G_{13} (Msi)	0.847	0.790	0.634	-	-	-
ν_{12}	0.25	0.31	0.25	0.30	0.28	0.34
ν_{23}	0.38	0.39	0.39	-	-	-
ν_{13}	0.25	0.31	0.25	-	-	-
V_f	0.60	0.60	0.60	-	-	-

Once a full 2-D (xy) mesh was created and given the appropriate properties, the elements were "extruded" in the Z direction to create 3-D elements with the correct properties. Since the same FEA mesh was used to create the different plies, mesh compatibility was maintained when plies of different orientation were stacked. Models with a non-zero TLR through-thickness angle, ψ, were created by extruding the 2-D geometry/mesh at an angle and manually meshing the empty areas of the rectangular unit cell box. All elements created by extrusion at an angle were inherently skewed. However, concern over severe error induced by misshapen elements was alleviated with straight forward model verification procedures discussed in the next section. Extrusion of the 2-D circular TLR perpendicular to the xy plane ($\psi=0$) resulted in a cylindrical TLR. Extrusion at an angle ($\psi\neq0$) maintained a circular cross-section on the xy plane, but created a TLR with an elliptical cross-section when viewed along the TLR longitudinal axis. Given that the cross-section can vary significantly in actual TLR materials, this variation was not considered significant as long as proper volume fractions were utilized in the interpretations of the results.

Once the 3-D mesh of the model was completed, scripts were used to locate and identify boundary nodes; and to apply displacement constraints, multi-point constraints, and loads for each of the six strain cases (see Chapter 2).

3.2.2. MODEL VERIFICATION

The built in check routines of COSMOS/M™ were consistently used to interrogate the quality of the FEA models. These commands and routines often proved grossly inadequate at identifying troubled areas of these very complex and detailed models.

Therefore other practical measures were also used to evaluate the quality of the models. Engineering judgment was used extensively in the trade off of model complexity and size versus accuracy and convergence.

To have some feeling for the validity of the unit cell modeling assumptions and the quality of the FEA models, control models were constructed and evaluated. Control models were made by copying an existing TLR model and changing the material properties and materials directions so that the model simulated an unreinforced laminate, that is without TLR and its ensuing microstructure. For the uniformly applied loads described in Chapter 2, the resulting stress should be uniform throughout the control models. Many poorly constructed models with misshaped elements were identified with this technique. Control cases were run for each of the six different load cases, thereby checking the elements for all six stress components.

In addition to validating the quality of the FEA mesh, the method of calculating engineering constants was also validated. The stiffnesses were calculated for the control cases of a unidirectional laminate, a two layer model with a [0/0] layup. These calculated values exactly matched the material input properties, within adequate precision. In addition to model validation, the control models were used extensively as a control to determine the effects of the addition of TLR.

3. 3.   STIFFNESS AVERAGING MODEL (TEXCAD)

As was discussed in section 1.5, simple stiffness averaging methods can be used to predict the fiber dominated macroscopic elastic constants reasonably well. Isostrain is assumed across the entire unit cell. A unit cell is composed of N discrete unidirectional

segments, each with a known volume fractions, V, and stiffness, $[C]$. The average

stiffness of this unit cell can be calculated by transforming each segments stiffness to

global coordinates, and summing the fractional contribution of all segments:

$$[C]^{avg.} = \sum_{m=1}^{N} \left(V_m [T]_m^T [C]_m [T]_m \right)$$

Equation 3-1.

$[T]$, and its transpose, $[T]^T$, are the well know stress transformation matrices of tensor

algebra (see for example [150]).

The limitations and application of stiffness averaging concepts, and other textile

modeling techniques, are discussed in more detail in [123]. The publicly available software

"TEXCAD," (Textile Composite Analysis for Design) was used to perform the stiffness

averaging for the TLR materials in this work. TEXCAD is described in references [138,

139, 155] and is included in the review found in [123]. TEXCAD was developed to run on

a desktop computer with sufficient ease of use to enable effective utilization as a design

tool. For these reasons, stiffness averaging by way of TEXCAD was selected for

comparison with the FEA unit cell approach described in Chapter 2.

3. 4. FLANGE-SKIN MODEL

The problem of a flanged skin in bending was selected as the problem of practical

interest for this study.   It is a problem having high inter-laminar stresses and whose failure

modes are dominated by the response to those stresses. In reference [156], the authors

proposed this problem as a simplified test of the bond strength between a skin and a

secondarily bonded or co-cured stiffener when the dominant loading in the skin is bending

along the edge of the stiffener. An illustration of the stiffener-skin interface is shown in

Figure 3-7. The test is performed by putting a flanged skin specimen in three or

four point bending, as shown in

Figure 3-8 and Figure 3-9. The flange-skin specimen is a representation of a larger

stiffened skin structure. This simple and relatively inexpensive test captures the same

failure mechanisms as in the larger structure. In addition to being a problem that could be

modeled in some detail with a reasonable computational effort, the experimental portion of

the study reported in [156] involved detailed observations of specimen failure.

A two dimensional generalized plane strain model was used to model the flanged

skin in reference [156]. Due to the three dimensional nature of TLR, the flange-skin

problem was modeled in three dimensions in this work.

The specimen with a 20° tapered flange, shown in

Figure 3-8, was modeled with the twenty node "SOLID" element of

COSMOS/M™. The SOLID element is a three dimensional "brick" element with three

translational degrees of freedom per node. "Prism" or "wedge" shaped elements were

judiciously used by collapsing one side of the brick. Quasi-isotropic layups, [45/0/-

45/90]$_{6s}$, of AS4-3501-6 graphite-epoxy lamina were used in both the flange and skin. As

was the case in the unit cell models, each ply was 0.006 inches thick. The dimensions of

the specimen are shown in

Figure 3-8. The width of the specimen was carefully selected so that at least one

unit cell could be fully represented across the width in the Y direction. The edges of the

specimen, the XZ planes at the maximum and minimum Y coordinates, were constrained

to have zero Y direction displacements, thus placing the model in plane strain. The finite

element mesh for this problem is shown in Figure 3-10. As failure has been shown to

begin near the tip of the flange, only the region near the flange tip was modeled with a fine

mesh. In the fine mesh region extended four plies into the flange and four plies into the

skin, with each ply and each TLR modeled by separate elements with the proper material

properties. The coarse mesh region was modeled with smeared properties of a quasi-

isotropic laminate composed of AS4-3501-6 lamina, with and without TLR. Input

material properties are listed in Table 3-3. Symmetric boundary conditions were used at

the specimen centerline so that only half of the specimen was actually modeled. Boundary

conditions representing three point bending were applied as shown in Figure 3-10 and a

force of 4.36 lbs was applied to each node across the width at the centerline of the

specimen.

**Table 3-3 Material input properties for the coarse mesh region of the
flange-skin FEA model.**

"Smeared" Properties for Quasi-Isotropic Laminates with and without 2% TLR Gr-Ep Lamina (AS4-3501-6)			
	No TLR	Graphit/Epoxy	Steel
E_x (Msi)	7.58	7.07	7.72
E_y (Msi)	7.58	7.06	7.72
E_z (Msi)	1.43	1.76	2.04
G_{xy} (Msi)	2.937	2.71	2.99
G_{yz} (Msi)	0.651	0.582	0.846
G_{xz} (Msi)	0.651	0.584	0.846
ν_{xy}	0.29	0.30	0.29
ν_{yz}	0.26	0.29	0.27
ν_{xz}	0.26	0.21	0.27

Four different versions of this basic model were analyzed. A control model

without TLR, and three models with TLR throughout the specimen. The control model

without TLR is shown in Figure 3-10. This baseline model was duplicated and TLR was

added by changing the material properties for certain elements in the fine mesh region, and

changing the properties for all the elements in the coarse mesh region. Three variations

were examined: a graphite-epoxy TLR with a diameter of 0.025 inches, a graphite-epoxy

TLR with a diameter of 0.008 inches, and a steel TLR with a diameter of 0.008 inches.

The volume fraction of the TLR was two percent in all three cases. The material input

properties for the TLR were the same as those used for unit cell models and are listed in

Table 3-2. The properties used for the coarse mesh were "smeared" by calculating the

laminate properties with the TEXCAD software discussed in the previous section. These

"smeared" properties for a quasi-isotropic laminate with and without TLR are listed in

Table 3-3. The FEA mesh for the stiffener-skin models with TLR is shown in Figure 3-11.

The primary objective of this modeling effort was to examine the effect of the TLR

on the material in regions in between the TLR. Considering the limitation of available

computational resources, a careful study of the results of the unit cell analyses was used to

determined that the modeling objectives could be met by neglecting the microstructural

features of pure resin regions and curved fibers next to the TLR. The shape of the TLR

was also approximated to be a square. Correct proportions and properties for the TLR

and lamina materials were maintained, thereby resulting in the proper structural response

being translated to the regions between the TLR. After several iterations, a uniform three

dimensional grid was selected with the elements being 0.0082 inches square and 0.006

inches thick with an aspect ratio of 1.4. These element dimensions allowed the individual

lamina to be modeled separately and the different diameter TLR to be modeled with an

integer multiple of the basic element size. Thus the same element grid was used in all four

variations of the flange-skin model. Figure 3-12 is a close-up view of these elements with

the different material properties being shown. Even with these approximations, the final

model contained 6,804 elements and 32,818 nodes.

The "bond" feature of COSMOS/M was used to join the fine mesh region to the

coarse mesh of the rest of the model. This bonding of surfaces consisted of using multi-

point constraints to tie together the displacements of nodes associated with the adjoining

faces. The disparity between the element size of the fine mesh and that of the coarse mesh

was too large for this method to work very accurately. Hence, error was introduced in the

areas that were bonded. This error appeared in the stress results as severe stress

concentrations at the "bonded" points. Another limitation of these models was the general

refinement of the finite element mesh. The fine mesh was not small enough to accurately

capture the severe stress gradients in and near the TLR. The regions of interest were four plies away from the "bond" points and the stress gradients between the TLR were much less severe than those within the TLR. For these reasons, it was felt that these models were adequate for addressing the question of damage initiation in the regions between the individual TLR at the interface between the skin and flange.
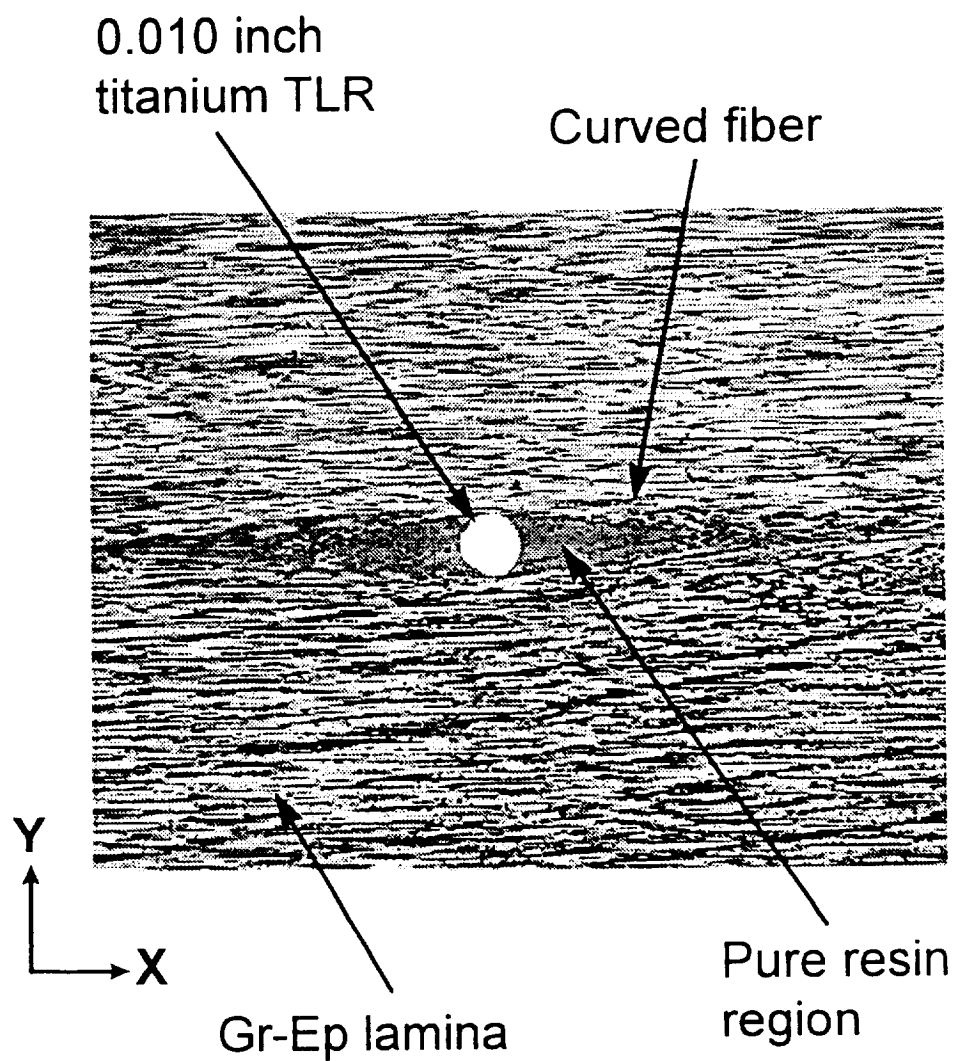
Figure 3-1 Micrograph showing curved fibers and pure resin regions of a graphite-epoxy laminate with a titanium TLR. Z-Fiber™ sample courtesy of Foster-Miller Inc. and Aztex Inc.
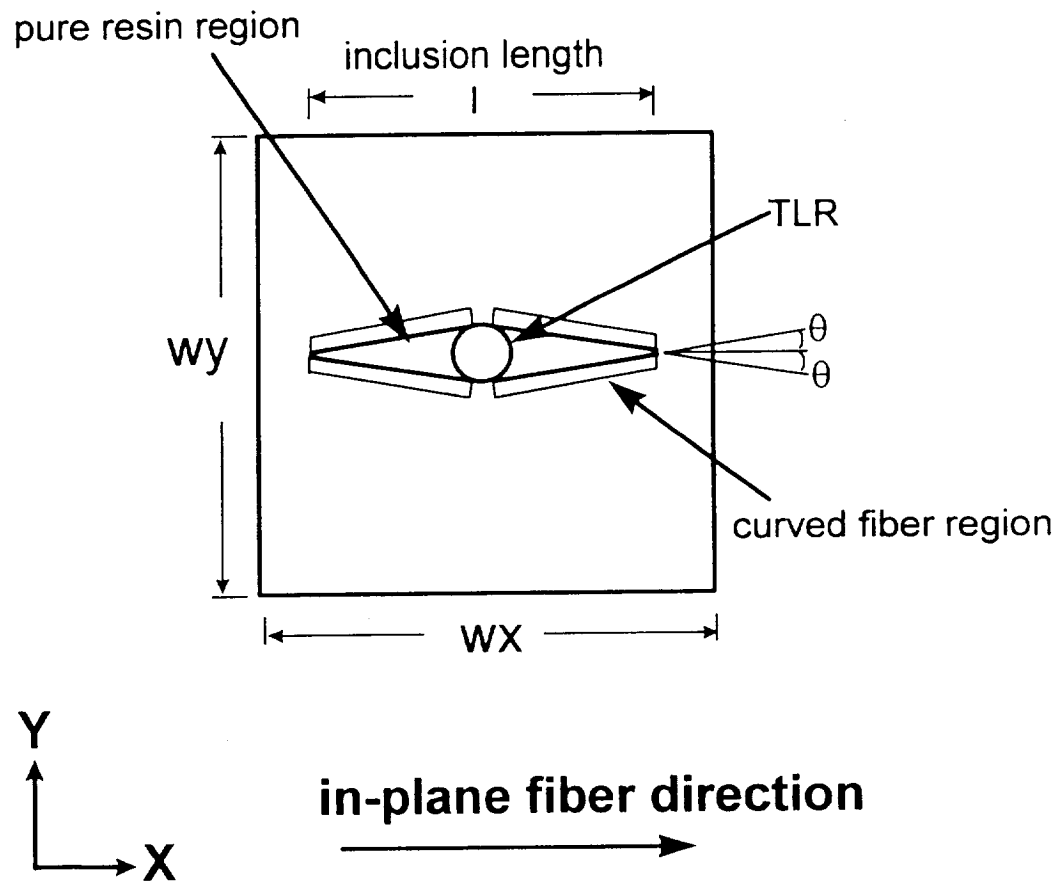
Figure 3-2 Schematic of TLR microstructure showing curved fiber and pure resin regions.
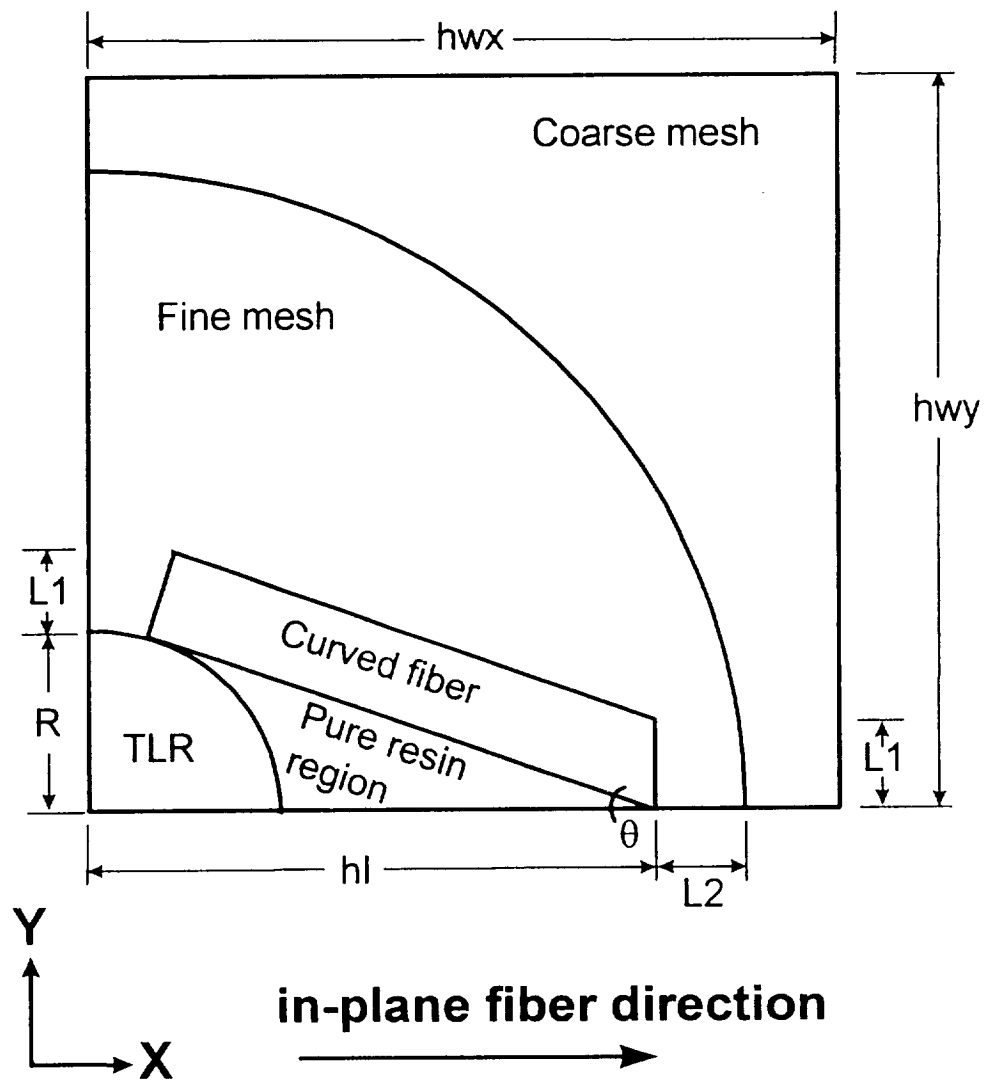
Figure 3-3 Schematic of ¼ model of TLR lamina with all necessary dimensions and parameters labeled.
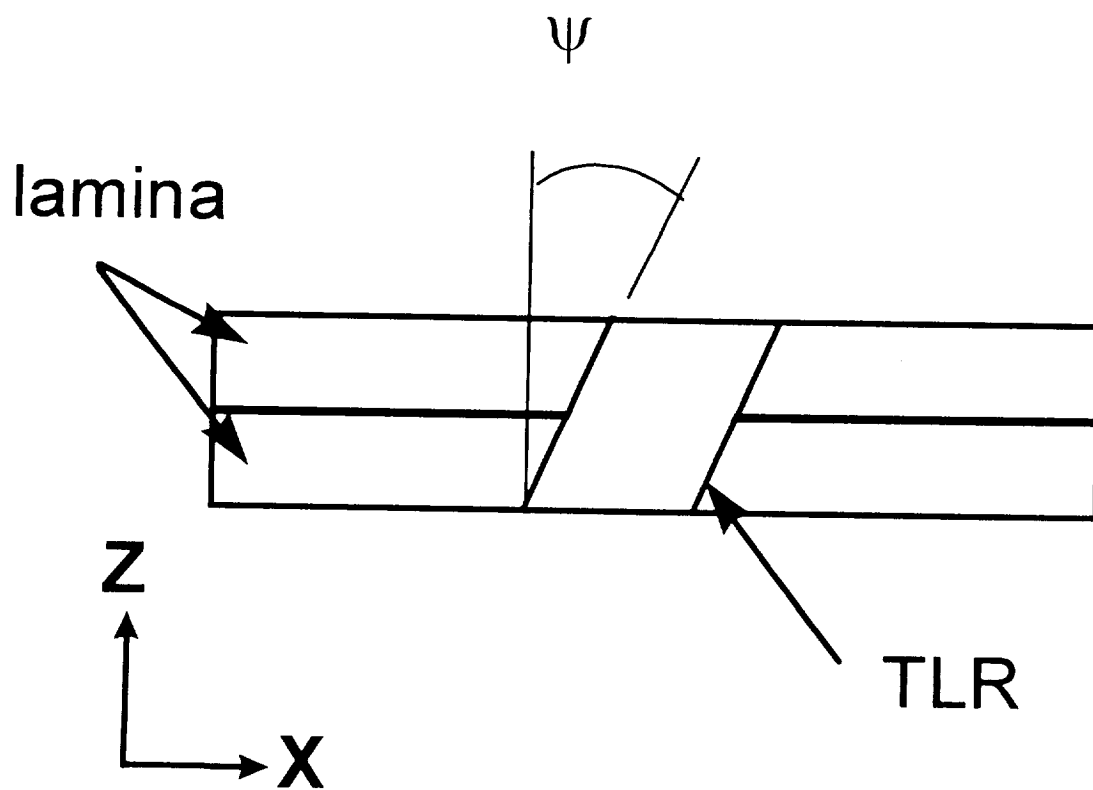
Figure 3-4 Definition of TLR through-thickness angle ψ.

Z **Y** **X**

TLR

pure resin regions
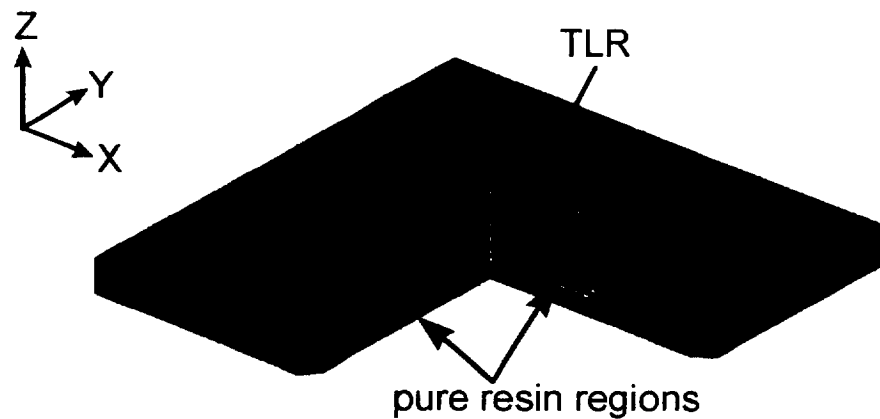
[0/90] two ply unit cell model color coded
for material properties (1/4 cut away)

curved fiber

Z **Y** **X**

zero degree ply

TLR at ψ = 45 degrees

90 degree ply
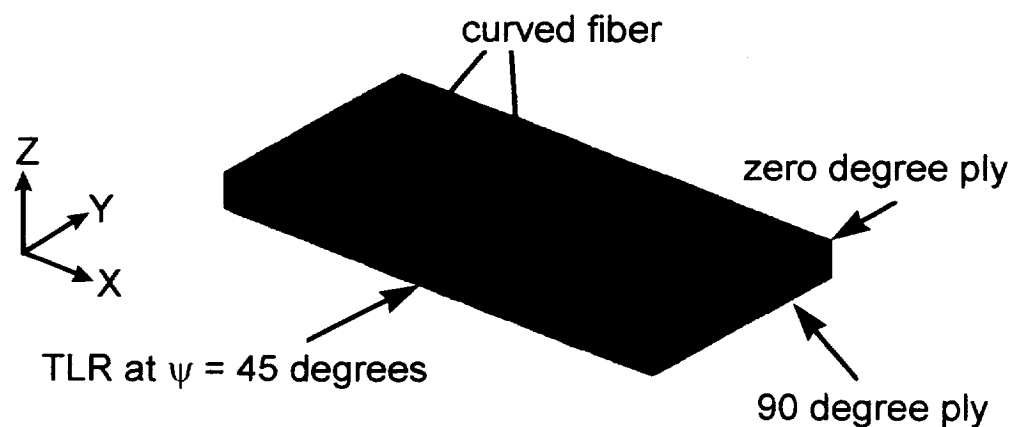
[0/90] two ply unit cell model color coded
for material direction (1/2 cut away)

**Figure 3-5 Typical finite element unit cell models with the element color
coded for material properties (above) and for material directions.**
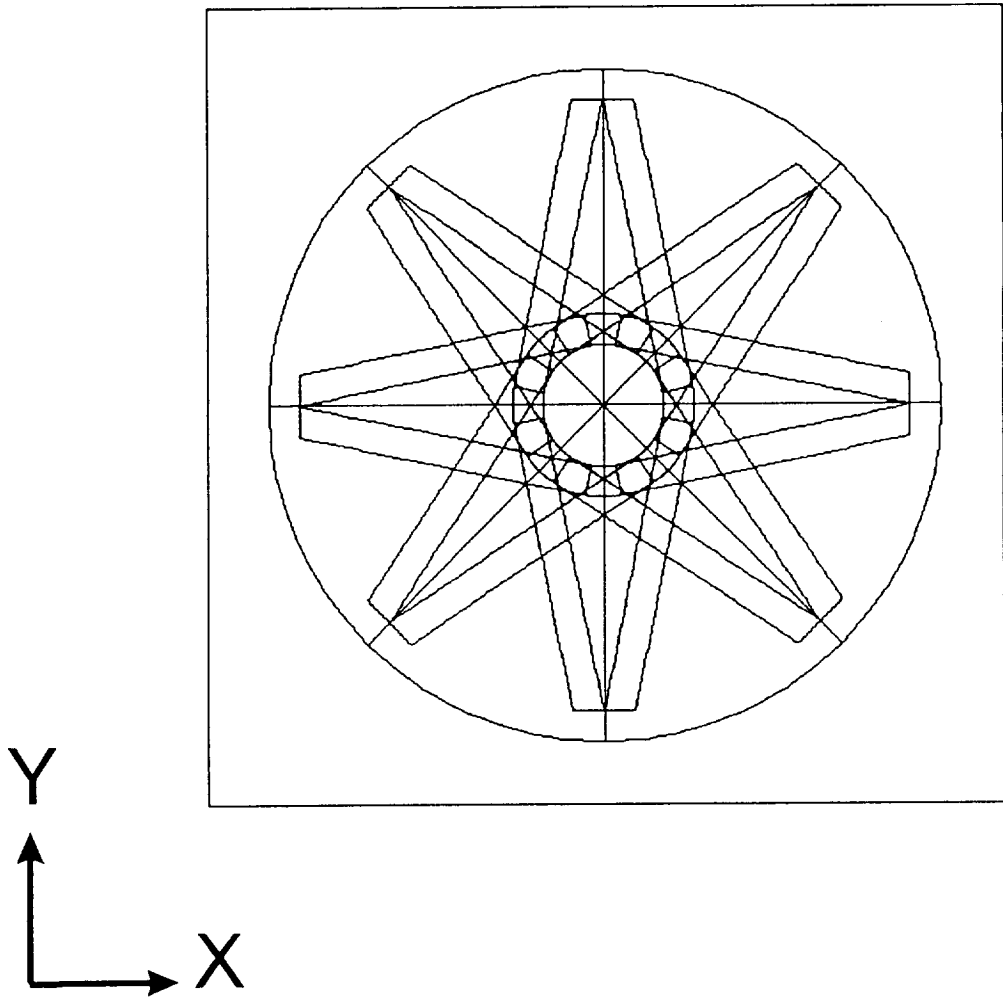
Figure 3-6 2-D geometry unit cell geometry.
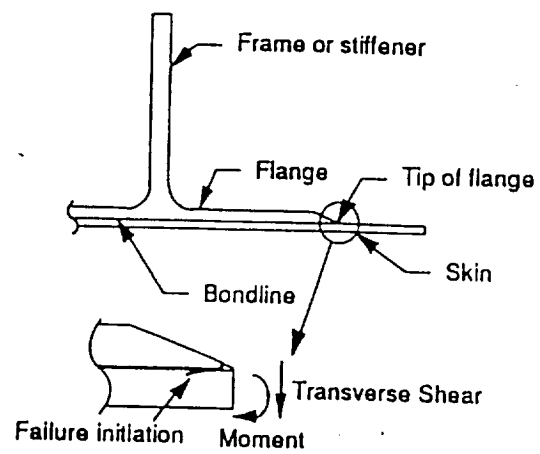
Figure 3-7 Illustration of stiffener-skin interface [156].
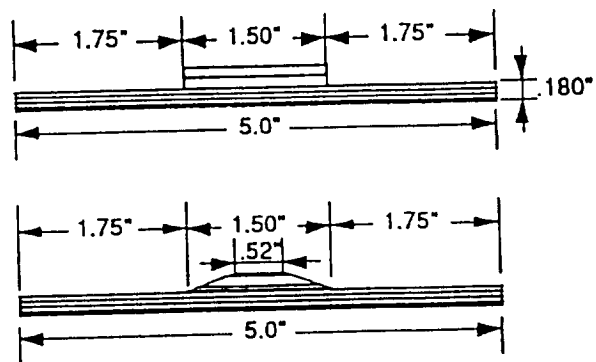
Figure 3-8 Proposed flange-skin test specimens for simulation of the stiffener-skin disbond problem in a stiffener pull-off test [156].
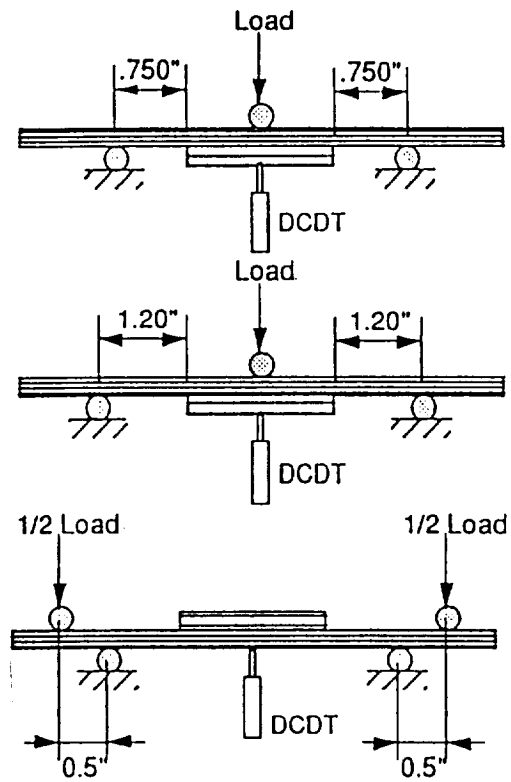
Figure 3-9 Bending test configurations for flange-skin test [156].
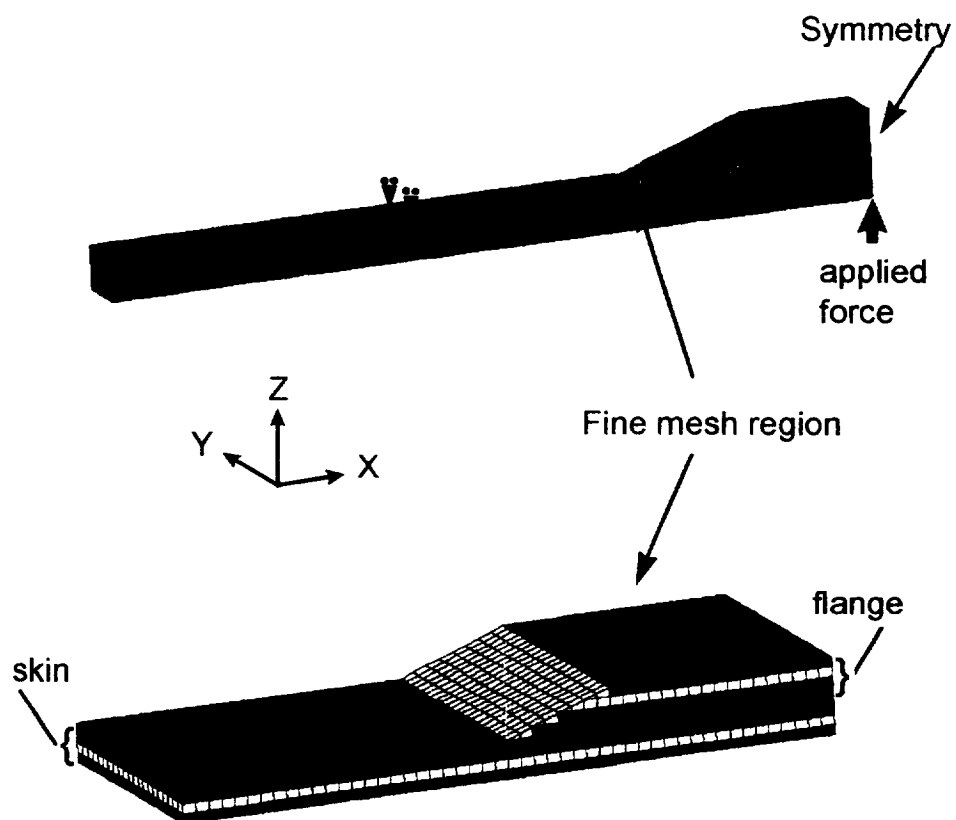
Figure 3-10 Finite element model of the flange-skin specimen without TLR.
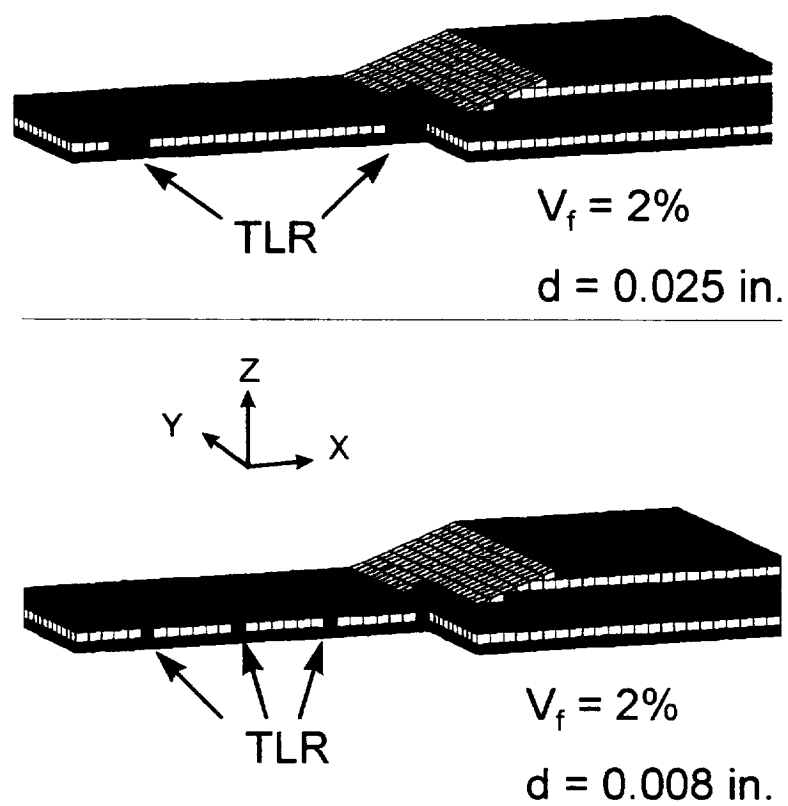
Figure 3-11 Fine mesh regions of flange-skin FEA models with TLR.
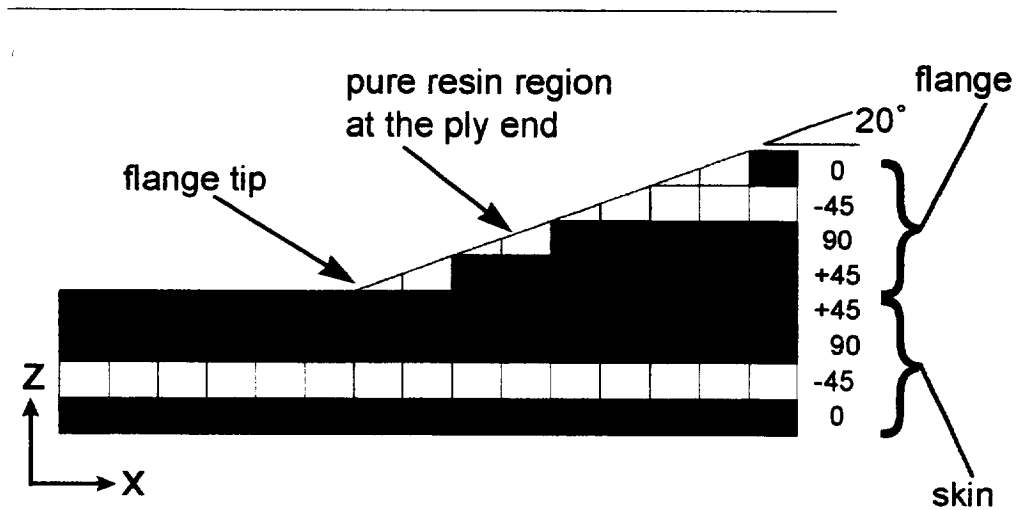
Figure 3-12 Details of the fine element mesh for the flange-skin model.

CHAPTER 4
ELASTIC PROPERTIES - STIFFNESS

The nine independent engineering constants, E_x, E_y, E_z, G_{xy}, G_{xz}, G_{yz}, v_{xy}, v_{xz}, and v_{yz}, completely define the stiffness of an orthotropic material. As noted in Chapter 2, a TLR material is not orthotropic in the strictest sense. However, in the macroscopic sense the assumption is a reasonable one. The engineering constants are used for a physical interpretation of the elastic behavior of materials and structures. Extensional modulus, E, relates the normal strain to normal stress and is the "stiffness" of a material undergoing elongation. Shear modulus, G, relates the shear strain to shear stress. The Poisson's ratio, v, refers to the lateral contraction of a material under a uni-directional extensional loading. The subscripts refer to the coordinate directions and relate each stiffness with its corresponding stress and strain component.

These nine engineering constants were calculated by using two methods: 1) a stiffness averaging technique using TEXCAD analysis software, and 2) a unit cell analysis using FEA. The results of these analyses are listed in Table 4-1 through Table 4-3. The focus of the following discussions will be on the extension and shear moduli, E's and G's, which have physical meaning that can be grasped fairly easily. This chapter begins by discussing the results for the control cases without TLR, followed by discussions of the effects of various important TLR parameters. The chapter closes with a brief summary discussion of the important findings and their significance.

Table 4-1 TEXCAD and FEA stiffness results for control cases, without TLR.

Control Values	Layup	E_x (Msi)	E_y (Msi)	E_z (Msi)	G_{xy} (Msi)	G_{xz} (Msi)	G_{yz} (Msi)	ν_{xy}	ν_{xz}	ν_{yx}	ν_{yz}	ν_{zx}	ν_{zy}
TEXCAD													
c2a	[0/90]	10.36	10.36	1.43	0.847	0.651	0.651	0.03	0.36	0.03	0.36	-	-
c2b	[+45/-45]	2.92	2.92	1.43	5.027	0.651	0.651	0.73	0.10	0.73	0.10	-	-
c2qua	[+45/0/-45/90]	7.58	7.58	1.43	2.937	0.651	0.651	0.29	0.26	0.29	0.26	-	-
c2c	[0/0]	19.40	1.26	1.26	0.847	0.847	0.456	0.25	0.25	0.02	0.38	-	-
FEA													
c2a	[0/90]	10.36	10.36	1.43	0.847	0.593	0.593	0.03	0.36	0.03	0.36	0.05	0.05
c2b	[+45/-45]	2.92	2.92	1.43	5.027	0.605	0.605	0.73	0.10	0.73	0.10	0.05	0.05
c2qua	[+45/0/-45/90]	7.58	7.58	1.43	2.937	0.599	0.602	0.29	0.26	0.29	0.26	0.05	0.05
c2c	[0/0]	19.40	1.26	1.26	0.847	0.846	0.457	0.25	0.25	0.02	0.38	0.02	0.38
Input													
AS4/3501-6		19.4	1.26	1.26	0.847	0.847	0.457	0.25	0.25	-	0.38	-	-

Table 4-2 TEXCAD stiffness results for all cases with TLR.

TEXCAD	Layup	E_x (Msi)	E_y (Msi)	E_z (Msi)	G_{xy} (Msi)	G_{xz} (Msi)	G_{yz} (Msi)	ν_{xy}	ν_{xz}	ν_{yx}	ν_{yz}	ν_{zx}	ν_{zy}
c2a	[0/90]	9.83	9.83	1.77	0.813	0.634	0.634	0.04	0.29	0.04	0.29	-	-
c2ap15	[0/90]	9.82	9.83	1.71	0.813	0.652	0.634	0.04	0.31	0.04	0.30	-	-
c2p7a	[0/90]	9.84	9.81	1.48	0.815	0.715	0.632	0.03	0.39	0.03	0.34	-	-
c3a	[0/90]	9.82	9.82	1.77	0.812	0.634	0.634	0.04	0.29	0.04	0.29	-	-
c2abig	[0/90]$_9$	9.83	9.83	1.77	0.813	0.634	0.634	0.04	0.29	0.04	0.29	-	-
c4a	[0/90]	10.28	10.28	1.49	0.841	0.648	0.648	0.03	0.34	0.03	0.34	-	-
c5a	[0/90]	9.40	9.40	2.34	0.787	0.625	0.625	0.04	0.21	0.04	0.21	-	-
c2b	[+45/-45]	2.80	2.80	1.77	4.746	0.634	0.634	0.73	0.08	0.73	0.08	-	-
c2c	[0/0]	18.31	1.28	1.60	0.813	0.818	0.450	0.28	0.20	0.02	0.31	-	-
c2qua	[+45/0/-45/90]	7.20	7.20	1.77	2.779	0.634	0.634	0.29	0.21	0.29	0.21	-	-
c2a-kev	[0/90]	9.81	9.81	1.49	0.815	0.637	0.637	0.03	0.34	0.03	0.34	-	-
c2a-ti	[0/90]	10.10	10.10	1.73	0.922	0.740	0.740	0.04	0.36	0.04	0.36	-	-
c2a-st	[0/90]	10.37	10.37	2.04	1.024	0.846	0.846	0.05	0.36	0.05	0.36	-	-
c2a-sfm	[0/90]	-	-	-	-	-	-	-	-	-	-	-	-
c2a-dhm	[0/90]	10.23	10.23	1.79	0.838	0.651	0.651	0.03	0.28	0.03	0.28	-	-

Table 4-3 FEA results for stiffness for all cases with TLR.

FEA	Layup	E_x (Msi)	E_y (Msi)	E_z (Msi)	G_{xy} (Msi)	G_{xz} (Msi)	G_{yz} (Msi)	ν_{xy}	ν_{xz}	ν_{yx}	ν_{yz}	ν_{zx}	ν_{zy}
c2a	[0/90]	9.60	9.60	1.76	0.836	0.576	0.576	0.04	0.29	0.04	0.29	0.05	0.05
c2ap15	[0/90]	9.59	9.59	1.74	0.835	0.577	0.576	0.04	0.29	0.04	0.29	0.05	0.05
c2p7a	[0/90]	9.59	9.59	1.64	0.836	0.576	0.576	0.04	0.31	0.04	0.31	0.05	0.05
c3a	[0/90]	9.56	9.56	1.76	0.831	0.577	0.577	0.04	0.28	0.04	0.28	0.05	0.05
c2abig	[0/90]+B38	9.61	9.61	1.76	0.838	0.574	0.574	0.04	0.29	0.04	0.29	0.05	0.05
c4a	[0/90]	10.22	10.22	1.48	0.844	0.591	0.591	0.03	0.34	0.03	0.34	0.05	0.05
c5a	[0/90]	8.78	8.78	2.33	0.860	0.569	0.569	0.06	0.21	0.06	0.21	0.06	0.06
c2b	[+45/-45]	2.86	2.86	1.76	4.564	0.588	0.588	0.71	0.09	0.71	0.09	0.05	0.05
c2c	[0/0]	17.72	1.27	1.59	0.826	0.815	0.451	0.31	0.19	0.02	0.31	0.02	0.38
c2quasi	[+45/0/-45/90]	7.07	7.06	1.76	2.714	0.582	0.584	0.30	0.21	0.29	0.21	0.05	0.05
c2a-kev	[0/90]	9.58	9.58	1.49	0.841	0.579	0.579	0.04	0.34	0.04	0.34	0.05	0.05
c2a-ti	[0/90]	9.67	9.67	1.68	0.854	0.664	0.664	0.04	0.31	0.04	0.31	0.05	0.05
c2a-st	[0/90]	9.70	9.70	1.94	0.856	0.751	0.751	0.04	0.27	0.04	0.27	0.05	0.05
c2a-sfm	[0/90]	9.57	9.57	1.76	0.799	0.576	0.576	0.04	0.29	0.04	0.29	0.05	0.05
c2a-dhm	[0/90]	9.86	9.86	1.78	0.835	0.594	0.594	0.04	0.28	0.04	0.28	0.05	0.05

4. 1.   CONTROL CASES

Four different lamina stacking sequences, or layups, were selected for this study: a cross-ply laminate, [0/90]; an angle-ply laminate, [+45/-45]; a uni-directional laminate, [0/0]; and a quasi-isotropic laminate, [+45/0/-45/90]. The elastic response of these four layups captures many of the important aspects of the behavior of laminated composites. The results for the control cases, that is laminates without TLR, are listed in Table 4-1. Also shown are the input properties for the AS4-3501-6 lamina materials used throughout this work. Both the TEXCAD and FEA results for the [0/0] laminate are within one percent of the input properties. With the exception of G_{xz} and G_{yz}, the TEXCAD and FEA results for the other unreinforced laminates were in agreement also. The G_{xz} and G_{yz} values differed by 7-9 percent. Hence TEXCAD and FEA agreed very well for the control cases. Since it was the objective of this work to study the effect of adding TLR to a laminate, the discussions and figures in the following sections will focus on the percent change in the properties in question. The percent change is defined as the difference between two values, divided by the control value. The change is relative to the control case for each specific layup and analysis method. A positive percent change indicates an increased value while a negative percent change indicates a decreased value.

4. 2.   LAMINA STACKING SEQUENCE (LAYUP)

Figure 4-1 through Figure 4-3 are plots of the effect of TLR on the different layups. The [0/90] layup, with a 0.025inch diameter Gr-Ep TLR at 1.9 percent volume fraction will be used as a baseline and will appear in all plots in this chapter.

In general, adding TLR to an otherwise 2-D laminate slightly reduces the in-plane stiffness in the X direction, E_x. This reduction of in-plane stiffness was under seven percent in all layups and can be attributed to the replacement of in-plane material with the softer TLR inclusion. The effect on the Y direction stiffness, E_y, was similar, with the exception of the uni-directional laminate, where the TLR caused a one percent increase in E_y. A possible explanation for this difference is the greater Poisson effect of a uni-directional laminate under transverse (Y direction) loading. The addition of the TLR would restrict the Poisson contraction in the Z direction. Such restriction could cause resistance to the applied load and thereby result in an effective increase in the stiffness in the Y direction. This increase in stiffness offsets the softening due to the added pure resin regions of the TLR inclusion. Although these effects are fairly small, it is important to understand the mechanics of the material if implications for strength are to be made.

The effect of TLR on Z direction stiffness, E_z, is shown in Figure 4-3. The addition of the stiff Gr-Ep TLR oriented in the Z direction resulted in a 23 percent to 27 percent improvement in the overall material Z direction stiffness. The [0/0] laminate had a slightly higher value for the same likely reasons as just discussed for E_y.

The shear stiffnesses G_{xy}, G_{xz} and G_{yz} were reduced in a similar manner and for similar reasons as the in-plane extensional stiffnesses, E_x and E_y, that is the replacement of in-plane stiffness with softer material of the TLR inclusion. For this amount of TLR (1.9 percent), these reductions were relatively small, only nine percent in the worst case.

4. 3.   TLR THROUGH-THICKNESS ANGLE

The effect of the through-thickness angle of the TLR, ψ, was studied by evaluating this parameter at values of 0° (baseline), 15° and 45°. A value of $\psi = 0°$ has the TLR normal to the plane of the laminate. The variation of ψ had no effect on the reduction of the in-plane stiffnesses, E_x and E_y. This finding is not surprising in that the models used herein varied ψ without changing the volume fractions of the constituents (see section 3.2 for details). Only the orientation of the TLR was changed.

The TLR through-thickness angle did have an effect on extensional stiffness, E_z (see Figure 4-4). Increasing ψ lowered the E_z. This trend is consistent with the fact that an angled TLR has less stiffness in the Z direction. The stiffness averaging method used in TEXCAD predicts that the increase in E_z, will drop from 23 percent to 3 percent when the TLR angle is changed from 0° to 45°. The FEA analysis predicts a change from 23 percent to 15 percent for the same values. It is likely that TEXCAD under-predicts the positive contribution of a TLR at 45°. In the more detailed FEA model, the TLR has a larger contribution than what is assumed by simple stiffness averaging.

Changing the TLR angle did not significantly affect the small reductions of the shear stiffnesses G_{xy} and G_{yz}. Likewise, the FEA calculated changes in G_{xz} were also not affected. However, as can be seen in Figure 4-5, TEXCAD predicted that the TLR effect on G_{xz} would change from negative three percent to positive ten percent. This change can be accounted for by the fact that 45° is the optimum orientation for maximum shear stiffness. Stiffness averaging captures this effect, and as the small amount of TLR rotates away from 0° toward 45°, the increased shear stiffness contribution of the TLR offsets

the softening effect of the added pure resin regions. This effect is not observed in the FEA results, suggesting that actual microstructure would not respond according to G_{xz}'s predicted by stiffness averaging.

4. 4. UNIT CELL THICKNESS AND TLR DIAMETER

The thickness of the unit cell and the diameter of the TLR were studied by maintaining a 1.9 percent TLR volume fraction and adjusting other model parameters. A thick unit cell was modeled with the FEA method by duplicating the [0/90] baseline in the thickness direction, resulting in a [0/90]$_9$ laminate model. A small diameter FEA model with the same TLR volume fraction was created by scaling down the in-plane dimension of the unit cell while leaving ply thickness constant. The diameter of the TLR was reduced from the baseline 0.025 inch to 0.010 inch, with unit cell outer dimension adjusted accordingly. Since these models all had the same volume fractions, it was expected that the stiffness averaging method would predict the same values for each case. The FEA models were used to determine if a thickness effect, or a TLR-diameter/ply-thickness effect were possible. As shown in Table 4-2 and Table 4-3, changing these thickness did not affect the calculation of the engineering constants. For all nine constants, the results calculated from the three different models were all within one percent of each other. Therefore, changing the ratio of TLR-diameter/ply-thickness and changing the number of plies did not change the effect of adding TLR. Getting the same results for the [0/90] and the [0/90]$_9$ models was particularly important, as it confirms that potential boundary reaction problems at the top and bottom surfaces did not affect calculation of engineering constants.

4. 5.   TLR VOLUME FRACTION

The TLR volume fraction was varied from the baseline 1.9 percent in two cases. A 0.3 percent TLR model was created by keeping unit cell outer dimensions constant, and decreasing the TLR diameter from 0.025 inch to 0.010 inch. The TLR inclusion was scaled accordingly. A 4.9 percent TLR model was created by decreasing the unit cell in-plane dimensions (W_x and W_y) while maintaining the same 0.025 inch TLR diameter. In order to fit the TLR inclusion within the unit cell borders and maintain adequate FEA mesh, the ratio of inclusion-length/TLR-diameter (l/d) was reduced from five to three. It was felt that this change would not obscure the import influence of the amount of TLR.

As can be seen in Figure 4-6, increasing the TLR volume fraction significantly decreased the in-plane X direction stiffnesses, E_x. An identical result was found for E_y. The stiffness prediction calculated using TEXCAD was consistently lower than that from FEA. This trend is most prominent in the case with 4.9 percent TLR, where the TEXCAD and FEA methods predicted a reduction in E_x of nine percent and 15 percent, respectively. This difference may be explained by the fact that the TEXCAD models do not account for the curved in-plane fiber. In addition, in the FEA models the pure resin regions shield the TLR and keep it from carrying load and contributing to the overall stiffness. Stiffness averaging assumes that all segments contribute their share of stiffness and do not interact with each other.

Unlike for the in-plane stiffnesses E_x and E_y, the TEXCAD and FEA results for out-of-plane stiffness, E_z, were within one percent of each other, in both percent change from control and in actual E_z values (see Figure 4-7). Increasing the TLR volume fraction

significantly increased the positive effect on Z direction stiffness. A 1.9 percent addition

of TLR increased E_z by 23 percent while adding 4.9 percent TLR resulted in a 64 percent

improvement. Adding even a small amount of a very stiff material in a trans-laminar

fashion has a significant impact on the otherwise compliant Z direction elastic response.

The effect of TLR volume fraction on the in-plane elastic shear response, G_{xy}, can

be seen in Figure 4-8. The TEXCAD results show a steadily increasing reduction of G_{xy}

with increasing TLR volume fraction. As discussed before, more TLR results in larger

amounts of the relatively compliant pure resin regions. However, the FEA results show a

minimal effect. This difference is likely due to the presence of the curved fibers in the

FEA models. Angled fibers can carry more shear load. Hence, the small amount of in-

plane curvature caused by inserting the TLR may be contributing to the effective

resistance to shear, and thus providing stiffness that offsets the added compliance of the

pure resin regions. This difference is most prominent in the case of 4.9 percent TLR,

where the angle of the curved fibers is slightly higher than that of the other cases. This

greater fiber curvature was a result of the shortened TLR inclusion length for that case.

For the out-of-plane shear stiffnesses G_{xz} and G_{yz}, in both the TEXCAD and FEA

results, increasing TLR volume fraction increased the reduction caused by adding TLR.

There was no fiber curvature in the out-of-plane, or z, direction in these models. This

effect was small however, with the change in G_{xz} and G_{yz} only being negative four percent

at the worst case 4.9 percent TLR.

4. 6.   TLR MATERIAL

The effect of varying the properties of the TLR was examined by creating and comparing models with four different TLR materials: Graphite-Epoxy (baseline), Kevlar®-Epoxy, Titanium and Steel. As can be seen in Table 3-2, listed in order of increasing longitudinal modulus, E, these materials rank K-EP, Titanium, Gr-Ep and Steel. They rank K-EP, Gr-Ep, Titanium and Steel with increasing shear modulus, G. In addition to allowing a determination of the relative importance of E and G, these materials are readily available and have been used for TLR in various experimental studies.

The results for the effect of the different materials on the X direction stiffness, E_x is shown in Figure 4-9. An identical result was found for E_y, hence the figure refers to the results of both E_x and E_y. In the TEXCAD results, the reduction in these in-plane stiffnesses decreased as the TLR modulus increased. It is likely that increasing the stiffness of the TLR material added sufficient stiffness to compensate for the softening effect of the pure resin regions, at least as calculated by stiffness averaging. In the case with steel TLR, the positive effect of the added stiffness of the TLR and negative effect of the pure resin regions offset each other, resulting in a net overall effect of zero percent change. This trend was not the case in the FEA results, where the in-plane stiffness reduction remained fairly constant at about negative seven percent. As suggested in previous sections, the pure resin regions shield the TLR in plies oriented in the loading direction and prevent it from contributing to the over all stiffness. Therefore, the high transverse modulus of steel and titanium TLR could not contribute to overall stiffness, and the FEA in-plane stiffness results were all about the same.

In Figure 4-10, the relative ranking of the changes in Z direction stiffness, E_z, follows the same order as that for the increasing TLR modulus, E. Adding steel TLR resulted in a 35 percent and 42 percent increase according to the FEA and TEXCAD analyses, respectively. As with the in-plane stiffness results, the TEXCAD analysis consistently predicted a greater out-of-plane stiffness, E_z, than did the FEA analysis. This difference was the greatest for the case with the stiffest TLR material, steel.

This difference between the TEXCAD and FEA results can be seen with a much greater magnitude in the in-plane shear, G_{xy}, results. As shown in Figure 4-11, with stiffness averaging, the larger shear stiffness of titanium and steel caused significant increases in G_{xy}. These large effects were not evident in the FEA results, where changing material had a minimal effect on G_{xy}. As was discussed earlier in section 1.5, stiffness averaging over predicts matrix dominated properties such as in-plane shear stiffness, G_{xy}.

This difference between TEXCAD and FEA was also evident in the out-of-plane shear stiffnesses G_{xz} and G_{yz}, although to a much lesser extent. The G_{xz} and G_{yz} results were identical and the effects on G_{xz} shown in Figure 4-12 are representative for both G_{xz} and G_{yz}. As can be seen in the figure, the TLR only had an effect on inter-laminar shear stiffness in the cases with steel and titanium TLR; that have a shear stiffness an order of magnitude higher than that of either the composite TLR or the unreinforced lamina (see Table 3-2).

4. 7.   TLR CREATED MICROSTRUCTURE - RESIN REGIONS AND CURVED FIBERS

During the insertion of TLR the straight in-plane fibers are pushed aside, creating regions of pure matrix and curved fibers next to the TLR. As has been discussed above, these microstructural features play an important role in the mechanical response of TLR materials. To study the effect of this microstructure, the baseline [0/90] TLR model was modified to create two new cases. The first case is referred to as the straight fiber model (SFM). The regions of curved fibers were not included in this model. In the FEA model, this was done by simply changing the material properties of the elements that constituted the curved fiber volume. It is important to note that all TEXCAD cases were effectively SFM models, as properties of curved fibers were not included in any of the stiffness averaging. The second varied microstructure model is referred to as the drilled hole model (DHM). In the DHM, neither the curved fibers nor the pure resin regions were included, resulting in a microstructure that could have been created by drilling a hole and then inserting the TLR.

The results for the in-plane extensional stiffnesses E_x and E_y are shown in Figure 4-13 (only E_x results are plotted as the E_y results were identical). The SFM results were essentially the same as those of the baseline. For the DHM TEXCAD results, not including the pure resin region caused the reduction in in-plane stiffness to change from negative five percent for the baseline to negative one percent for DHM. Therefore, for stiffness averaging, it was the addition of the softer pure resin regions that dominated the reduction of in-plane properties. In the FEA results, the reduction only changed from negative seven percent to negative five percent, a much smaller effect.

The curved in-plane fibers and pure resin regions did not play a significant role in the TLR effect on out-of-plane or Z direction stiffness, E_z, (see Figure 4-14). Compared to the 23 percent change in E_z for the baseline, the DHM resulted in a 25 percent increase. The SFM and DHM Z direction stiffness results for TEXCAD and FEA agreed relatively closely.

The in-plane shear, G_{xy}, results are shown in Figure 4-15. There was minimal TLR effect in the DHM which had no curved fiber and no pure resin regions. Considering the pure resin regions only, that is the SFM, adding TLR reduced the in-plane shear stiffness by about four to five percent. This is consistent with the lower shear stiffness of pure matrix. Considering the curved fibers and resin regions, that is the baseline FEA case, the in-plane shear stiffness was again minimally affected. This finding supports the hypothesis, discussed in section 4.4, that the curved fibers contribute shear stiffness that offsets the softness of the neat resin.

The inter-laminar or out-of-plane shear stiffnesses G_{xz} and G_{yz} were only minimally affected by the presence of the curved fiber and pure resin regions. The change was only negative three percent in the base line, and zero percent in the DHM.

4. 8.   SIGNIFICANCE AND APPLICATION

The addition of small amounts of TLR (less than five percent) had small effects on the in-plane extensional and shear stiffnesses, E_x, E_y, and G_{xy}. However, adding only a few percent of very stiff TLR resulted in relatively large improvements in the out-of-plane stiffness, E_z. The longitudinal modulus of the TLR is an order of magnitude greater than that of the unreinforced laminate in the Z direction. With the exception of the titanium and

steel TLR cases, the inter-laminar shear properties, G_{xz} and G_{yz}, were mildly degraded, even in the material with 4.9 percent TLR. Both steel and titanium have a shear stiffness an order of magnitude larger than that of the unreinforced lamina.

These findings suggest that using TLR with an extremely high stiffness will result in a significant improvement in the corresponding elastic constant. Although a 20 to 60 percent improvement is considerable, it is important to realize that increasing a small number by 60 percent still results in a small number. The thickness direction properties of composite laminates are an order of magnitude lower than the in-plane properties. In addition, the large improvements in inter-laminar stiffness suggested by these analyses may not be achievable in real materials. In these models, a perfect bond was assumed between the TLR and the surrounding medium, allowing full transfer of inter-laminar loads from the lamina into the TLR. In real TLR materials, bonding would not be "perfect." There will always be microcracks in and around the TLR and the pure resin regions. Such microcracks are caused by the different thermal expansion of the different materials during processing, and by disbonding of the TLR from the surrounding medium due to high inter-laminar stresses. For these reasons, it is unlikely that an order of magnitude higher intrinsic stiffnesses of a TLR can be fully translated into the laminate on a volume averaging basis.

The slight reductions in the in-plane properties have been generally attributed to the replacement of stiff in-plane material with the relatively soft TLR inclusion materials. In these models, neither changes to in-plane fiber volume fraction nor increases in laminate thickness were considered. Rather a direct substitution was made. In a real laminate

adding two to five percent volume must cause a change either in the overall thickness, in the fiber volume fraction, or in both. In various references on TLR, the authors have noted the added thickness caused by adding the TLR (see for example [62, 66]). Once such a change is accounted for, the already small reductions in in-plane stiffnesses become even less of an issue.

Being able to predict the engineering constants quickly and easily is still an extremely valuable asset for design purposes. Comparing the TEXCAD and FEA analyses used here, there was less than ten percent difference in all cases of in-plane extensional stiffness, E_x and E_y. The maximum difference for Z direction stiffness, E_z, was six percent for the steel TLR case, and less than three percent in all other cases. The TEXCAD and FEA in-plane shear G_{xy} results differed by more than ten percent only in the steel TLR case and the 4.9 percent TLR case. The differences between TEXCAD and FEA results for the inter-laminar shear stiffnesses, G_{xz} and G_{yz}, ranged from zero to 21 percent in all cases examined. These things considered, stiffness averaging offers a quick, easy and reasonably effective method to estimate the engineering constants.

Effect of Ply Orientation on E_x
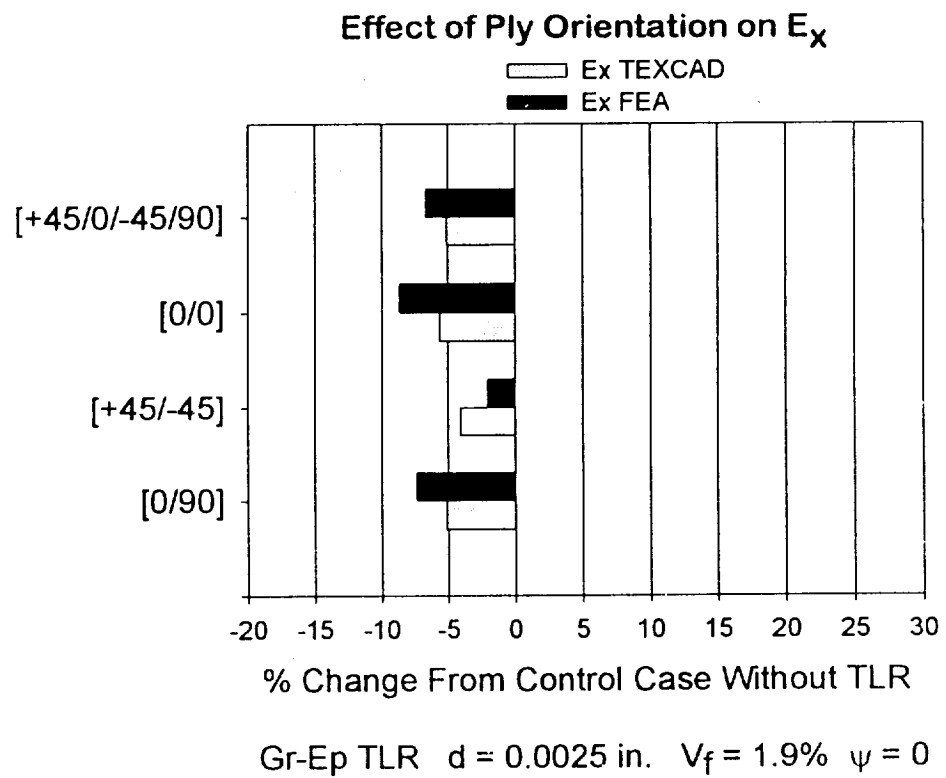
Figure 4-1 Effect of various ply orientations on the TLR induced changes to laminate E_x.

Gr-Ep TLR   d = 0.0025 in. V_f = 1.9% ψ = 0

% Change From Control Case Without TLR

Effect of Ply Orientation on E$_\gamma$

☐ Ey TEXCAD
■ Ey FEA

[+45/0/-45/90]

[0/0]

[+45/-45]

[0/90]

-20 -15 -10 -5 0 5 10 15 20 25 30

% Change From Control Case Without TLR

Gr-Ep TLR d = 0.0025 in. V$_f$ = 1.9% ψ = 0
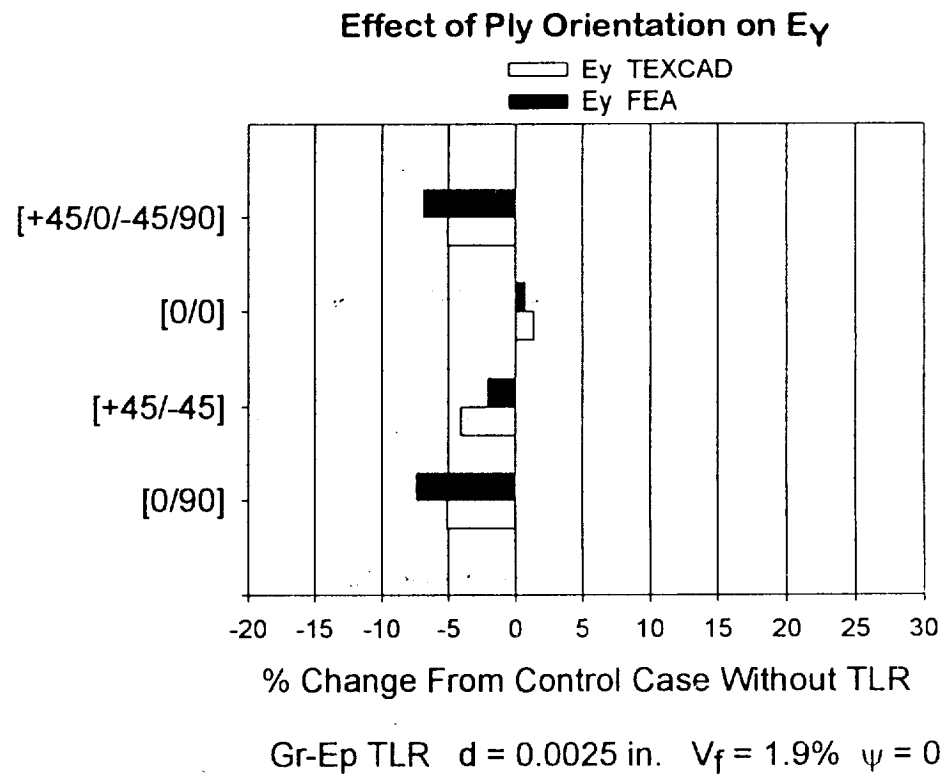
Figure 4-2 Effect of various ply orientations on the TLR induced changes to laminate E$_y$.

Effect of Ply Orientation on E_z

Legend:
- Ez TEXCAD
- Ez FEA

Categories (top to bottom):
- [+45/0/-45/90]
- [0/0]
- [+45/-45]
- [0/90]

X-axis: -20, -15, -10, -5, 0, 5, 10, 15, 20, 25, 30

% Change From Control Case Without TLR

Gr-Ep TLR   d = 0.0025 in. V_f = 1.9% ψ = 0
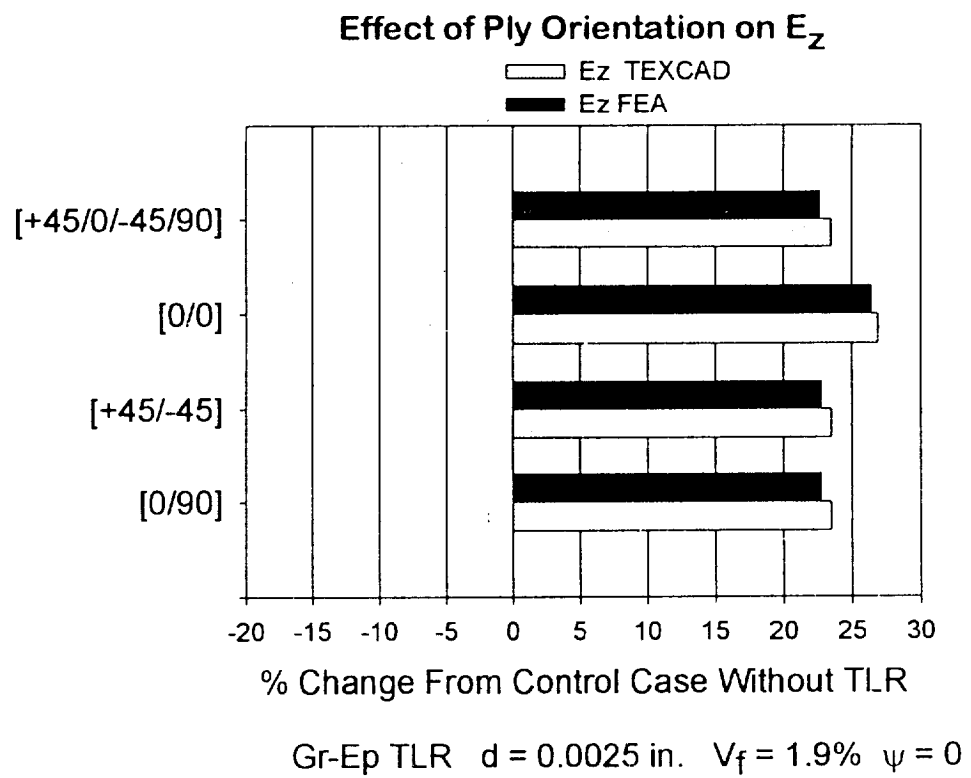
Figure 4-3 Effect of various ply orientations on the TLR induced changes to laminate E_z.

Effect of TLR Through Thickness Angle, ψ, on E_z

☐ Ez TEXCAD
■ Ez FEA

% Change From Control Case Without TLR

[0/90] Gr-Ep TLR d = 0.0025 in. V_f = 1.9%
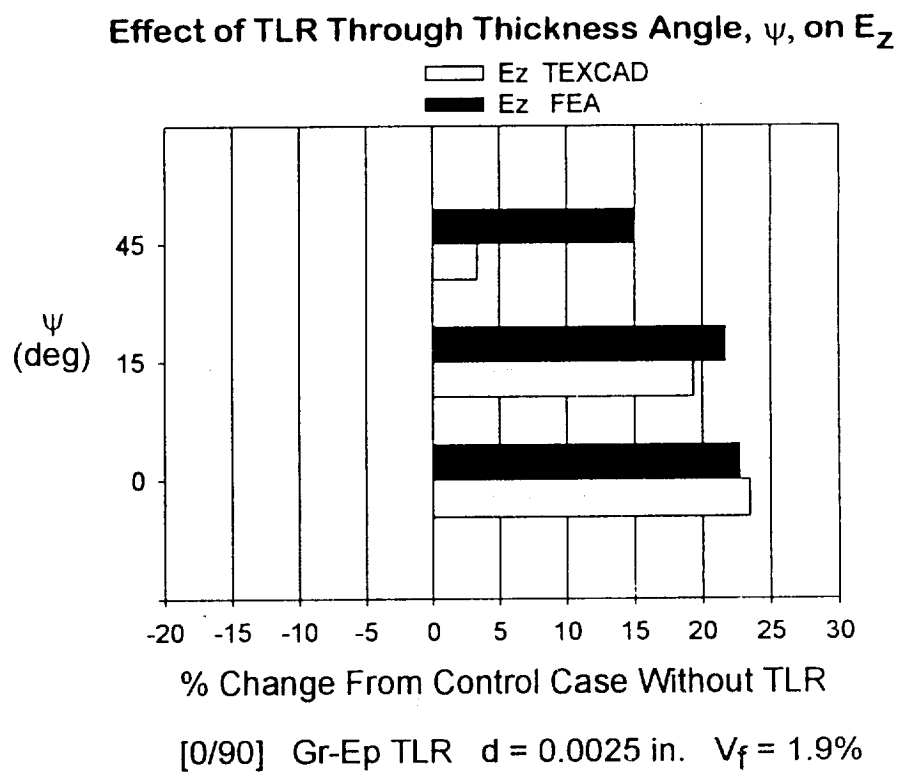
Figure 4-4 Effect of TLR through-thickness angle on TLR induced changes to laminate E_z.
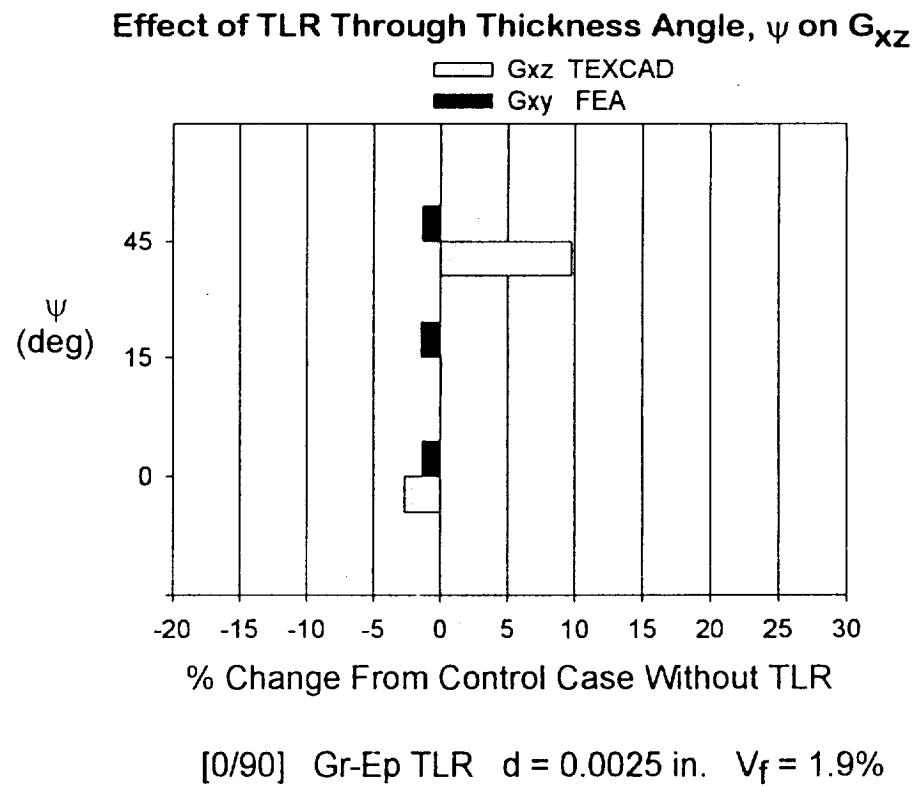
Figure 4-5 Effect of TLR through-thickness angle on TLR induced changes to laminate G_{xz}.

Effect of TLR Volume Fraction, V_f, on E_x

Ex TEXCAD
Ex FEA

TLR V_f
(%)

4.9

1.9

0.3

-20 -15 -10 -5 0 5 10 15 20 25 30

% Change From Control Case Without TLR

[0/90] Gr-Ep TLR d = 0.0025 in. ψ = 0
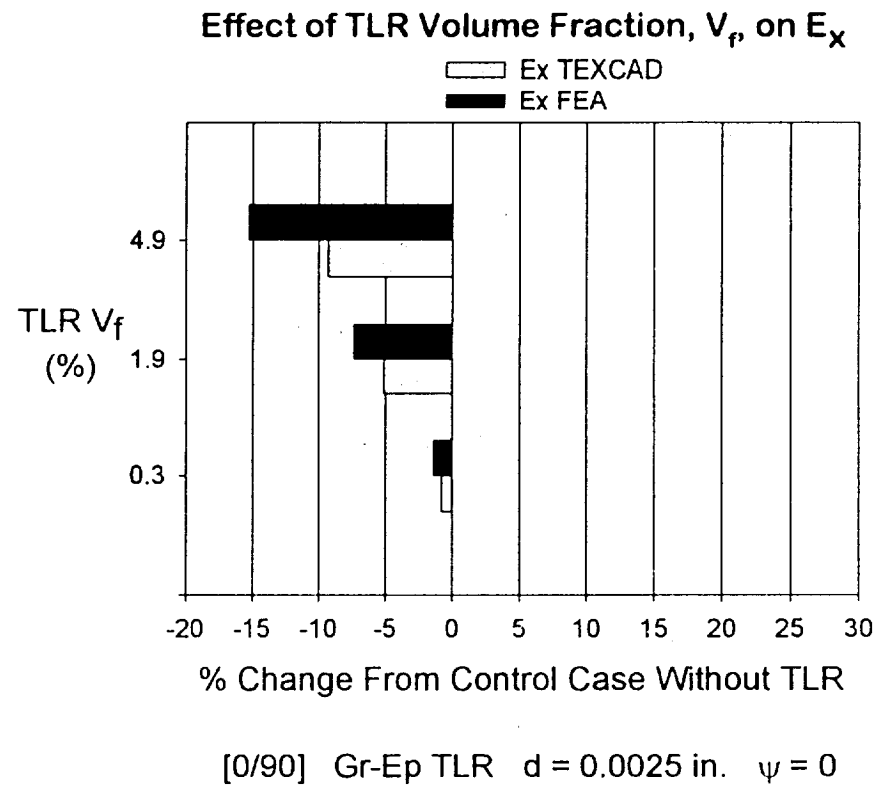
Figure 4-6 Effect of TLR volume fraction on TLR induced changes to laminate E_x.

Effect of TLR Volume Fraction, V_f, on E_z
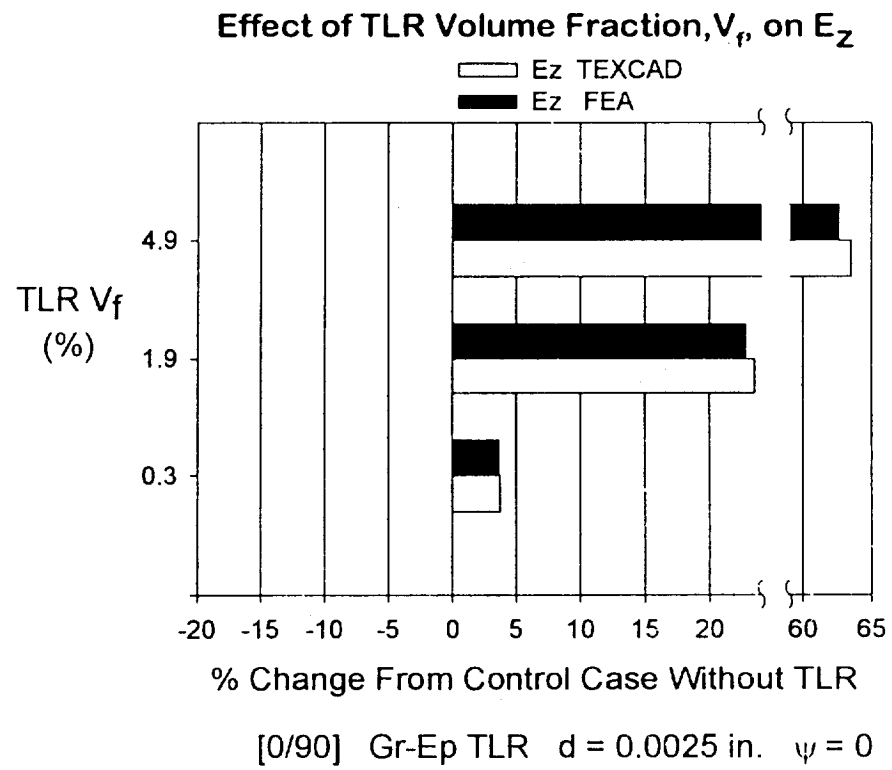
Figure 4-7 Effect of TLR volume fraction on TLR induced changes to laminate E_z.

Effect of TLR Volume Fraction, V_f, on G_{xy}

☐ Gxy TEXCAD
■ Gxy FEA

TLR V_f
(%)

4.9

1.9

0.3

-20 -15 -10 -5 0 5 10 15 20 25 30

% Change From Control Case Without TLR

[0/90] Gr-Ep TLR d = 0.0025 in. $\psi = 0$
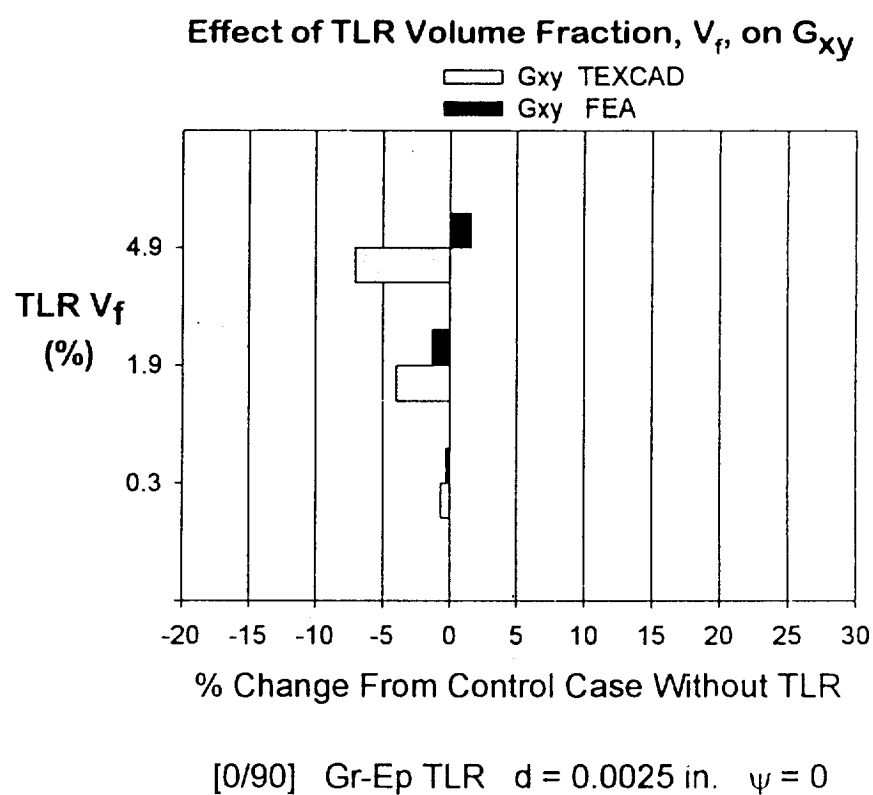
Figure 4-8 Effect of TLR volume fraction on TLR induced changes to laminate G_{xy}.

Effect of TLR Material on E_x

□ Ex TEXCAD
■ Ex FEA

Steel

Titanium

K-Ep

Gr-Ep

-20 -15 -10 -5 0 5 10 15 20 25 30

% Change From Control Case Without TLR

[0/90]   d = 0.0025 in. $\psi = 0$ $V_f = 1.9\%$
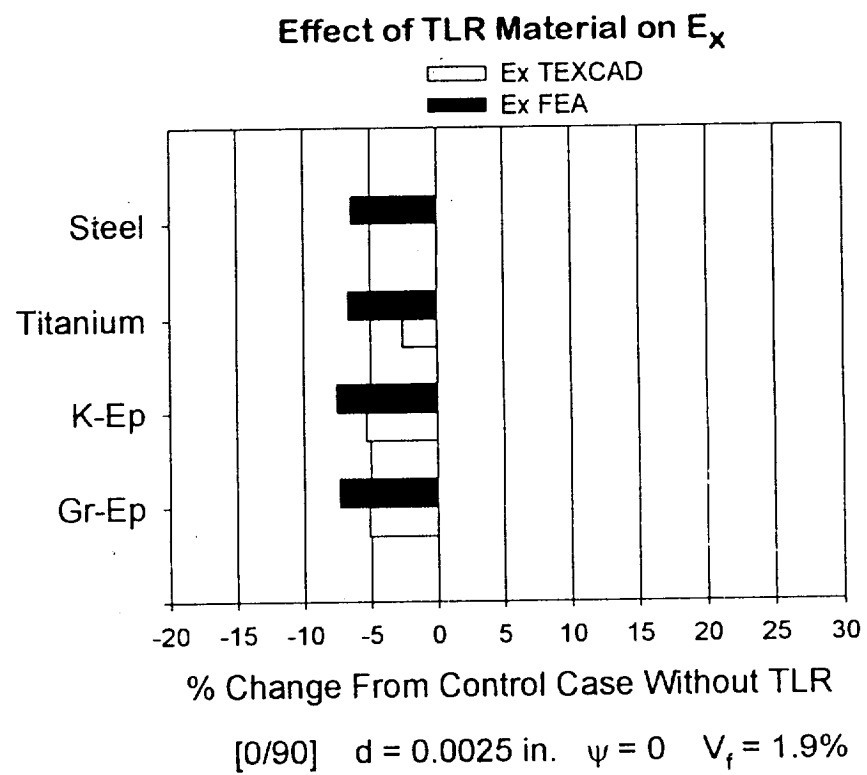
Figure 4-9 Effect of TLR material on TLR induced changes to laminate E_x.

Effect of TLR Material on E$_z$

% Change From Control Case Without TLR

[0/90]   d = 0.0025 in. $\psi = 0$ V$_f$ = 1.9%
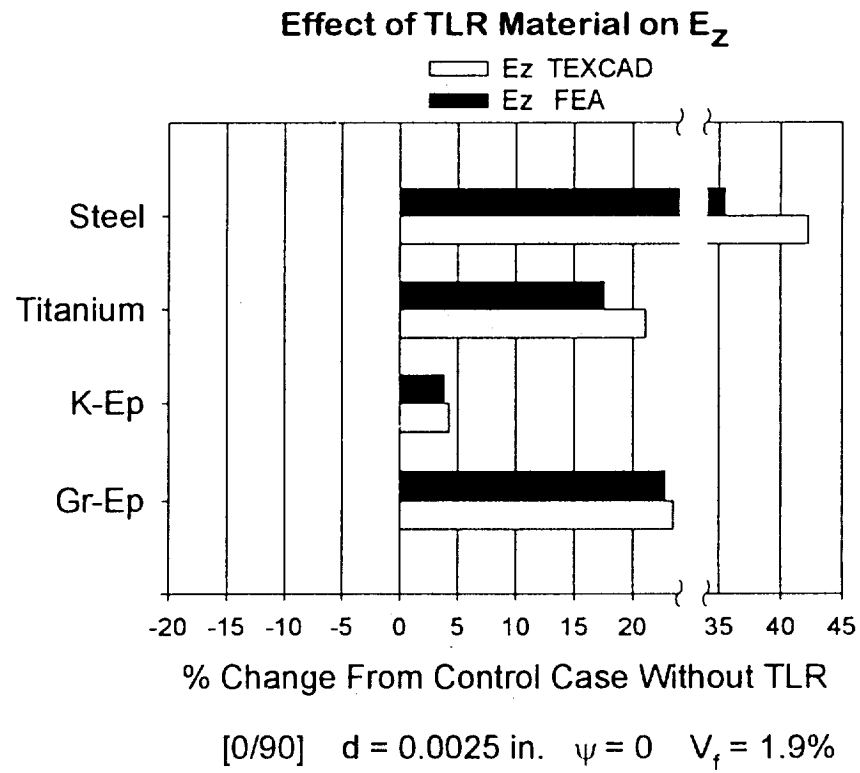
Figure 4-10 Effect of TLR material on TLR induced changes to laminate E$_z$.
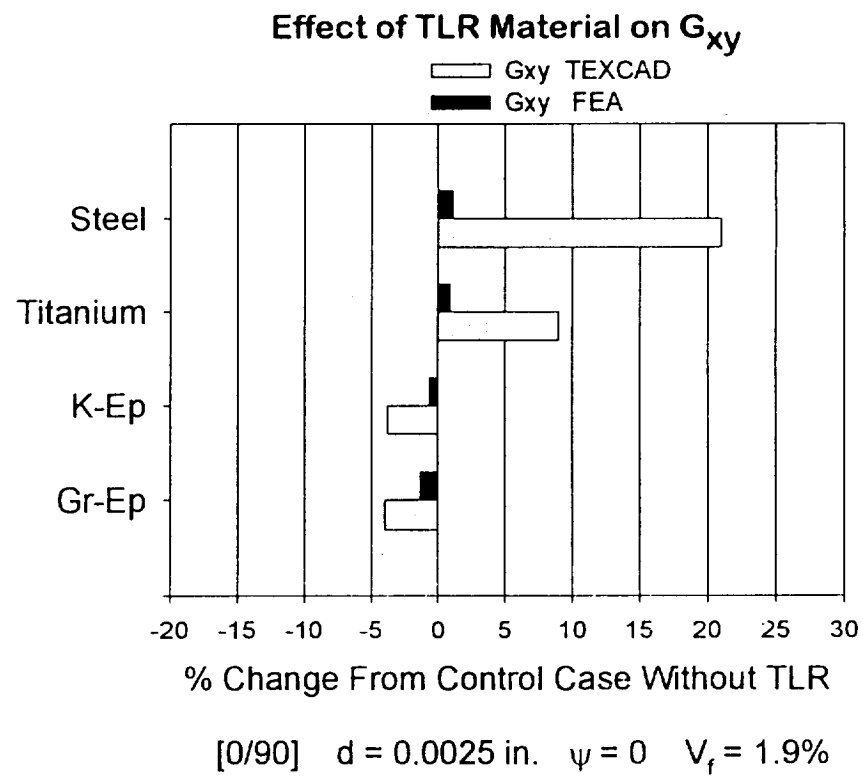
Figure 4-11 Effect of TLR material on TLR induced changes to laminate G_{xy}.

Effect of TLR Material on G_{xz}

% Change From Control Case Without TLR

[0/90]   d = 0.0025 in. $\psi = 0$ V_f = 1.9%
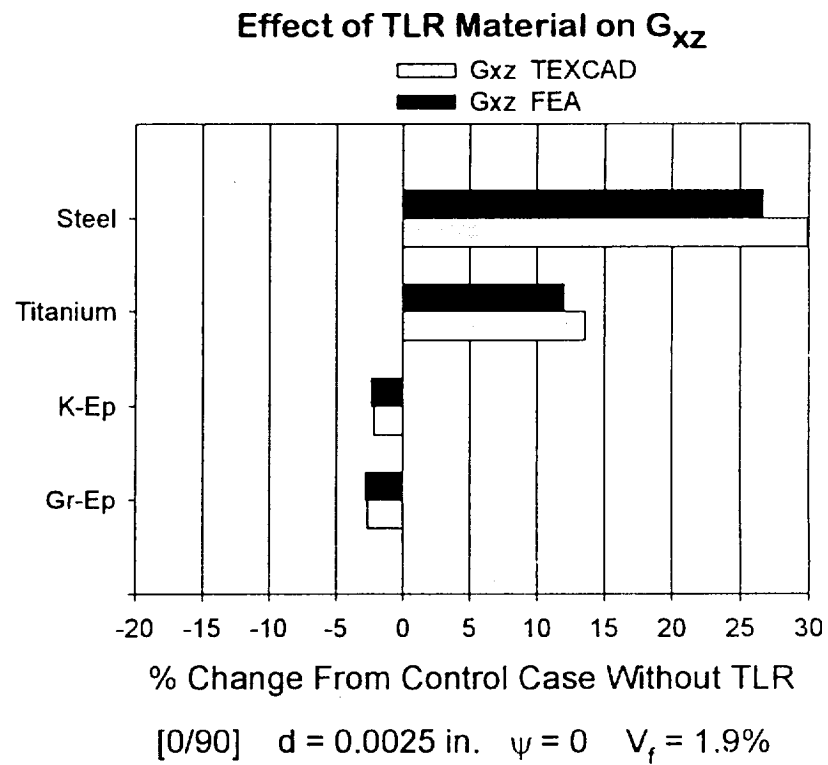
Figure 4-12 Effect of TLR material on TLR induced changes to laminate G_{xz}.

Effect of Pure Resin Regions and Curved Fiber on E_x

Ex TEXCAD

Ex FEA

Drilled Hole

Straight Fiber

Baseline

-20 -15 -10 -5 0 5 10 15 20 25 30

% Change From Control Case Without TLR

[0/90]   Gr-Ep TLR   d = 0.0025 in. $\psi = 0$ $V_f = 1.9\%$
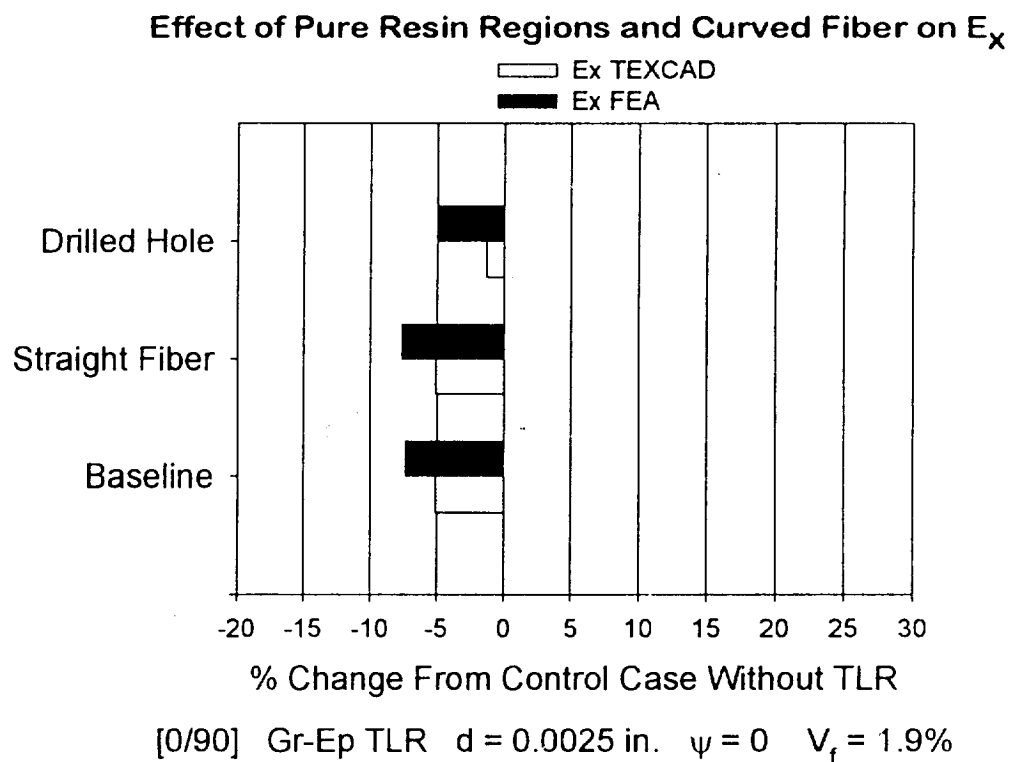
Figure 4-13 Effect of pure resin regions and curved fiber on TLR induced changes to E_x.

Effect of Pure Resin Regions and Curved Fibers on E_z

[0/90] Gr-Ep TLR d = 0.0025 in. $\psi = 0$ $V_f = 1.9\%$
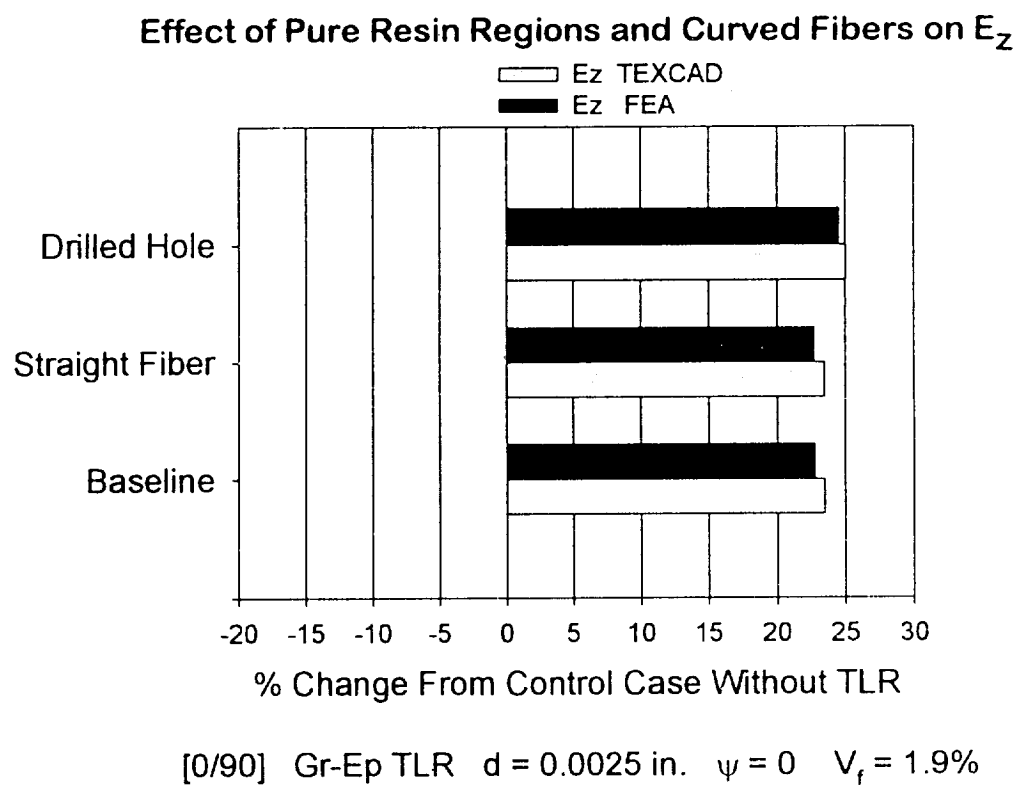
Figure 4-14 Effect of pure resin regions and curved fiber on TLR induced changes to E_z.
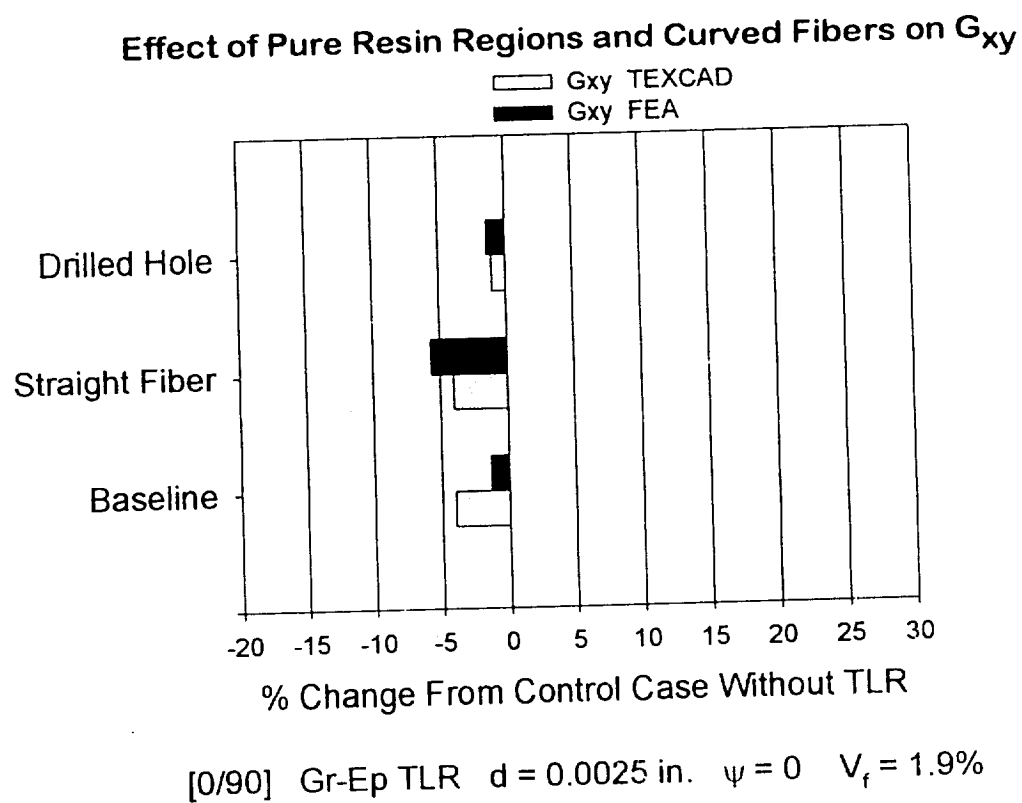
Figure 4-15 Effect of pure resin regions and curved fiber on TLR induced changes to G_{xy}.

CHAPTER 5
STRESS AND IMPLICATIONS FOR STRENGTH

A large number of different "failure mechanisms" for composite laminates can be found in the literature. There is not a consensus on the names of many of them. However, most failure events can be broken down into combinations and sequences of three simple mechanisms: fiber failure, transverse crack formation, and delamination. Stated another way, laminate failure can most always be traced to cracks forming transverse to the fiber direction in a the uni-directional ply, and/or cracks forming between the plies and/or fibers breaking.

The strength of any material is the stress at which failure, however defined, occurs. In the following sections the effect of adding TLR will be discussed in terms of stress and implications for failure and strength. After a brief examination of the in-plane tension and compression response, the discussion will focus on the "Achilles' Heel" of laminates, that is delamination. A strength of materials approach is used to examine the initiation of delamination.

5. 1.   IN-PLANE STRENGTH - TENSION AND COMPRESSION

Unless instability under compression is considered, the tension and compression linear elastic responses of materials as modeled by FEA are equivalent. The term compression will be used here, but the stress concentration results of the FEA should apply equally to tension failure.

As discussed in Chapter 1, many researchers have found that adding TLR reduces the in-plane properties of composites. Many discussions cay be found in the literature about how the microstructure associated with TLR affects the in-plane tension and compression response. Pure resin regions and curved or broken in-plane fibers are associated with the reduction of in-plane tension and compression properties. While this hypothesis is conceptually sound, there have been few detailed experimental or analytical studies focusing on the mechanisms of in-plane property reduction due to the addition of TLR.

The top portions of Figure 5-1 through Figure 5-3 show the microstructural features of pure resin regions and curved fibers associated with TLR. The figures contain close-up views of the elements color coded for material property, hence showing model details. In Figure 5-1 a "drilled hole model," (DHM) is shown. The TLR laminate is modeled as if a hole were drilled in the uni-directional lamina and the TLR inserted. This simplification does not include pure resin regions and curved fibers. Figure 5-2 shows a close up of the "straight fiber model," (SFM). In this case the resin regions have been added, but all the in-plane fibers are assumed to remain straight. Figure 5-3 shows the baseline model which includes both pure resin regions and curved fibers. As discussed in Chapter 3, these three FEA models were all copies of the same finite element mesh, with the materials properties for elements appropriately assigned in each case.

The bottom portions of Figure 5-1 through Figure 5-3 display the stress distributions around the TLR. These plots have the same view of the elements in and around the TLR as the plots in the top portions. However, in the stress plots the color

coding corresponds to stress level. A 10 ksi compressive load was applied in all cases (see Chapter 2 for loading details) and the plots all have the same stress scale, zero to negative 50 ksi. As expected for a filled hole, in the drilled hole model there was a strong stress concentration adjacent to the TLR. In the three figures, the stress concentrations are noted and are evidenced by the concentration of color at the extremes of the stress scale. Comparing the stress plots for the three models, it can be seen that adding the pure resin regions lessened this stress concentration and shielded the TLR from carrying in-plane compressive load. Addition of the curved fiber lessened the stress concentration even further, and spread the concentrated stress over a larger area. This finding is consistent with the practice of stitching dry fiber preforms rather than prepreg materials. In a dry fiber preform, the stitching needle and thread push in-plane fiber aside creating fiber curvature that lessens the stress concentration. By stitching prepreg, where the in-plane fibers are held in place by the resin, the needle and thread poke a hole and break in-plane fibers, resulting in a larger stress concentration and lower in-plane strengths. While having fibers that curve around the TLR may be better than effectively drilling a hole, the curved fibers themselves offer a potentially weak region where failure can start, resulting in a lower in-plane compression strength than laminates without TLR.

Compression failure of laminated composite materials is a complex set of mechanisms with terms such as "brooming,", "shear kinking," "kink band formation," and "sublaminate buckling" commonly used in the literature. No matter which particular compression failure theory one subscribes to for a given situation, it stands to reason that the concentration of applied compressive stress caused by adding TLR, will lower the so called "compression strength" of the laminate. Additionally, curved fiber regions in plies

aligned with the applied load should present a weak area, because these curved fibers are not oriented in the direction of compressive stress like the rest of the ply.

In [80] the mechanism of reduced compression was investigated in terms of the in-plane fiber curvature caused by the surface loops and knots associated with stitching. Such curvature is out-of-plane with respect to the laminate. However, in-plane curvature also occurs as shown in the models in this work, that is curvature due to in-plane fibers curving around the TLR inclusion. Such curved fiber imperfections are likely to play an important role in compression failure unless the curvature is small enough to be on the same scale as the inherent waviness of the lamina. Quantitative measurement of fiber waviness is extremely difficult and exact values are not known. Fiber waviness is quite variable with the magnitude depending on the quality of processing. However, the addition of very small diameter (0.010 inches) discontinuous TLR in the form of Z-Fiber™ was found to have a negligible affect on compression strength [131]. The non-effect of very small diameter TLR on compression strength would not be evident in the FEA studies done in this work, because the in-plane lamina were modeled as perfectly straight material with uniform material properties.

5. 2.   DELAMINATION INITIATION

Many experimental and analytical studies have concluded that TLR restricts or impedes the growth of delamination. However, there has been little or no detailed study of whether TLR can delay the onset or initiation of delamination. In the following sections the question of delamination initiation is addressed. The answer to this question has important design implications. The strength of materials approach used in this work is

first described and then a discussion of the results of the FEA analysis is given.

Comparison with experimental work is done in the last section where important

mechanisms are discussed in the light of experimental findings reported in the literature.

5. 2. 1.   STRENGTH OF MATERIALS APPROACH

In the approach used here, it is assumed that a delamination will start in one of two

ways. Either a crack will form directly between plies due to an inter-laminar stress

exceeding the inter-laminar strength of the material, or a delamination may evolve from a

transverse crack formed within a ply when a transverse tensile stress exceeds the

transverse strength (90° strength) of the uni-directional lamina. In the second case,

delamination is assumed to be initiated when the transverse crack is formed. In both types

of failure initiation, a maximum stress failure criterion is assumed. This approach is a

strength of materials approach, as opposed to a fracture mechanics approach, and hence is

only valid in addressing the beginning or initiation of damage. Damage progression is not

considered.

Two stress components will be studied for the direct formation of delamination:

the inter-laminar normal stress, σ_z, and the inter-laminar shear stress, τ_{xz}. These stresses

will be examined at the interface between plies. The maximum transverse tensile principal

stress, P1, will be studied for the formation of a transverse crack, and hence initiation of

delamination. Figure 5-4 illustrates the concept of the maximum transverse tensile stress.

Each individual lamina is transversely isotropic, with material properties being independent

of the direction perpendicular to the longitudinal fiber direction, or "1" direction in the

principal materials coordinates. Hence, a simple application of the two dimensional

maximum principal stress formula (Mohr's circle) yields the maximum transverse tensile stress in the ply, for a given state of global stress. This method is the same as that used in [156]. The stress at a point within the ply is transformed from the xyz global coordinate system to the 123 principal material coordinate system. The maximum transverse tensile stress, P1, can then be calculated by:

$$P1 = \frac{\sigma_{22} + \sigma_{33}}{2} + \sqrt{\frac{\left(\sigma_{22} - \sigma_{33}\right)^2}{2} + \tau_{23}^2}$$

Equation 5-1.

To examine the effect of TLR on delamination initiation, the stress results of the unit cell analyses were used. The results in this section are for the ε_z and γ_{xz} load cases for each unit cell model (see Chapter 2 for loading details). These two load cases represent inter-laminar normal and inter-laminar shear conditions, respectively. In a pure ε_z loading, the delamination is most likely to initiate directly from σ_z at the ply interface, or indirectly from P1 in an off-axis ply. The symbol $P1^z$ will be used to refer to the maximum transverse tensile stress under inter-laminar normal loading. Likewise for γ_{xz} loading, τ_{xz} and $P1^{xz}$ will be used to refer to the stresses that are most likely to lead to delamination initiation. The inter-laminar stresses σ_z and τ_{xz} are of interest at the interface between plies, hence the average stresses were calculated from the FEA results for the nodes at the interface. These interface nodes belong to the common face of adjacent elements on opposite sides of the interface. The $P1^z$ and $P1^{xz}$ stresses were calculated only at nodes within the off-axis plies (90° or 45° plies). The values for P1 did not include results for any nodes at the interface or ply boundaries.

The "nodal stress" output of COSMOS/M was used to generate these results. The "nodal stress" is the average of the values of element stress at the node for all the elements to which that node belongs. In order to avoid having the results unduly influenced by extreme values that could occur due to numerical error, and in order to obtain a measure of stress over certain regions of interest, a stress averaging technique was used. The "nodal stresses" were averaged over areas shown in Figure 5-5 and Figure 5-6. These areas were selected in order to minimize potential boundary effects and to examine the stress both inside and outside the TLR. The "in" area refers to the cross section the TLR at the ply interface. The "out" area refers to the area outside the TLR and includes nodes belonging to the microstructural features of pure matrix and curved fiber. The "lam" area refers to nodes out in the lamina that belong solely to elements with straight lamina properties. Thus comparisons of "in" and "out" average stress will illustrate potential load path changes where adding the TLR directs the load away from the interface into the TLR. Comparisons of the "out" and "lam" areas demonstrates the effects of the pure resin regions and curved fibers..

These average stresses have been normalized by the same averaged stress found in the control cases without TLR. With the exception of the models with 45° plies, in all control cases the applied 10 ksi σ_z or τ_{xz}, resulted in uniform 10 ksi stress throughout the unit cell. There was a small variation of stress in control cases that contained 45° plies. This variation was always less than two percent and was suspected to be a result of imperfect boundary conditions as previously discussed in section 2.2.2. This small variation was neglected and normalizing consisted of dividing the stress value by 10,000. For normalized stress values greater than 1.0, adding TLR caused that stress component

to increase. Likewise, normalized values less than 1.0 indicate that the stress at the point in question was lowered by the addition of TLR.

5.2.2.   UNIT CELL INTER-LAMINAR NORMAL LOADING

Values for the average normalized inter-laminar normal stress, σ_z, are shown in Figure 5-7. The shaded bar is the average of the values for all the nodes in the "in" area. The line above the bar denotes the peak values. In all cases of inter-laminar normal loading, the TLR picked up significant load: up to a factor of about 16 times the control value. The normalized σ_z for the "out" and "lam" areas is shown in Figure 5-8. As can be seen in the figure, the normal stress was lowered in all models, as measured over "out" or "lam" areas. With the exception of the model with TLR at a 45° degree angle through the thickness, all the peak values of the normalized inter-laminar stress, σ_z, are below one. Hence, adding TLR caused a load path change that resulted in the TLR carrying a significant portion of the normal stress, relieving the inter-laminar normal stress at the interface.

The distribution of normalized σ_z in the "in" and "out" areas is plotted in the scatter plot shown in Figure 5-9. The normalized, σ_z has a uniformly high value inside the TLR and a low value outside the TLR. In the control case, all data points would lie on a plane at a value of one. Hence the load path change is clearly evident with the bi-level distribution of normalized σ_z. Since the values are greater than one within the TLR, the TLR clearly picks up load, allowing the rest of the interface to carry less stress, with values less than one. These lower σ_z values between TLR pins (numbers less than 1.0) can be clearly seen in the scatter plot shown in Figure 5-10. Comparing the "out" and

"lam" values shown in Figure 5-10, it can be seen that the microstructural features of pure resin regions and curved fibers did not play a significant role in inter-laminar normal loading. While some areas of neat resin carry little stress, the limits of σ_z in the "out" area matches that found in the "lam" area for all three: baseline model, straight fiber model and the drilled hole model. With the exception of a wide range of values found at the nodes near the TLR, the σ_z distribution in the 45° TLR model is very similar (see Figure 5-11 and Figure 5-12). This lowering of interface stress is consistent in all the different models including the case with the lowest volume fraction of TLR and the case with the relatively soft Kevlar® TLR (see Figure 5-8).

The question of whether or not the results were affected by the method of introducing load at the boundaries is addressed by examining the inter-laminar stress results found at the mid-planes of both the [0/90] and the [0/90]$_9$ models. Both models gave almost identical results. A stress contour plot of the actual inter-laminar normal stress, σ_z, in the 18 ply model is shown in Figure 5-13.

The maximum transverse tensile stress, $P1^z$, for all models is shown in Figure 5-14. In general, adding TLR lowered the $P1^z$ within the off-axis plies in the area away from the TLR. All normalized $P1^z$ averages are below one. However, in the models with an angled TLR, the range of the $P1^z$ is much higher than one, suggesting that if the TLR is not oriented perpendicular to the plane of the laminate, a transverse crack will be more likely to form in an off-axis ply. As was the case in the inter-laminar normal stress, σ_z, results, the pure resin regions and curved fiber increased the range of $P1^z$.

Examining the data for the various parameters, the TLR volume fraction and TLR

material exerted the most influence on σ_z and P1^z. This finding makes sense in that one

would expect the amount and stiffness of the TLR to be important factors. An effective

single measure of these two parameters can be found in what will be referred to as the

"effective extensional load" of the TLR, or nEA. Multiplying the axial modulus of the

TLR, E, by the XY cross-sectional area of the TLR, A, and the number of TLR per unit

area, n, results in a number indicating the relative load carrying ability of the TLR. The

units of nEA are the same as those for stress. Values of nEA for the cases used in this

study are shown in Table 5-1. Plots of nEA versus σ_z and P1^z are shown in figures Figure

5-15 and Figure 5-16, respectively. As can be seen in the figures, there is a direct

relationship between nEA and the lessening of the stress between the TLR.

Table 5-1 TLR Effective extensional load for the different combinations of TLR parameters used in this study.

TLR Material	Vf (%)	n (1/in.)	d (in.)	nEA (psi)
Gr-EP	1.9%	38	0.025	0.38
Gr-EP	1.9%	242	0.010	0.39
Gr-EP	0.3%	38	0.010	0.06
Gr-EP	4.9%	100	0.025	1.01
K-Ep	1.9%	38	0.025	0.10
Titanium	1.9%	38	0.025	0.30
Steel	1.9%	38	0.025	0.56

As the data indicate, adding very stiff fibrous reinforcement in a trans-laminar

fashion increased the Z direction stiffness and reduced the inter-laminar stress between the

TLR. Assuming that in the real material, load is transferred between lamina by the TLR as

it was in these models, the initiation of an inter-laminar normal stress induced delamination

would require a higher applied load. The addition of TLR improved the resistance to a mode I induced delamination, even for the area between the individual TLR.

5.2.3. UNIT CELL INTER-LAMINAR SHEAR LOADING

Values for the normalized τ_{xz} are shown in Figure 5-17 and Figure 5-18. The shaded bar is the average of the values for all the nodes in the selected area. The line above the bar denotes the peak values. Unlike the results for σ_z, the TLR did not pick up the shear load in all the models. The shear stress was redirected away from the interface into the TLR only in the cases with titanium and steel TLR. It is of special interest to note that changing the angle of the TLR did not allow it to carry more shear as might have been expected. Even in the 45° TLR model, the τ_{xz} values in and outside the pin all range above and below one, leading to the suggestion that simply having angled TLR will not delay shear induced delamination initiation. This finding is evidenced in the bar charts of Figure 5-17 and Figure 5-18, the scatter plots shown in Figure 5-19 and Figure 5-20, and in the stress plots of Figure 5-21 and Figure 5-22. A shear stress load path change, with stress moving away from the interface and into the TLR only occurred in the cases where the shear modulus of the TLR was an order of magnitude higher than that of the un-reinforced laminate, that is in the titanium and steel TLR cases (see the material input properties, Table 3-2). The distribution of the shear stress τ_{xz} in the steel case is similar to that of the normal stress σ_z in the baseline case (see Figure 5-23, Figure 5-24 and Figure 5-25). The shear transfer to the TLR from the surrounding area is significant. However, the shear stress is not uniform within the TLR or in the surrounding area as it was in the σ_z results.

This non-uniformity of normalized shear stress was evident to an even greater degree in the results for the maximum transverse tensile stress, $P1^{xz}$ (see Figure 5-26 and Figure 5-27). Although the average $P1^{xz}$ was below one in both the "out" and "lam" areas, the range of the values goes much higher than one. It can be seen in Figure 5-27 that even in a steel TLR material, transverse cracks would be likely to initiate in the area close to the TLR, where high stress gradients exist. The fact that there was essentially no variation of $P1^{xz}$ in the drilled hole model suggests that the tendency for greater transverse cracking is due to presence of the pure resin regions.

As was the case for the normal stress, the TLR volume fraction and TLR material exerted the most influence on τ_{xz} and $P1^{xz}$. A TLR "effective shear load" can be defined as nGA, where G is the longitudinal-transverse shear modulus of the TLR, A is the XY cross-sectional area of the TLR, and n is the number of TLR per unit area. The number for nGA indicates the relative shear load carrying ability of the TLR. The units of nGA are the same as those for stress. Values of nGA for the cases used in this study are shown in Table 5-2. Compared to Gr-Ep or K-Ep TLR using two percent titanium or steel TLR results in an order of magnitude increase in nGA. The TLR material far outweighs the TLR volume fraction in the shear cases. As discussed above, the shear load path was significantly changed only when steel or titanium were used. This finding is also clearly evident in the plots of nGA versus τ_{xz} and $P1^{xz}$ shown in Figure 5-28 and Figure 5-29, respectively. Only values of nGA corresponding to steel and titanium TLR lowered the average and maximum τ_{xz} and the average $P1^{xz}$. However, the maximum values of normalized $P1^{xz}$ were much greater than one in the titanium and steel cases.

Table 5-2 TLR Effective shear load for the different combinations of TLR parameters used in this study.

TLR Material	Vf (%)	n (1/in.)	d (in.)	nGA (psi)
Gr-EP	1.9%	38	0.025	0.01
Gr-EP	1.9%	242	0.010	0.01
Gr-EP	0.3%	38	0.010	0.00
Gr-EP	4.9%	100	0.025	0.03
K-Ep	1.9%	38	0.025	0.01
Titanium	1.9%	38	0.025	0.12
Steel	1.9%	38	0.025	0.22

Considering the inter-laminar shear stress alone, these results imply that using a TLR with a very large shear modulus can delay the onset of delamination. In essence, adding small amounts of reinforcement with very high shear stiffness in a trans-laminar fashion enables the material to carry a higher inter-laminar shear load before a delamination would initiate directly. This finding is based on the assumption that in the real material, load is transferred between lamina by the TLR as it was in these models. However, transverse cracking would be even more likely to occur, allowing an indirect contribution to the initiation of a delamination. Hence it is unlikely that TLR can effectively prevent the initiation of delamination due to a mode II or inter-laminar shear type load dominance. As just discussed above, damage in the form of transverse cracks is more likely to begin in TLR material than un-reinforced material. Once cracks start to form near the TLR, the ability to transfer the shear stress into the TLR would be lowered and the inclination to delaminate is the same or greater.

5. 2.4.   EXPERIMENTAL RESULTS IN THE LITERATURE

The following two sections discuss the important mechanisms involved in some common mechanical tests that involve the creation of delaminations. The important concepts will be discussed in light of experimental evidence reported in the literature.

5. 2.4.1.   Delamination Initiation - Material Response

Testing to induce edge delamination under tensile loading is an example of a test developed to study the initiation and growth of delamination. Analytical and experimental work described in [36] was used to demonstrate that TLR could slow the growth of delamination and allow the specimen to carry a higher ultimate load before final failure. The TLR effect varied greatly depending on the layup, and no conclusive evidence was given that suggested that TLR delayed the initiation of delamination. The results of edge delamination tests with and without Z-Fiber™ are reported in [131]. The addition of only one percent volume of TLR practically doubled the load to initiate delamination. However, the initiation of delamination was determined by the change in slope of a load displacement curve, rather than detailed observations of failure in the specimen. It is possible that small and obscure delaminations occurred at or near the same value of load in specimens with and without TLR. In the specimens with Z-Fiber™, TLR bridging the delaminations could have carried load allowing the specimen to exhibit the same or similar overall load displacement response. Minor changes in the slope of the load displacement curve could have also been overlooked. Examples of the load displacement curves were not included in the paper.

The compression-after-impact (CAI) test is another test that has shown the benefit of TLR. As noted in Chapter 1, many studies on the low velocity impact of laminates with and without TLR have been reported in the literature. It is well documented that low velocity impact can result in large delaminations internal to the laminate that are not visible to the naked eye. The sublaminates created by the delaminations will buckle under compressive loading, resulting in failure of the specimen at a lower than anticipated load. The addition of TLR has been shown to improve both damage resistance, as shown by a smaller damage area for a given impact energy or force, and damage tolerance as shown by a higher failure load for a given damage size. In terms of damage tolerance, the TLR reinforces the sublaminates, preventing them from buckling at a low load. However, the question considered in this work is that of damage resistance. Even in the low velocity impact of traditional laminates without TLR, the exact sequence of damage and delamination formation is unclear. Nevertheless the sequence is likely to begin at some point with the formation of transverse cracks within plies and/or small delaminations between the plies. As the impact event continues with transverse displacement of the laminated plate, unstable growth of those original cracks/delaminations occurs. The presence of TLR may not prevent the onset of the initial cracks, but it can play a role in the growth of the delamination. This fact would explain how adding TLR results in both smaller damage areas for a given impact energy and higher compressive strengths for a given state of damage.

It is the resistance to the growth of delamination that can account for the improved performance of TLR laminates in many materials tests. This resistance to delamination growth can be traced to the fact the as a crack progresses past TLR, the individual TLR

often stay intact behind the crack front, thus bridging the crack faces. The TLR

consequently applies a traction across the crack faces in the wake of the advancing crack,

thereby affecting the energy and load required to further grow the crack. This concept is a

fracture mechanics problem, and section 1.5.3 sites important references using this

approach.

5. 2.4.2. Delamination Initiation - Structural Response

As noted in Chapter 1, many researchers have investigated using TLR in joining

applications. In stiffened structures where the stiffener is simply adhesively bonded or co-

cured, the relatively soft region between the stiffener and skin is often the weak point in

the design. Failure typically initiates at the tip of the stiffener flange or at the "noodle"

area underneath the web of the stiffener. Once initiated, the delamination will typically

grow in an unstable fashion along the area between the stiffener and skin causing the

structure to fail catastrophically. If TLR is used in conjunction with co-curing, the

stiffener typically does not separate catastrophically, and the structure carries a higher

ultimate load (see [21, 22, 25-31, 132]).

The fine points of the mechanisms of failure are rarely discussed in detail in reports

on structural tests, and although some authors may refer to TLR having delayed damage

initiation, care must be taken to understand how damage initiation is defined and

identified. It is likely that transverse cracks and small delaminations form at similar loads

in the same area of the structure but that TLR prevents the unstable growth of the

delamination, that is the separation of a stiffener. The TLR structure may have an overall

load response similar to that of an un-reinforced structure with two major differences; the

"damage initiation" as noted by a change in the over all structural response occurs at a

higher load, and ultimate failure is more gradual and occurs at a significantly higher load.

Although not discussed by all researchers who studied TLR for joining applications, this

concept can be found in literature as early as 1981 [22]. In that study TLR in the form of

stitching was used for hat stiffener attachment in marine applications. It was concluded

that stitching did not delay the initial formation of cracks, but it did allow the structure to

achieve a higher ultimate load.

The unit cell FEA results discussed in sections 5.2.2 and 5.2.3 support these

findings. Although extremely stiff TLR do carry high load in undamaged materials, it does

not prevent or delay transverse cracking and delamination.

A concept to enable the TLR to carry more of the inter-laminar load in undamaged

material is suggested in [132]. The idea proposed is to put a compliant rubber-like layer

between the stiffener and the skin. This layer has a lower transverse modulus than the skin

and stiffener material, thus forcing load to be carried by the TLR. If the TLR carries the

load, stress may be kept away form the areas where damage initiates, enabling higher loads

before delamination begins. Early FEA results look promising but experimental results

have yet to be reported.

5. 3.   SIGNIFICANCE AND APPLICATION

As suggested in section 5.1, in-plane tensile and compression property reduction

can be minimized with the use of small diameter TLR. If the structure will have holes or

other geometric discontinuities with very large stress concentrations, the potential of

minor in-plane property reduction caused by TLR is of limited concern. Therefore the most important questions in regard to TLR are how does it help and how much is needed?

The unit cell FEA results discussed in section 5.2.2 suggest that axially stiff TLR can pick up a significant amount of applied inter-laminar normal stress, σ_z, and consequently delay the initiation of delamination. However, perfect bonding between the TLR and surrounding laminate was assumed. Real materials will not have "perfect" bonding, but they will almost always have cracks in the pure resin regions, as well as cracks in and around the TLR. These imperfections would likely limit the load transfer to the TLR and prevent it from carrying the amount of stress suggested in the results for these models.

The unit cell FEA results discussed in 5.2.3 suggest that the tendency for delamination initiation from a direct inter-laminar shear stress can only be delayed with the use of a TLR with an extremely high shear stiffness, such as titanium and steel. However, even if extremely shear-stiff TLR are used, the tendency for transverse cracking is not reduced, but increased. Transverse cracks would then allow the formation of delaminations and further prevent shear stress transfer from the lamina into the TLR. The results of this detailed investigation of TLR materials could not conclusively prove that TLR delays damage initiation. The benefits of using TLR that have been shown experimentally and reported in the literature can all be explained by the restriction of damage propagation.

As has been shown repeatedly in the literature, TLR can be used to overcome the inherent weaknesses of composite laminates, and thus offers immense value in the design

of composite structures. For this value to be achieved, the design philosophy must be to contain a known or assumed crack size, rather than to prevent cracking in the first place. Such an approach is typical for designing aerostructures where impact damage is a critical driver. However, designing a stiffened structure with design ultimate loads beyond where stiffeners would "start" to debond is not practical in un-reinforced laminates, and can only be accomplished in mechanically fastened stiffeners or stiffeners attached with TLR.
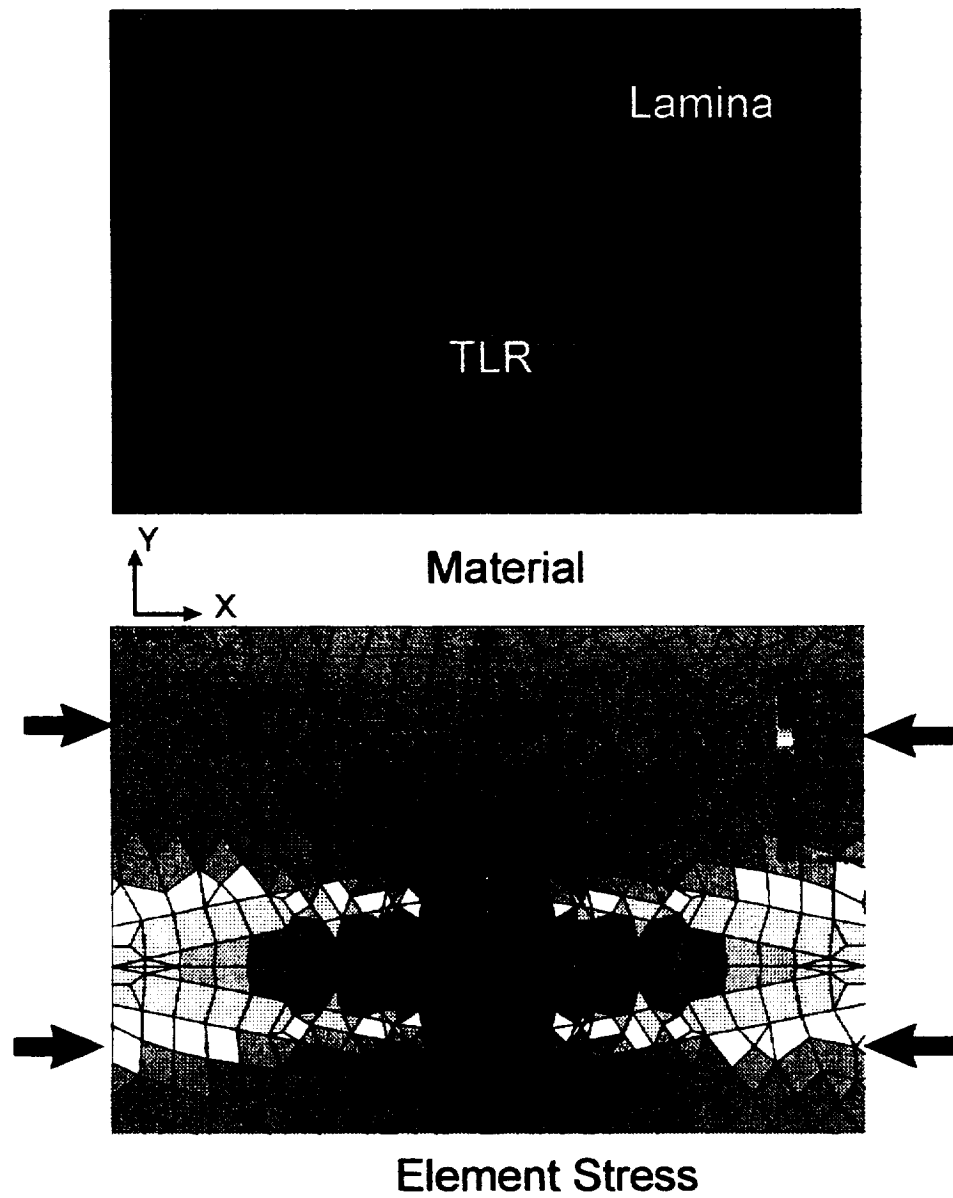
Figure 5-1 Normal stress σ_x in the 0° ply of the drilled hole model under compressive loading.
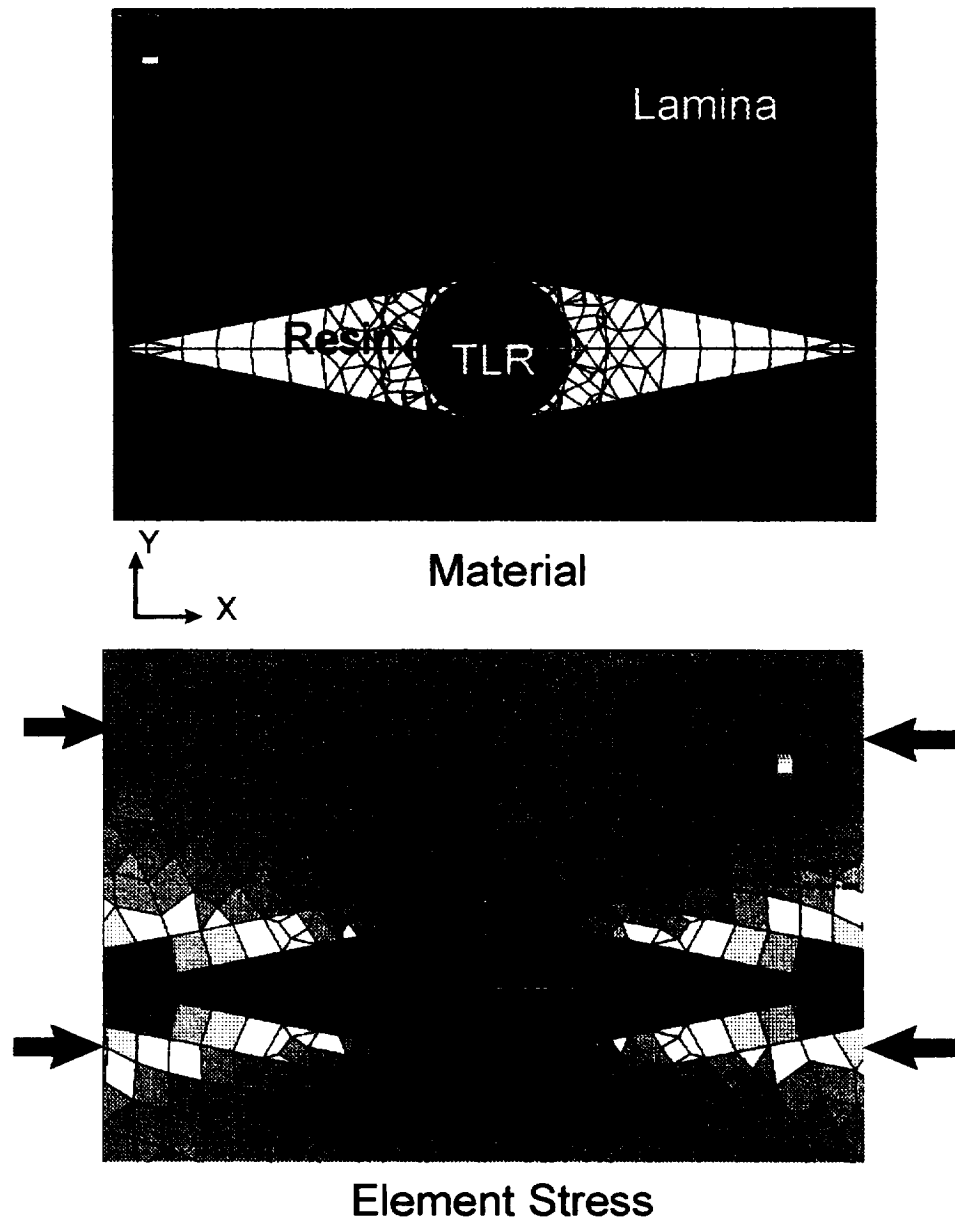
Figure 5-2 Normal stress σ_x in the 0° ply of the straight fiber model under compressive loading.
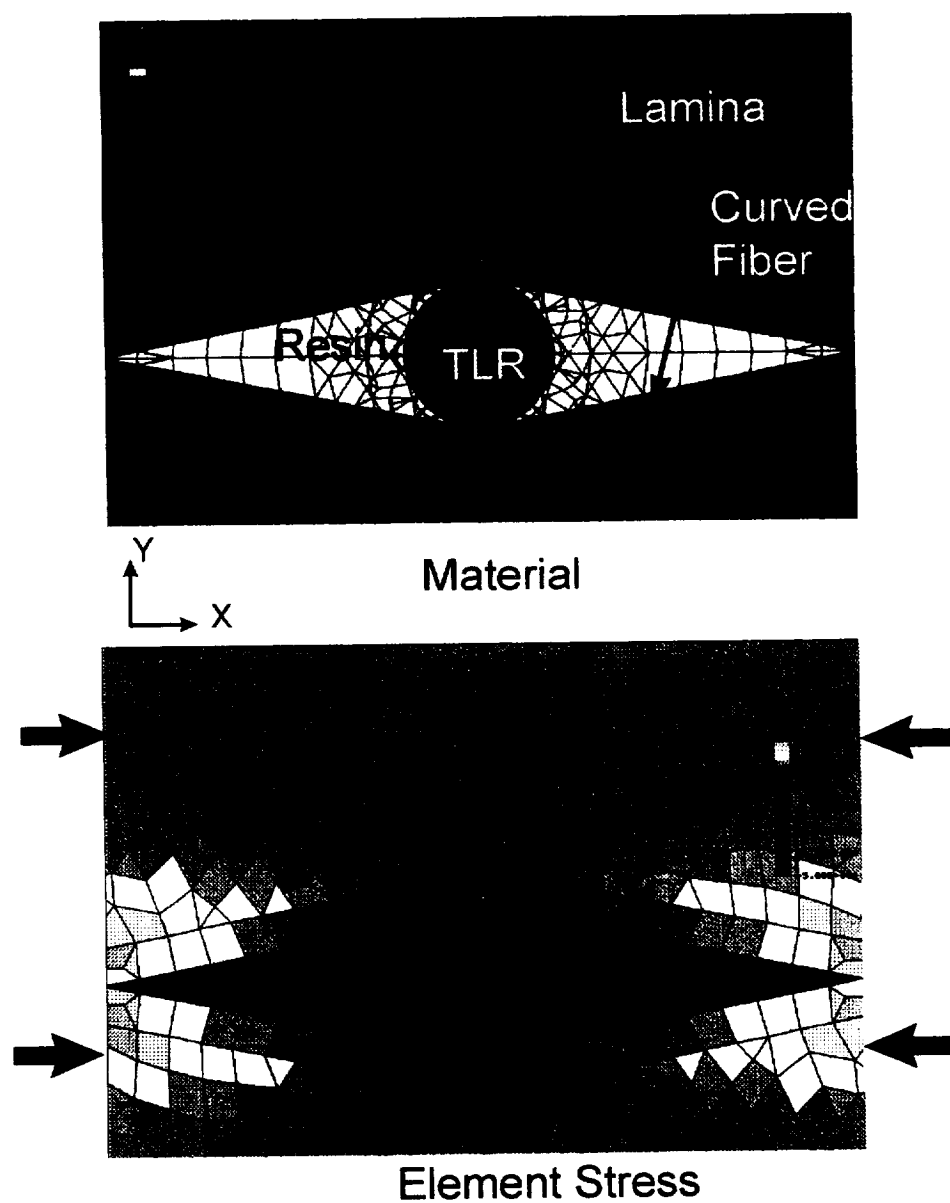
Figure 5-3 Normal stress σ_x in the 0° ply of the baseline model under compressive loading.

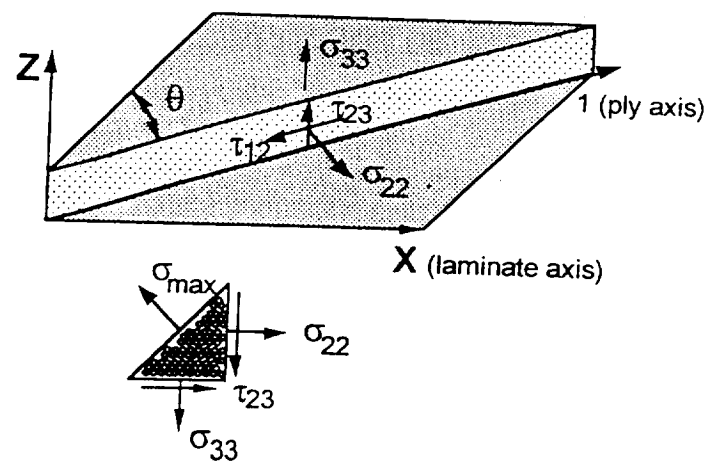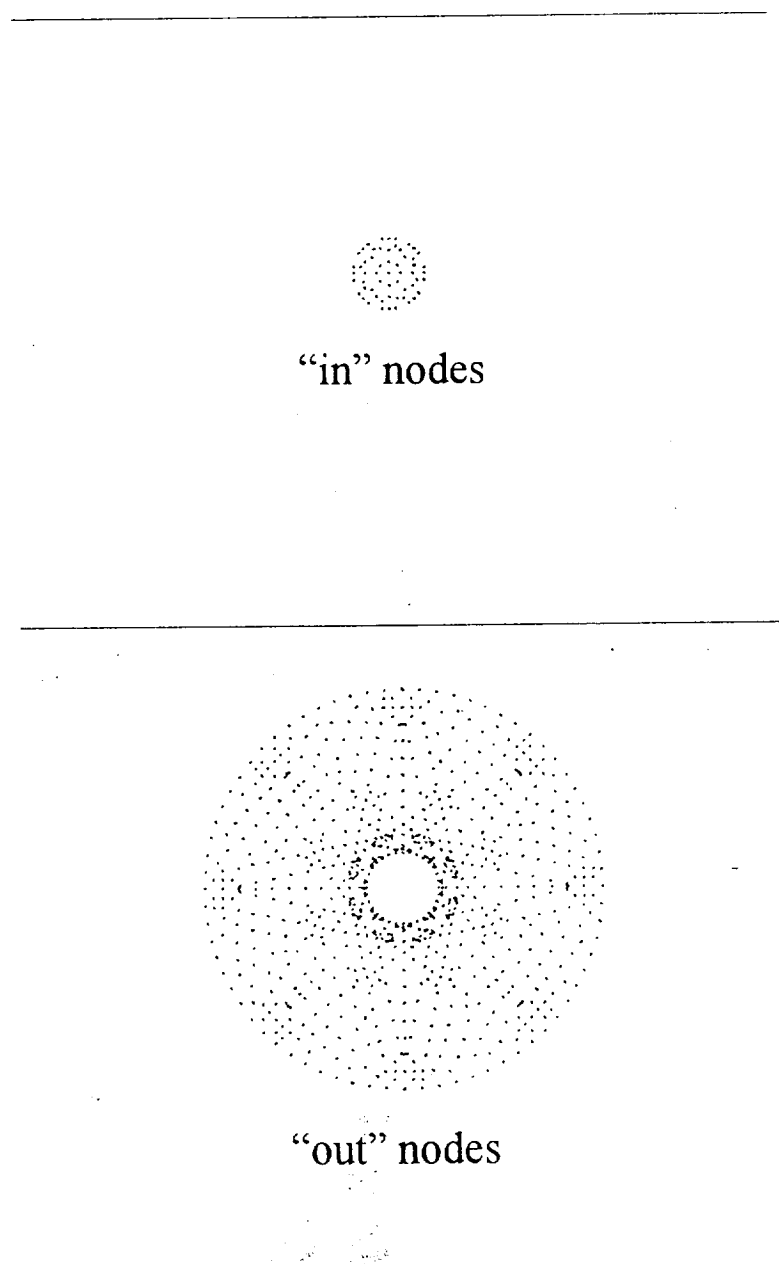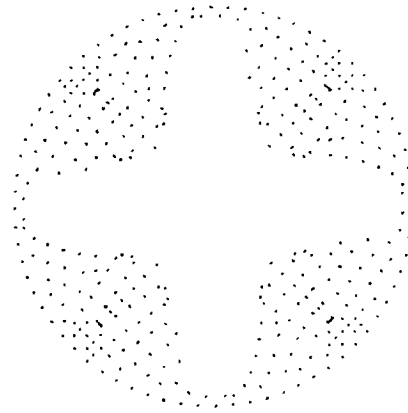**Figure 5-4 Illustration of the transverse state of stress in an angle ply [156].**
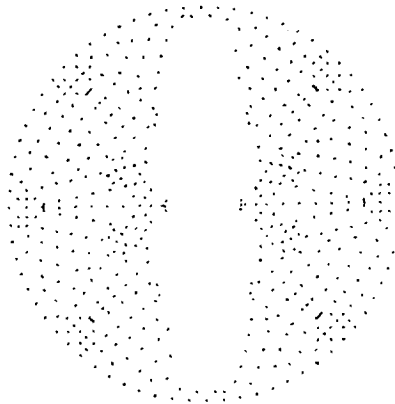
"in" nodes

"out" nodes

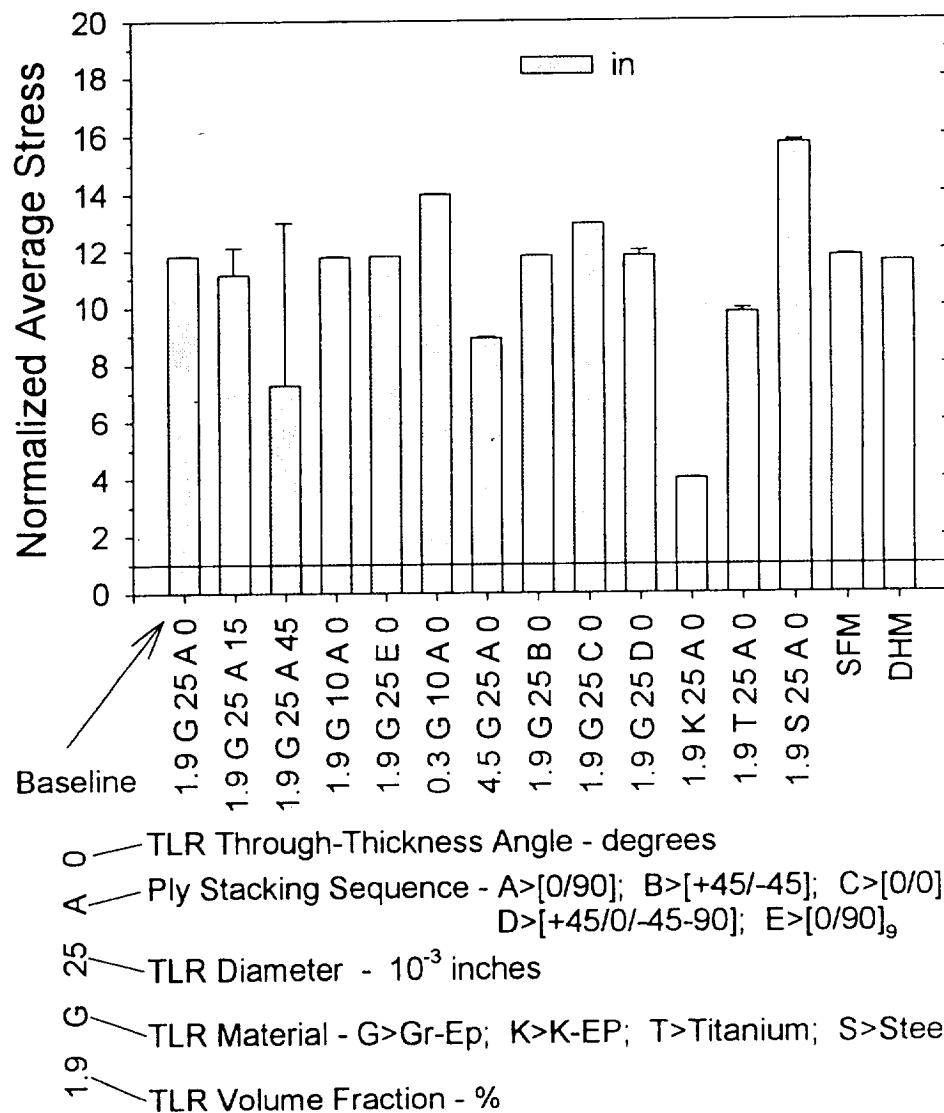Figure 5-5 Plane of nodes used to average stress inside and outside the TLR at the ply interface or within a ply.
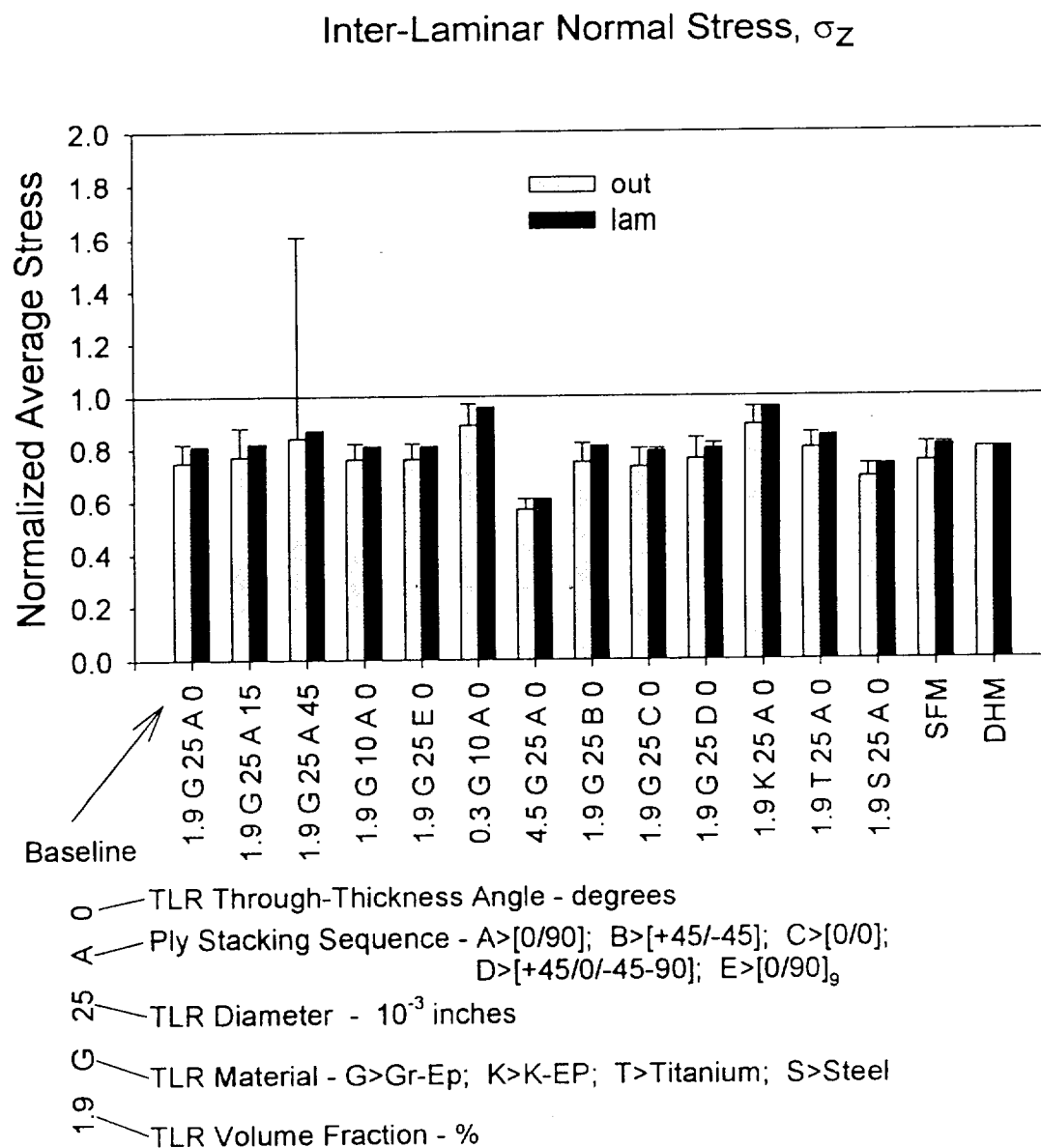
"lam" nodes
at ply interface

"lam" nodes
within a ply

Figure 5-6 Plane of nodes used to average the maximum transverse tensile stress over the area out in the lamina away from the TLR, at the ply interface and within the ply.

Inter-Laminar Normal Stress, σ_z

Baseline:

$\overset{\text{O}}{\underset{\text{}}{\diagup}}$ —TLR Through-Thickness Angle - degrees

$\overset{\text{A}}{\underset{\text{}}{\diagup}}$ —Ply Stacking Sequence - A>[0/90]; B>[+45/-45]; C>[0/0];
D>[+45/0/-45-90]; E>[0/90]$_9$

$\overset{\text{25}}{\underset{\text{}}{\diagdown}}$ —TLR Diameter - 10^{-3} inches

$\overset{\text{G}}{\underset{\text{}}{\diagdown}}$ —TLR Material - G>Gr-Ep; K>K-EP; T>Titanium; S>Steel

$\overset{\text{1.9}}{\underset{\text{}}{\diagdown}}$ —TLR Volume Fraction - %

Figure 5-7 Normalized inter-laminar normal stress, σ_z, at the ply interface averaged over the "in" area inside the TLR. The key below the figure explains the identifiers used on the X axis.

Inter-Laminar Normal Stress, σ_z

Baseline

$\underset{0}{\frown}$ TLR Through-Thickness Angle - degrees

$\underset{A}{\frown}$ Ply Stacking Sequence - A>[0/90]; B>[+45/-45]; C>[0/0];
D>[+45/0/-45-90]; E>[0/90]$_9$

$\underset{25}{\frown}$ TLR Diameter - 10^{-3} inches

$\underset{G}{\frown}$ TLR Material - G>Gr-Ep; K>K-EP; T>Titanium; S>Steel

$\underset{1.9}{\frown}$ TLR Volume Fraction - %

Figure 5-8 Normalized inter-laminar stress, σ_z, at the ply interface averaged over the "out" and "lam" areas outside the TLR. The key below the figure explains the identifiers used on the X axis.

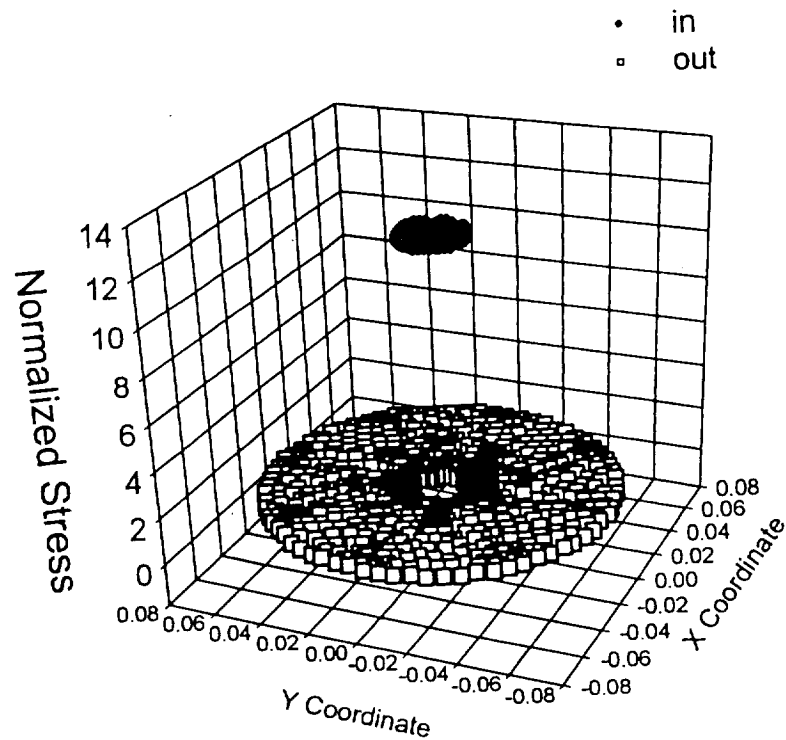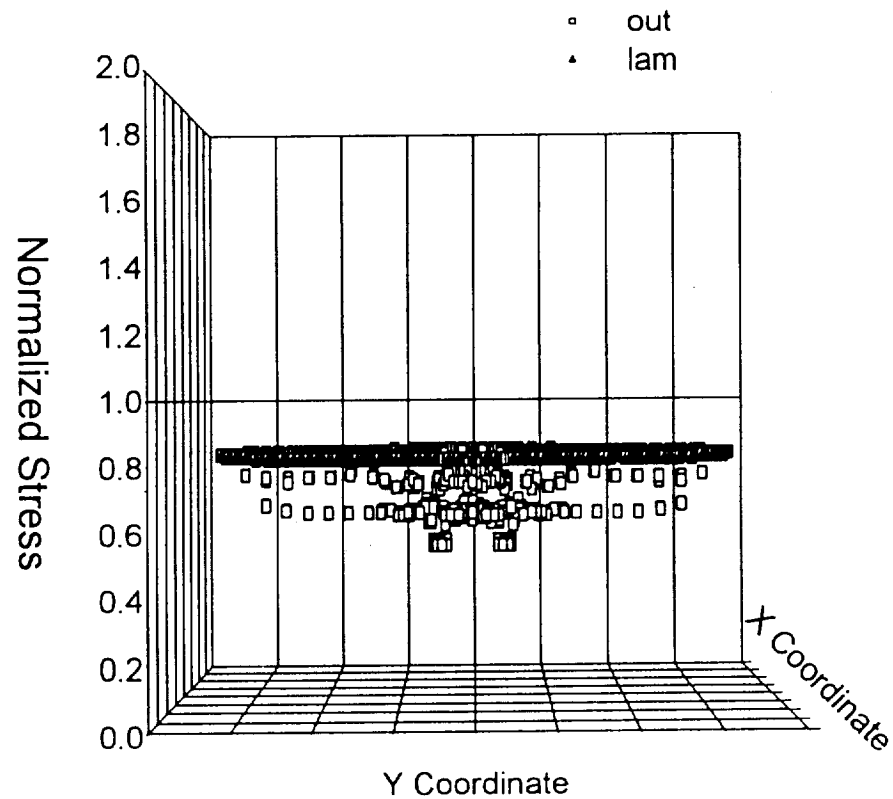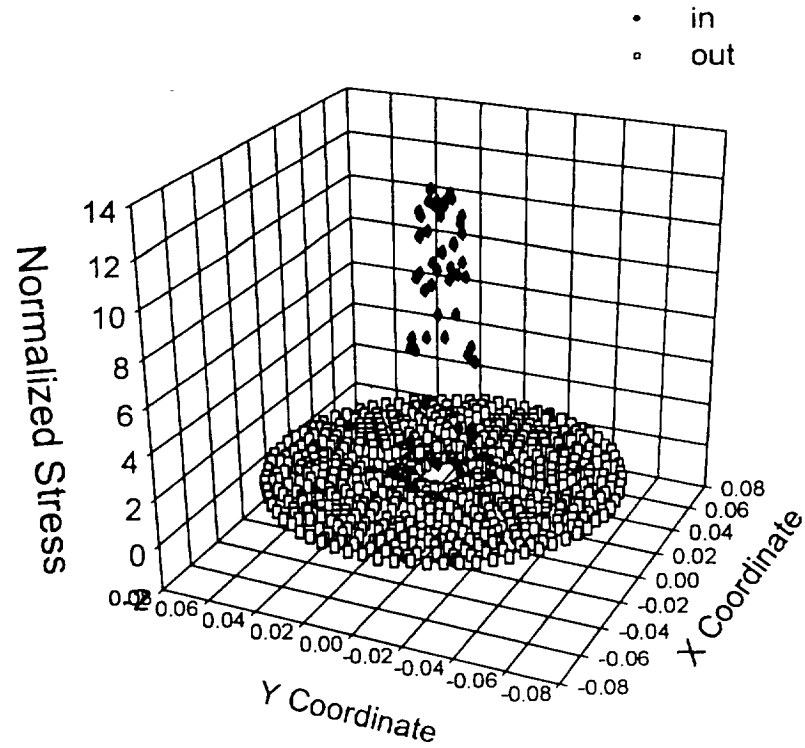Figure 5-9 Scatter plot of the normalized inter-laminar normal stress,σ_z, in the "in" and "out" areas at the ply interface of the [0/90] baseline model.

Figure 5-10 Scatter plot of the normalized inter-laminar normal stress, σ_z, in the "out" and "lam" areas at the ply interface of the [0/90] baseline model.

Figure 5-11 Scatter plot of the normalized inter-laminar normal stress, σ_z, in the "in" and "out" areas at the ply interface of the [0/90], $\psi=45°$ model.
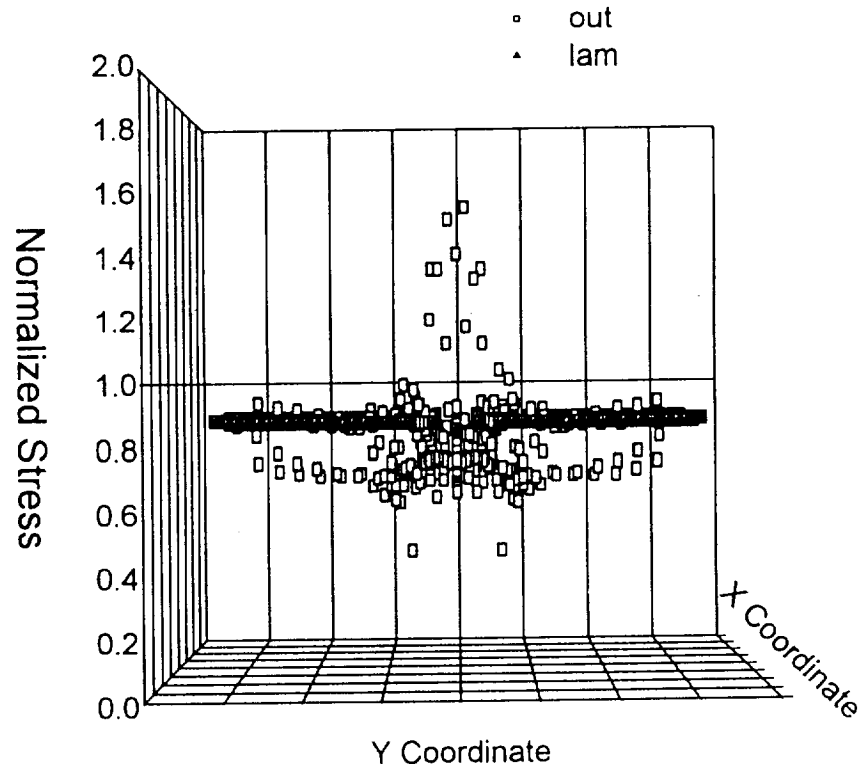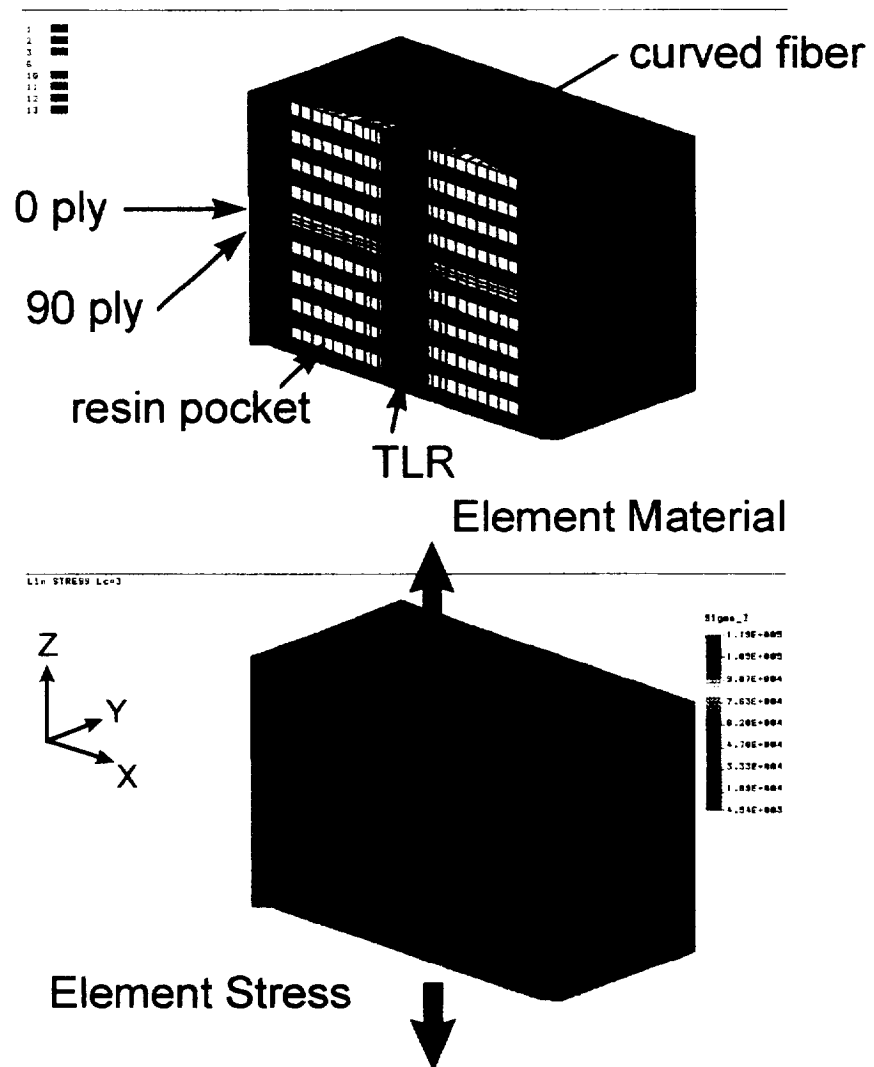
Figure 5-12 Scatter plot of the normalized inter-laminar normal stress, σ_z, in the "out" and "lam" areas at the ply interface of the [0/90], ψ=45° model.

Figure 5-13 Inter-laminar normal stress, σ_z, in the [0/90]$_9$ model under Z direction loading.

Maximum Transverse Tension Principal Stress, P1^z

o —TLR Through-Thickness Angle - degrees

A —Ply Stacking Sequence - A>[0/90]; B>[+45/-45]; C>[0/0];
D>[+45/0/-45-90]; E>[0/90]$_9$

25 —TLR Diameter - 10^{-3} inches

G —TLR Material - G>Gr-Ep; K>K-EP; T>Titanium; S>Steel

1.9 —TLR Volume Fraction - %
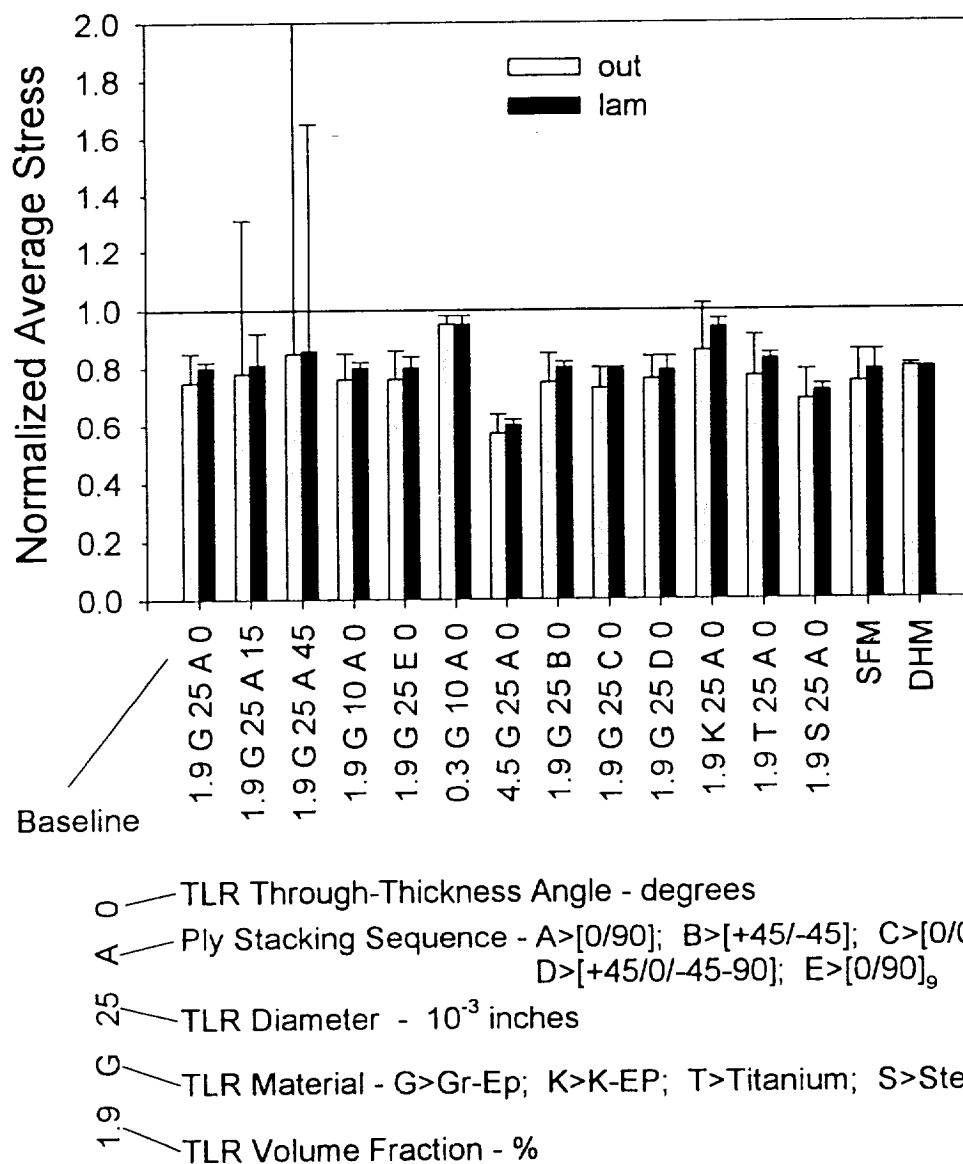
Figure 5-14 Normalized maximum transverse tensile stress under Z direction normal loading, P1^z, averaged over the "out" and "lam" areas within the off-axis ply. The key below the figure explains the identifiers used on the X axis.

TLR Effective Extensional Load versus σ_z in "lam" Area
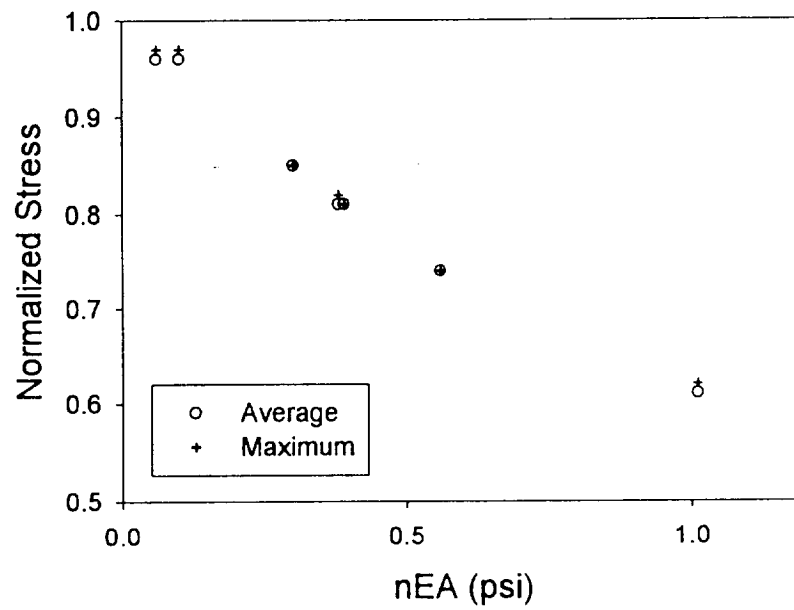
Figure 5-15 Effect of TLR effective extensional load, nEA, on the interlaminar normal stress, σ_z, in the "lam" area.

TLR Effective Extensional Load versus P1^Z in "lam" Area

Figure 5-16 Effect of TLR effective extensional load, nEA, on the maximum transverse tensile stress, P1^z, in the "lam" area.

Inter-Laminar Shear Stress, τ_{XZ}
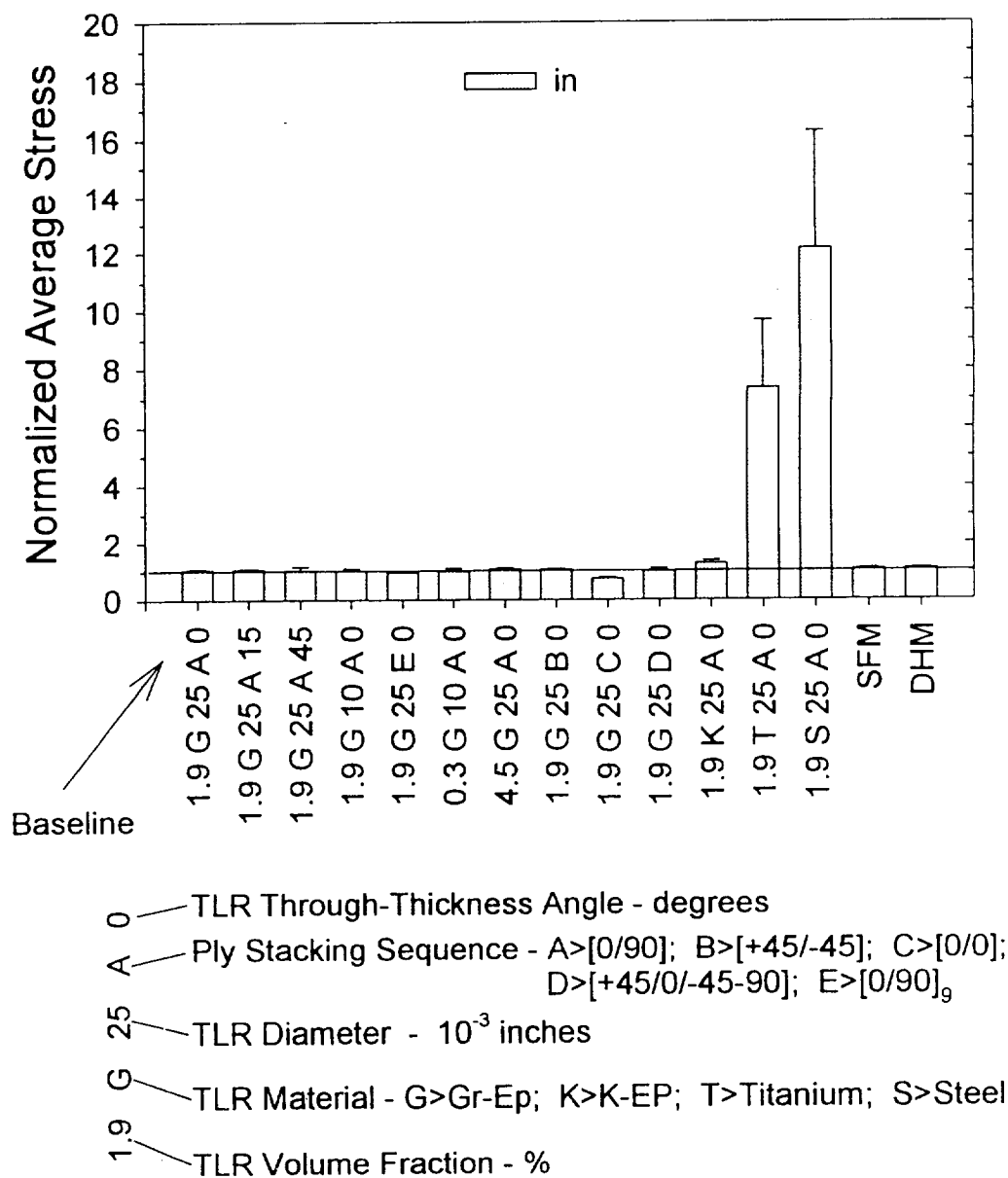
Figure 5-17 Normalized inter-laminar shear stress, τ_{xz}, at the interface averaged over the "in" area in the TLR. The key below the figure explains the identifiers used on the X axis.

Inter-Laminar Shear Stress, τ_{xz}
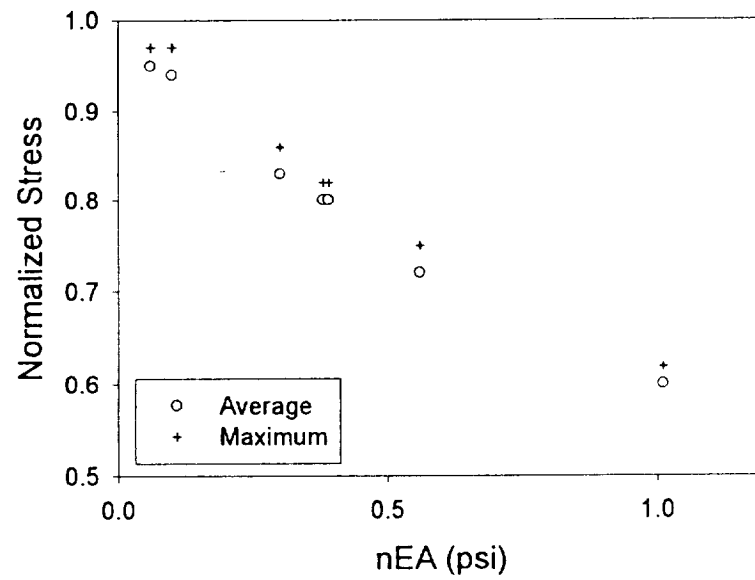

Key below figure:

$\underset{\text{O}}{}$ —TLR Through-Thickness Angle - degrees

$\underset{\text{A}}{}$ —Ply Stacking Sequence - A>[0/90]; B>[+45/-45]; C>[0/0]; D>[+45/0/-45-90]; E>[0/90]$_9$

$\underset{\text{25}}{}$ —TLR Diameter - 10^{-3} inches

$\underset{\text{G}}{}$ —TLR Material - G>Gr-Ep; K>K-EP; T>Titanium; S>Steel

$\underset{\text{1.9}}{}$ —TLR Volume Fraction - %
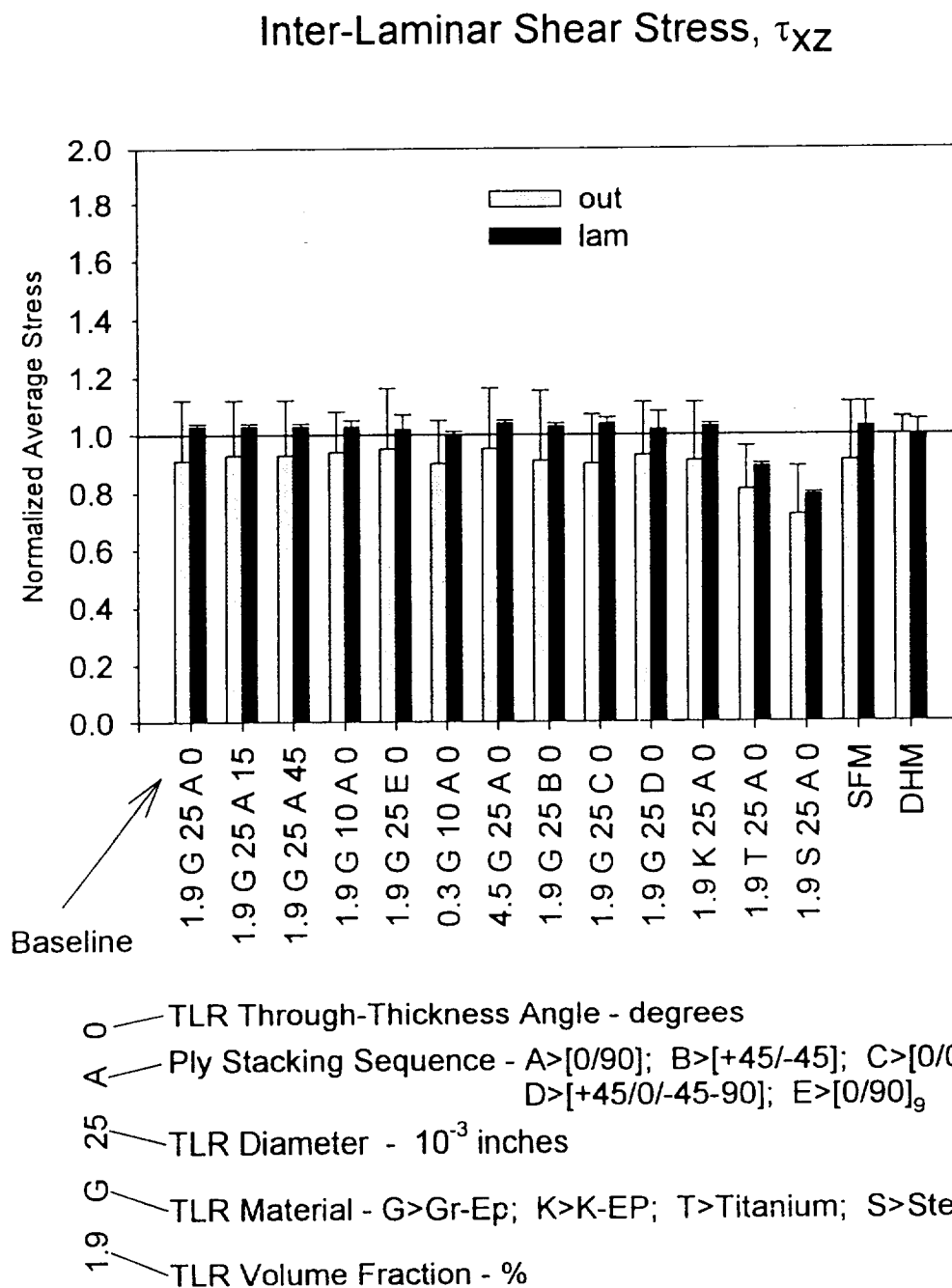
Figure 5-18 Normalized inter-laminar shear stress. τ_{xz}, at the interface averaged over the "out" and "lam" areas outside of the TLR. The key below the figure explains the identifiers used on the X axis.

Figure 5-19 Scatter plot of the normalized inter-laminar shear stress, τ_{xz}, over the "in," "out" and "lam" areas of the baseline model.

Inter-Laminar Shear Stress at the Ply Interface, τ_{xz}

Vf$_f$=1.9% d=0.025 TLR=Gr/Ep ψ=45

Figure 5-20 Scatter plot of the normalized inter-laminar shear stress, τ_{xz}, over the "in," "out" and "lam" areas of the model with the TLR at a through-thickness angle of 45°.
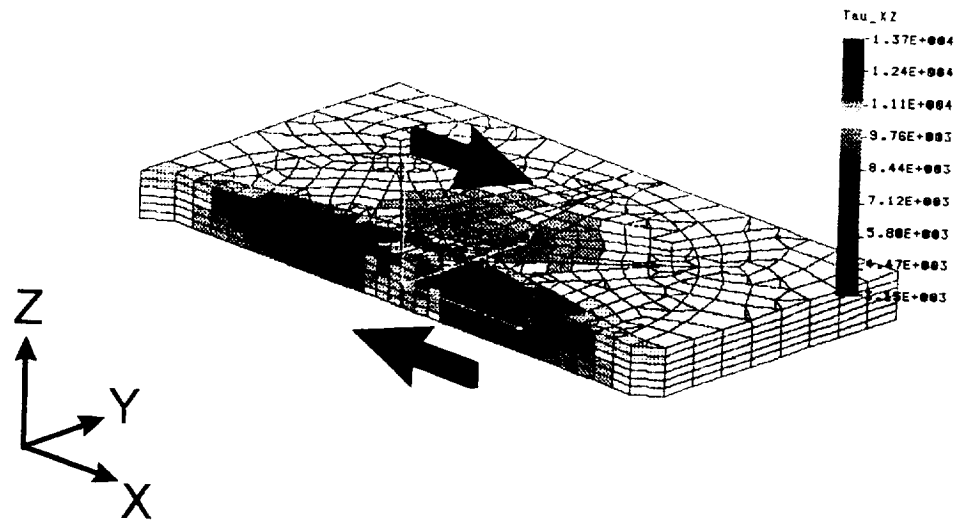
Figure 5-21   Inter-laminar shear stress, τ_{xz}, in the baseline model under γ_{xz} loading.
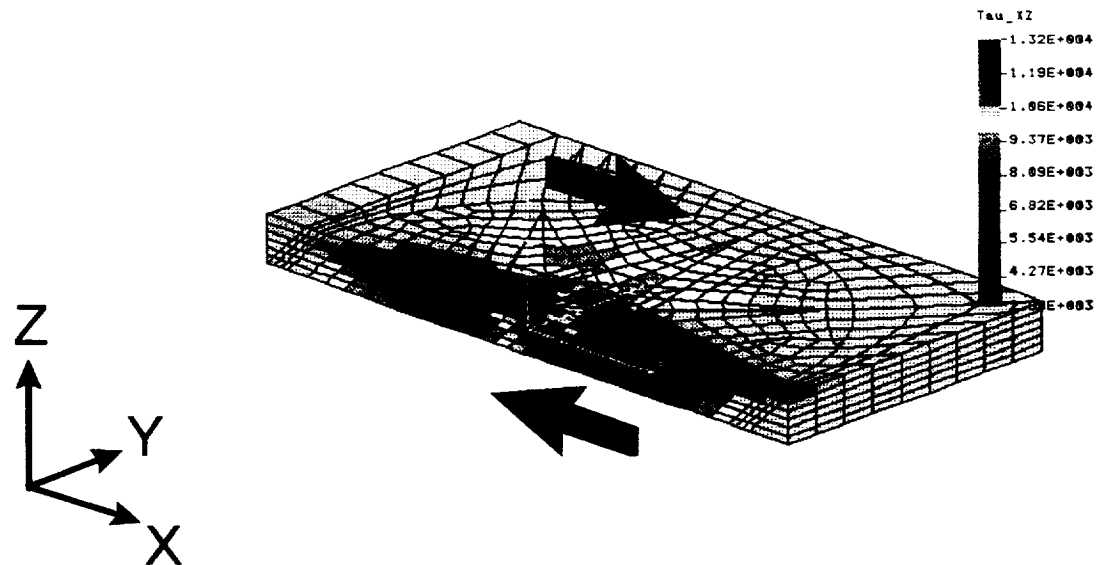
Figure 5-22 Inter-laminar shear stress, τ_{xz}, in the model with the TLR at a through-thickness angle of 45°, under γ_{xz} loading.

Inter-Laminar Shear Stress at the Ply Interface, τ_{xz}
V_f=1.9% d=0.025 TLR=Steel ψ=0
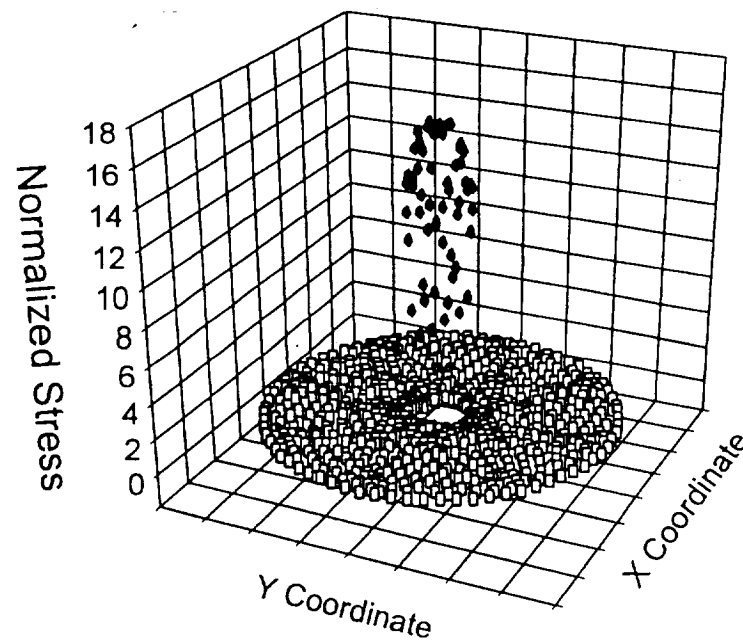
Figure 5-23 Scatter plot of the normalized inter-laminar shear stress, τ_{xz}, over the "in" and "out" areas at the interface in the Steel TLR model.

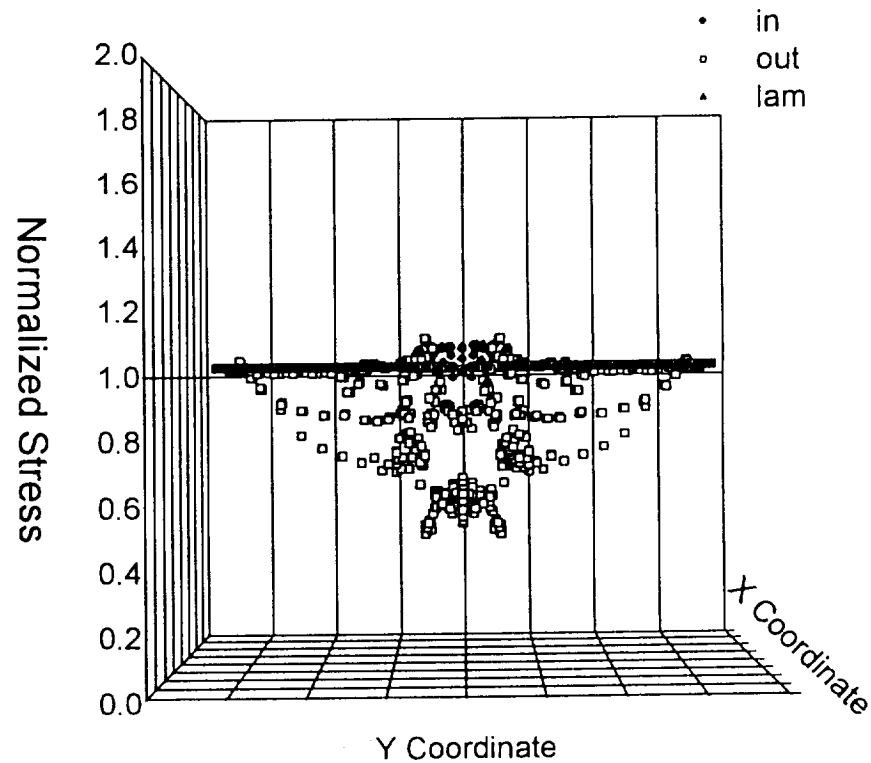Inter-Laminar Shear Stress at the Ply Interface, τ_{xz}
V_f=1.9% d=0.025 TLR=Steel ψ=0
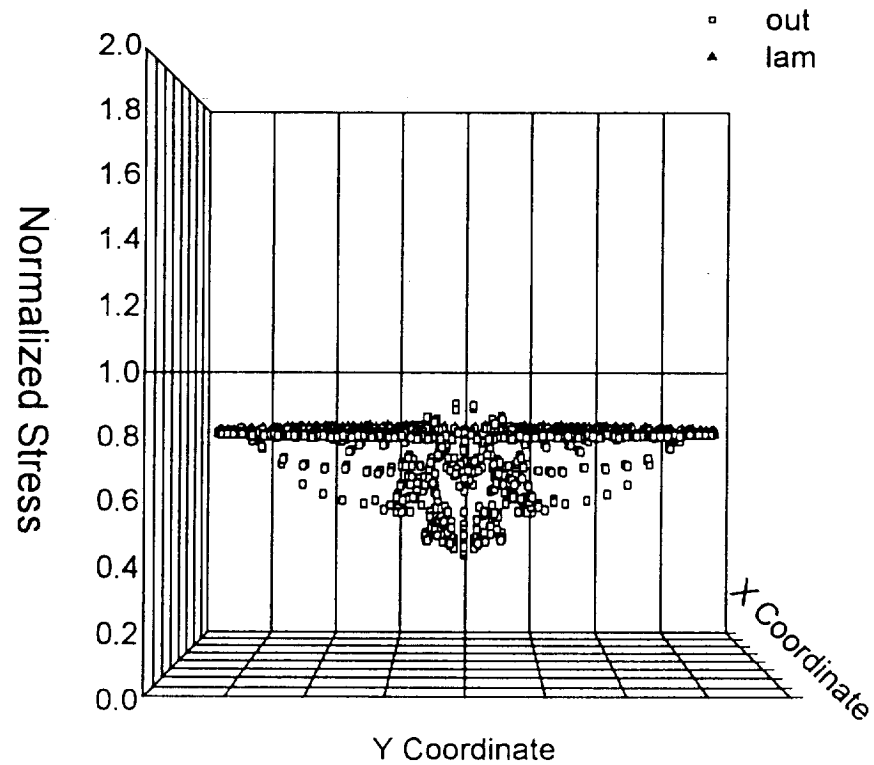
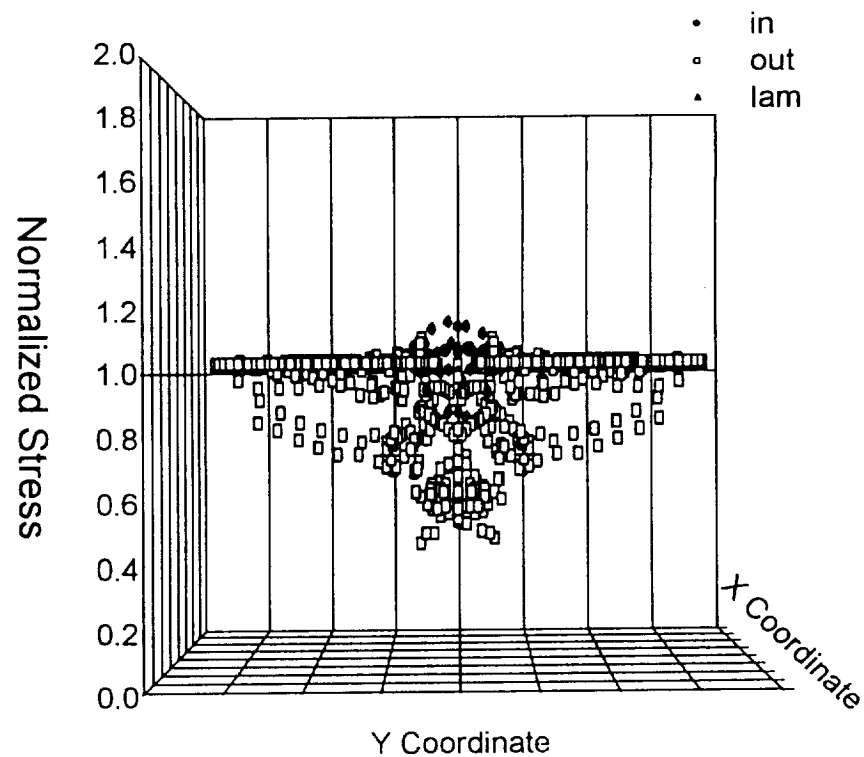**Figure 5-24 Scatter plot of the normalized inter-laminar shear stress, τ_{xz}, over the "out" and "lam" areas outside the TLR, at the interface of the steel TLR model.**
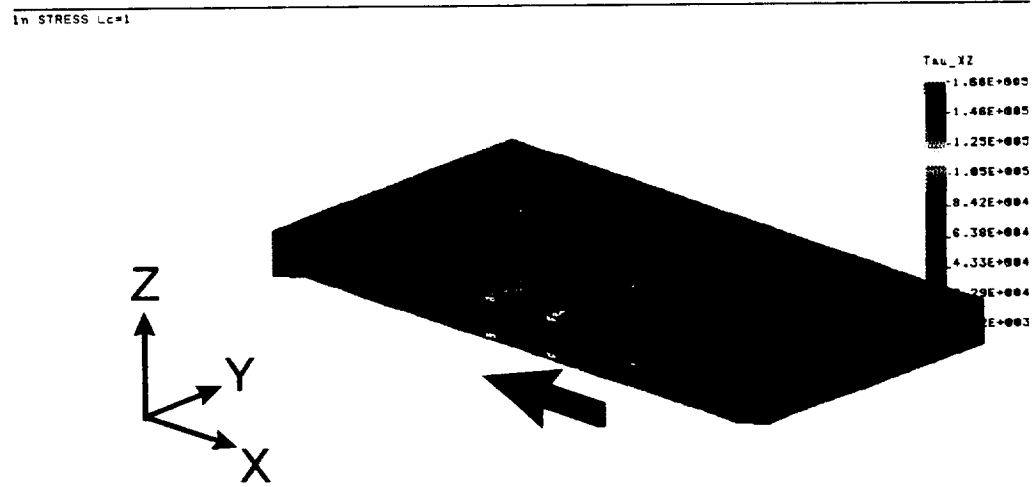
Figure 5-25 Inter-laminar shear stress, τ_{xz}, in the steel TLR model under γ_{xz} loading.

Maximum Transverse Tension Principal Stess, P1^{xz}

Baseline

$\underset{\longleftarrow}{0}$ TLR Through-Thickness Angle - degrees

$\underset{\longleftarrow}{A}$ Ply Stacking Sequence - A>[0/90]; B>[+45/-45]; C>[0/0]; D>[+45/0/-45-90]; E>[0/90]$_9$

$\underset{\longleftarrow}{25}$ TLR Diameter - 10^{-3} inches

$\underset{\longleftarrow}{G}$ TLR Material - G>Gr-Ep; K>K-EP; T>Titanium; S>Steel

$\underset{\longleftarrow}{1.9}$ TLR Volume Fraction - %
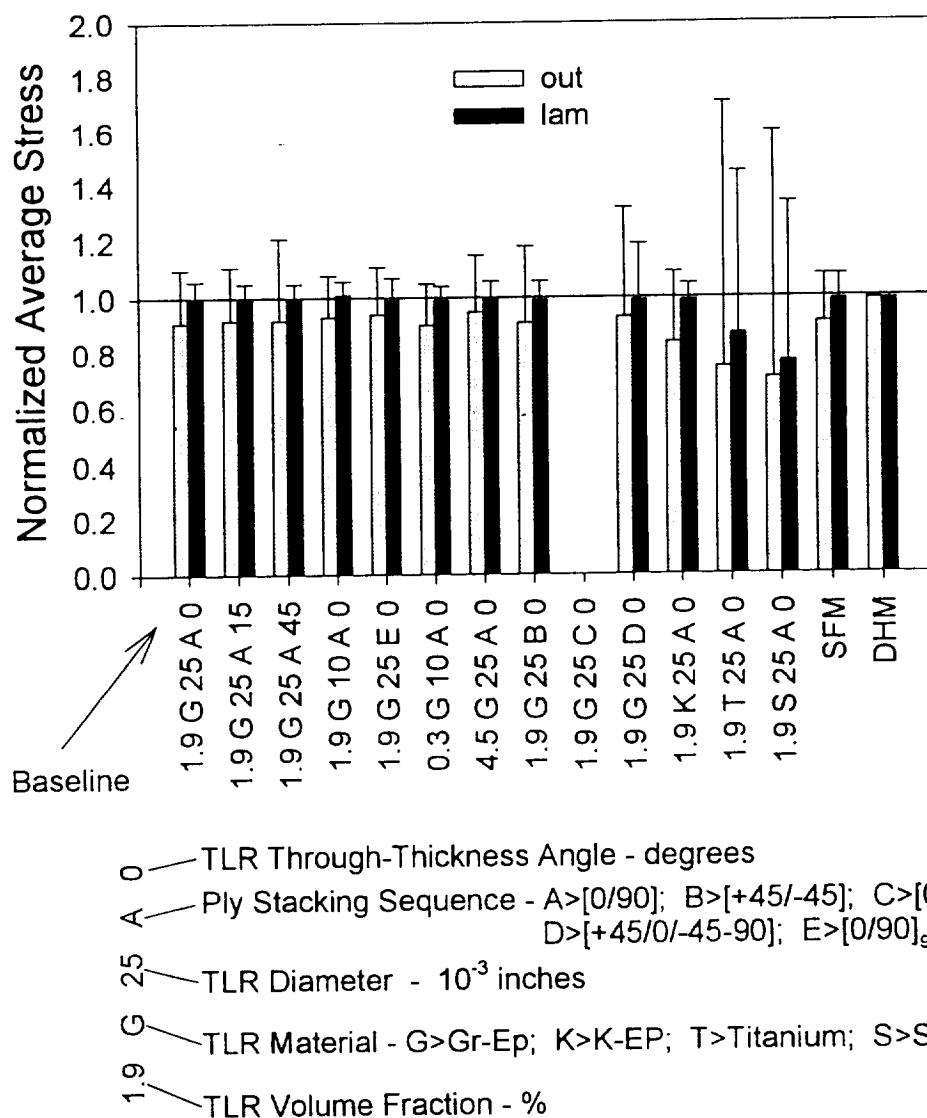
Figure 5-26 The normalized maximum transverse tensile stress, P1^{xz}, averaged over the "out" and "lam" areas for all model under γ_{xz} loading. The key below the figure explains the identifiers used on the X axis.
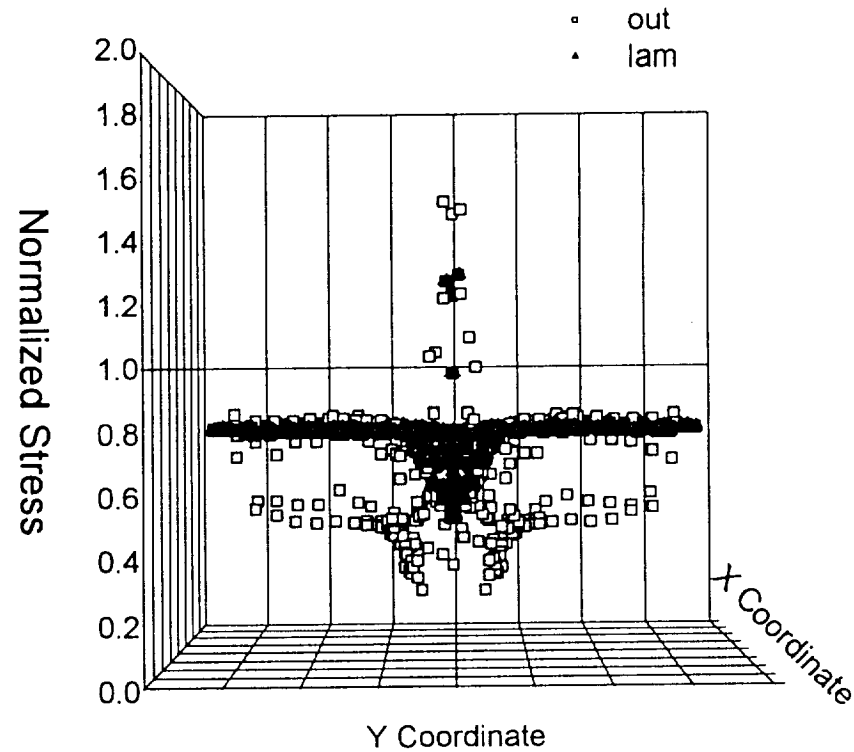
Figure 5-27 Scatter plot of the normalized maximum transverse tensile stress, $P1^{xz}$, over the "out" and "lam" areas within the 90° ply of the steel TLR model under γ_{xz} loading.

TLR Effective Shear Load versus τ_{xz} in "lam" Area
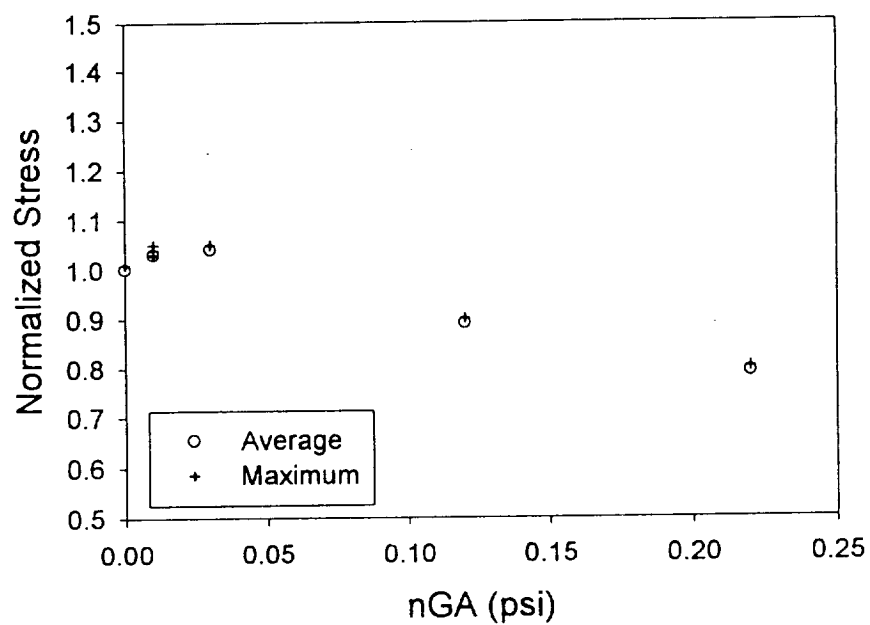
Figure 5-28 Effect of the TLR effective shear load, nGA, on the inter-laminar shear stress, τ_{xz}, in the "lam" area.

TLR Effective Shear Load versus $P1^{xz}$ in "lam" Area
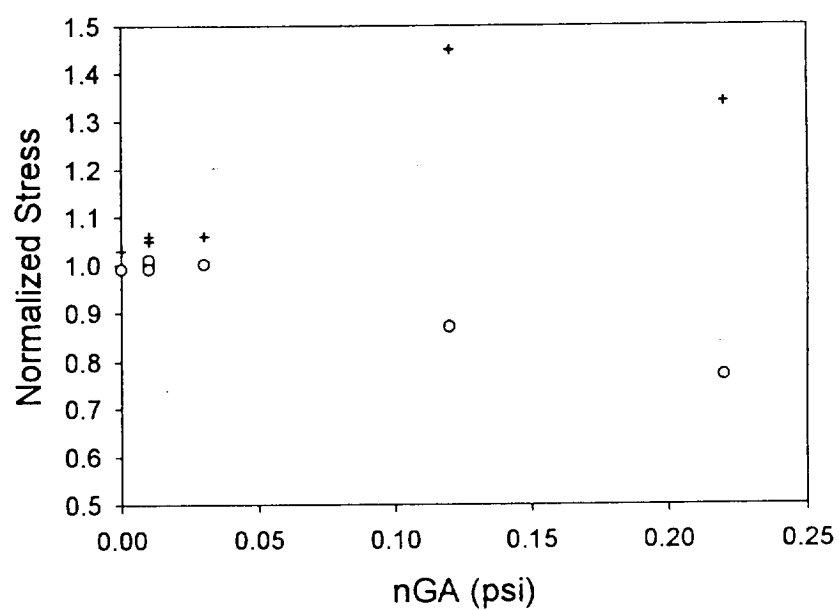
Figure 5-29 Effect of the TLR effective shear load, nGA, on the maximum transverse tensile stress, $P1^{xz}$, in the "lam" area.

CHAPTER 6
APPLICATION OF TLR TO AN INTER-LAMINAR DOMINATED PROBLEM

The results of the unit cell analysis presented in Chapter 5 were based on the assumption of a uniform loading applied to the unit cell. In actual structures made from composite materials, stress gradients in the regions where failure typically occur are not uniform, even over areas small enough to be on the scale of the unit cell. Hence the conclusions presented in the previous chapter need to be verified on a more realistic problem with non-uniform loading. In the following sections a simplified stiffener pull-off problem [156] is modeled and the results are presented in terms of damage initiation. A strength of materials approach similar to that discussed in Chapter 5 was used. This chapter closes with a few comments on the application and significance of the results.

6. 1.   SKIN-STRINGER DEBOND TEST AND MODEL

Secondarily bonding or co-curing frames or stringers to skins is one method of reducing or eliminating the use of fasteners. Such manufacturing techniques offers potential to provide an economical means of manufacturing composite stiffened structure. One potential problem with bonded or co-cured stiffener attachment is the disbonding of the stiffener from the skin. This disbonding typically results in the catastrophic failure of the structure.

The stiffener pull-off test is a common method of evaluating this weakness of bonded or co-cured composite stiffened structure. However, the typical stiffener pull-off

test specimen is expensive to fabricate and test, making the use of this test for materials screening impractical. A simplified test of the bond strength between a skin and a secondarily bonded or co-cured stiffener has been proposed for when the dominant loading in the skin is flexure along the edge of the stiffener [156]. An illustration of the stiffener-skin problem is shown in Figure 6-1. The test is performed by putting a flanged skin in three or four point bending, as shown in Figure 6-2 and Figure 6-3. The flange-skin specimen is thus a representation of larger stiffened skin structure. This simple and relatively inexpensive test captures the same failure mechanisms as in the larger structure. The authors of [156] used both detailed observations of failure and finite element analysis to determine that failure initiates at the tip of the flange, either at the interface between the stiffener and skin or in the topmost skin ply.

In order to model a problem of reasonable size that captures both the correct loads and failure mechanisms, the tapered flange-skin specimen shown in Figure 6-2 was modeled in three point bending. The model details are discussed in section 3.4. The FEA mesh is shown in Figure 6-4. Four different versions of this basic model were analyzed. The control model without TLR is shown in Figure 6-4. This baseline model was duplicated and TLR was added by changing the material properties for certain elements. Three variations were examined: a graphite-epoxy TLR with a diameter of 0.025 inches, a graphite-epoxy TLR with a diameter of 0.008 inches, and a steel TLR with a diameter of 0.008 inches. The FEA mesh for the stiffener-skin models with TLR is shown in Figure 6-5. As discussed in section 3.4, there were two major limitations associated with these large models: the FEA mesh was not fine enough to accurately capture the severe stress gradients associated with the different and discontinuous materials of the composite

microstructure, and error was introduced by using the COSMOS/M "bond" feature to join

regions of incompatible mesh. In spite of these limitations, it was felt that these models

were sufficient to address the issue of damage initiation between individual TLR.

6. 2.   EFFECT OF TLR ON DAMAGE INITIATION

Use of the finite element method results in detailed stress and strain information at

every point in the model. The following discussion will focus on the stress results for

selected regions of interest. These regions of interest, shown in Figure 6-6, are at the

interface between the skin and flange and within the topmost +45 ply of the skin. These

regions correspond to where failure was observed to have initiated [156]. In order to

avoid potential boundary effects, the results will be shown only for internal nodes. Values

for nodes within three elements of the edge of the specimen are not shown. The given

stress results consist of the "nodal stress" output from COSMOS/M, defined as the

average of the values of element stress at the node for all the elements to which that node

belongs.

Contour plots of the inter-laminar normal and shear stresses for the four models

are shown in Figure 6-7 through Figure 6-10. The stress scale is kept constant for all four

of the figures. The range of stress shown does not include the maximum stresses

encountered in the TLR, but rather allows a comparison of what is happening between the

TLR in the various models.

As required physically, the inter-laminar normal and shear stresses are zero at the

surface of the skin not covered by the flange. In the case without TLR (Figure 6-7) there

is a concentration of both normal and shear stress just behind the flange tip. This

concentration is a result of both the geometrical and material discontinuities where the bottom ply of the flange ends. This concentration of stress is partially due to the artificially sharp corner in the FEA model. The real material would have a corner of some radius. Nonetheless, it is in this region that failure initiated according to the experimental observations in [156]. The objective of this analysis was not to determine exact stress values, but rather to study the effect of the TLR. The inter-laminar stresses for the models with TLR are shown in Figure 6-8 through Figure 6-10. As can be seen in the figures, the areas of stress concentrations remain, but are somewhat reduced.

It is difficult to make quantitative comparisons with contour plots such as those shown in Figure 6-7 through Figure 6-10. To gain a better feel for stress state at the interface, three dimensional surface plots of the inter-laminar normal stress for the cases without TLR and with steel TLR are shown in Figure 6-11 and Figure 6-12. In the case without TLR, the stress concentration just behind the flange tip is clearly visible as a ridge of high stress. A somewhat shorter ridge of stress is evident in the surface plot of the results for the model with steel TLR. The locations of the TLR are clearly indicated by the sharp spikes. The values in and next to the TLR are known to be inaccurate due to the very high stress gradients and coarse finite element mesh.

Although the three dimensional surface plot gives a different perspective of the stress state at the interface, quantitative comparisons of models with and without TLR are still difficult. To make such comparisons, the normalized stress was calculated and plotted for a row of nodes across the width of the model. The point of intersection of this Y direction row of nodes and the XZ plane is shown in Figure 6-6. The normalized stress

was calculated by taking the value of stress at a node in a model with TLR and dividing it by the value of stress for the same node in the control model without TLR. Values less than one indicate that adding the TLR lowered the stress at that point. The normalized shear and normal stresses at the interface between the flange and skin and the normalized maximum transverse tensile stress within the top $+45°$ ply of the skin are shown in Figure 6-13 through Figure 6-15. The results for all three models with TLR are plotted in each figure. The position across the width (Y direction) begins and ends three elements in from the edge of the specimen. The TLR locations are marked on the plot with both the small diameter and large diameter TLR position being indicated in the same figure. The values for the nodes that reside inside the TLR are not plotted. Although there may be some question as to the accuracy of the values for the nodes inside of and next to the TLR, this discussion is focused on the area between the TLR and the initiation of damage therein.

The normalized inter-laminar normal stress, σ_z, at the interface between the flange and skin is shown in Figure 6-13. The normalized stress for both models with Gr-Ep TLR stay at or near a value of one. Therefore it was concluded that adding two percent of Gr-Ep TLR did not lower the tendency to delaminate due to a high σ_z. However, adding the steel TLR did lower the normal stress. The normalized values were in the 0.80 to 0.85 range in the regions between the steel TLR. Hence, compared to a structure without TLR, the addition of steel TLR would result in higher loads being required to get the area between the TLR to fail due to the inter-laminar normal stress.

The same trend was observed in the normalized inter-laminar shear stress, τ_{xz}, at the flange-skin interface (see Figure 6-14). Only the steel TLR made a difference in the

stress in the unreinforced regions between the TLR. There was also no significant gradient of stress across the region between the TLR, a distance six times the diameter of the TLR.

Interpreting these results alone leads to a conclusion similar to that discussed in the previous chapter; only an extremely stiff TLR such as steel can pick up the inter-laminar loads and relieve the inter-laminar stress in the region between the TLR. Such an effect would delay the onset of a delamination caused by direct inter-laminar stress.

However there is also the question of transverse cracking. As discussed in section 5.2, if within the ply the maximum transverse tensile principal stress, P1, is higher than the transverse tensile strength of the lamina, a transverse crack will form. The normalized maximum transverse tensile stress, P1, is plotted in Figure 6-15. There are fewer points plotted because this region of the model was represented by only the mid-side nodes of the 20 node brick elements. These results are consistent with those of the inter-laminar stresses; only the steel TLR decreased the propensity to transverse crack within the top 45° ply of the skin. This finding was also discussed in the results of the previous chapter. However, unlike in Chapter 5, these large coarse models do not allow examination of the stresses next to the TLR where the likelihood of transverse cracking may be increased.

6. 3. SIGNIFICANCE AND APPLICATION

As was the case in the unit cell models, these flange-skin models were proposed with the limiting assumptions of perfect bonding and complete load transfer between the lamina and the TLR. These assumption are unlikely to hold true in most real TLR composites. If these limitations are set aside, the results of the flange-skin modeling can

be interpreted to conclude that only TLR with a stiffness on the order of that of steel can be effective at preventing the initiation of delamination. However, as noted in the literature review discussed in Chapter 1, Kevlar® threads have been used by many researchers to increase the performance of laminates in many inter-laminar dominated tests. This fact, along with the lack of prevention of damage initiation by Kevlar®-epoxy and graphite-epoxy TLR, leads to the hypothesis that the true benefit of TLR lies only in its ability to retard the growth of damage, and not in an any potential capability to prevent it from initiating.
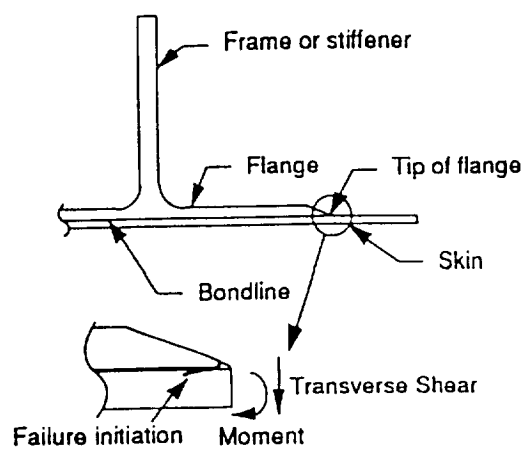
Figure 6-1 Illustration of stiffener-skin interface [156].
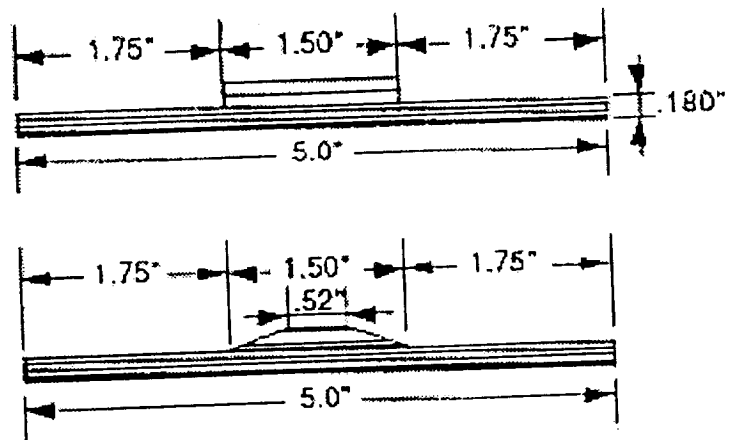
Figure 6-2 Proposed flange-skin test specimens for simulation of the stiffener-skin disbond problem in a stiffener pull-off test [156].
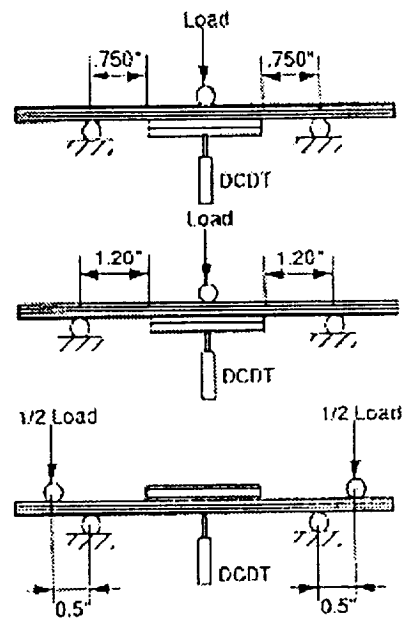
Figure 6-3 Bending test configurations for flange-skin test [156].
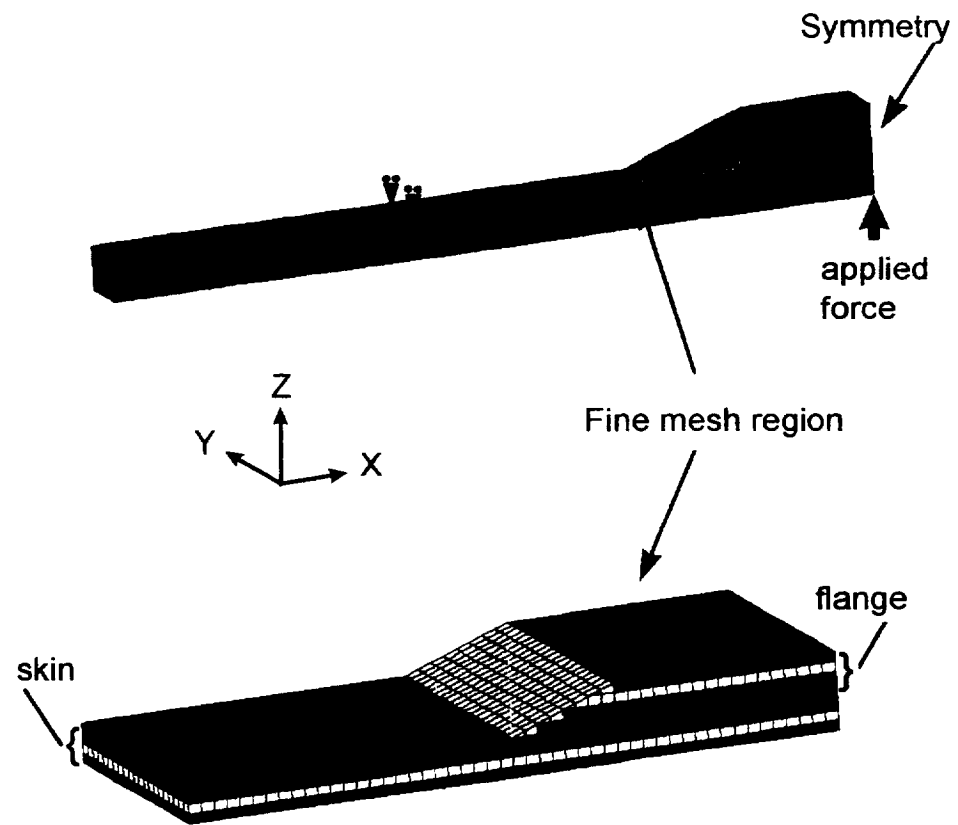
Figure 6-4 Finite element model of the flange-skin specimen without TLR.
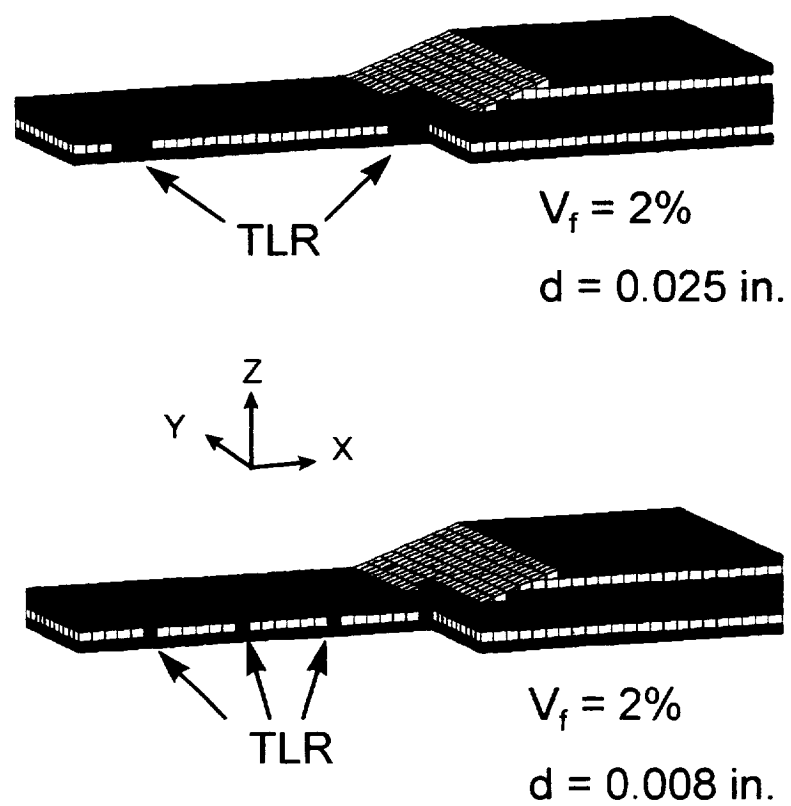
Figure 6-5 Fine mesh regions of flange-skin FEA models with TLR.
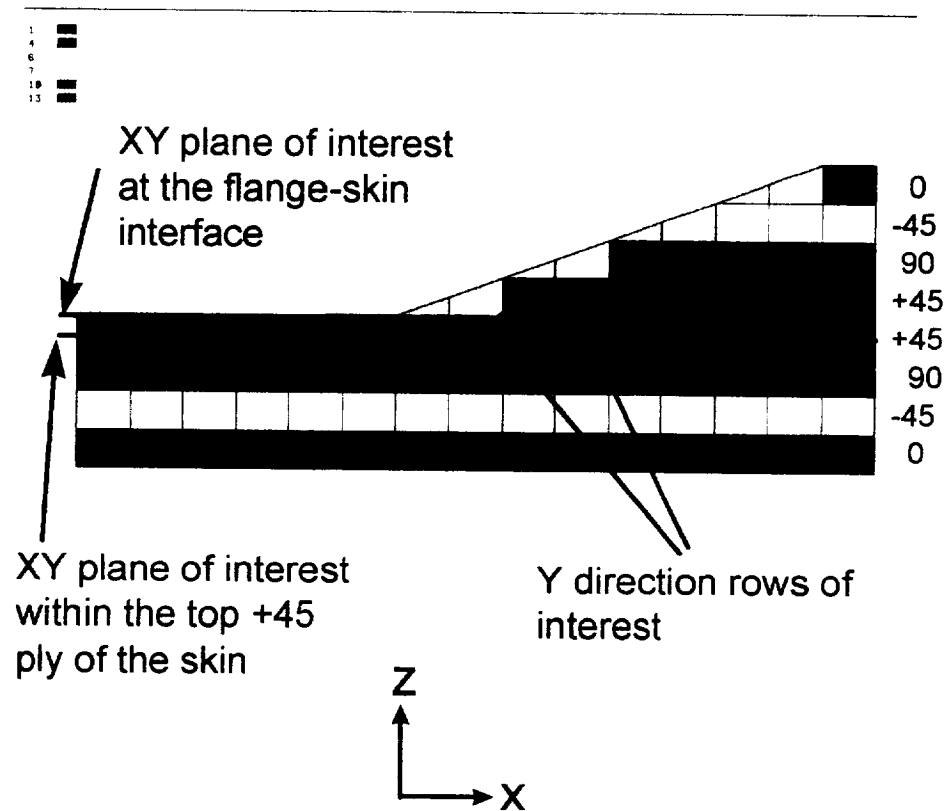
Figure 6-6 Regions of interest in the flange-skin specimen model over which stress is plotted in subsequent figures.
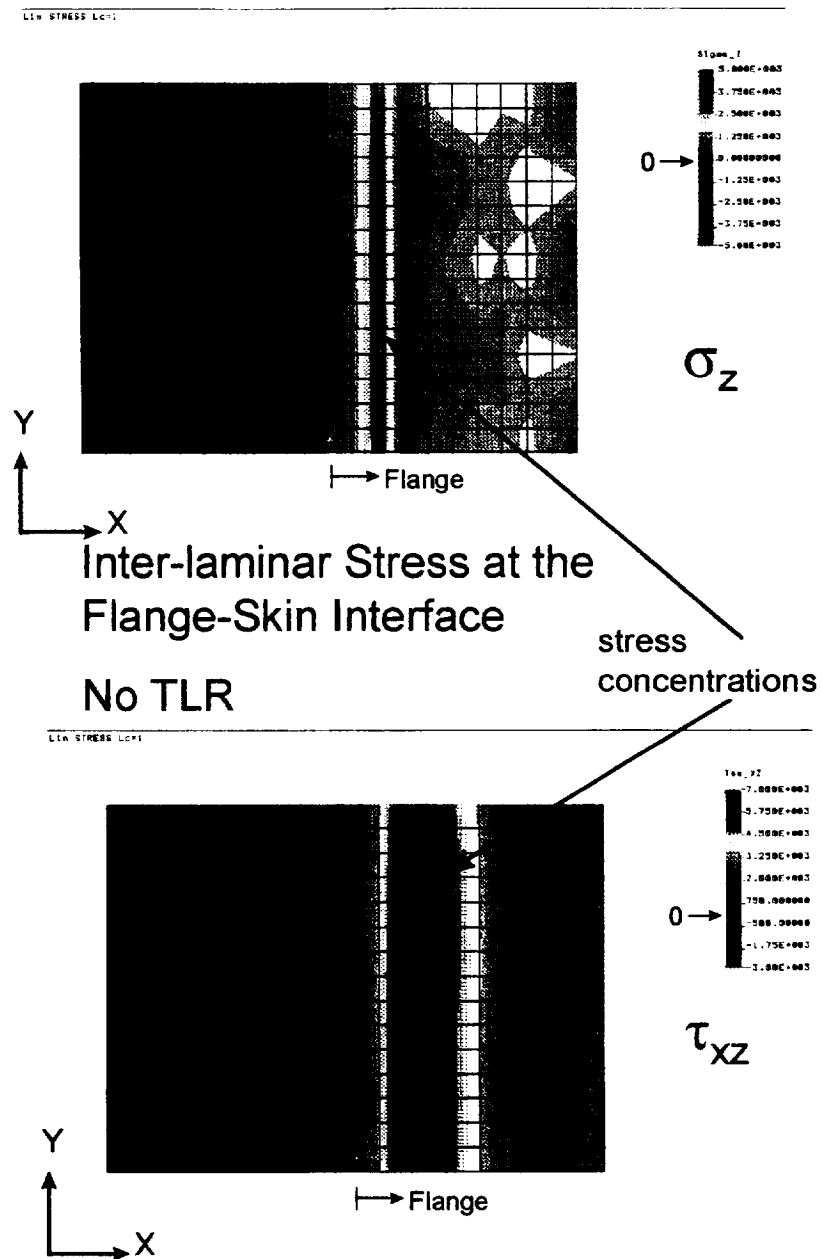
Figure 6-7 Inter-laminar normal and shear stresses at the flange-skin interface in the control model without TLR.
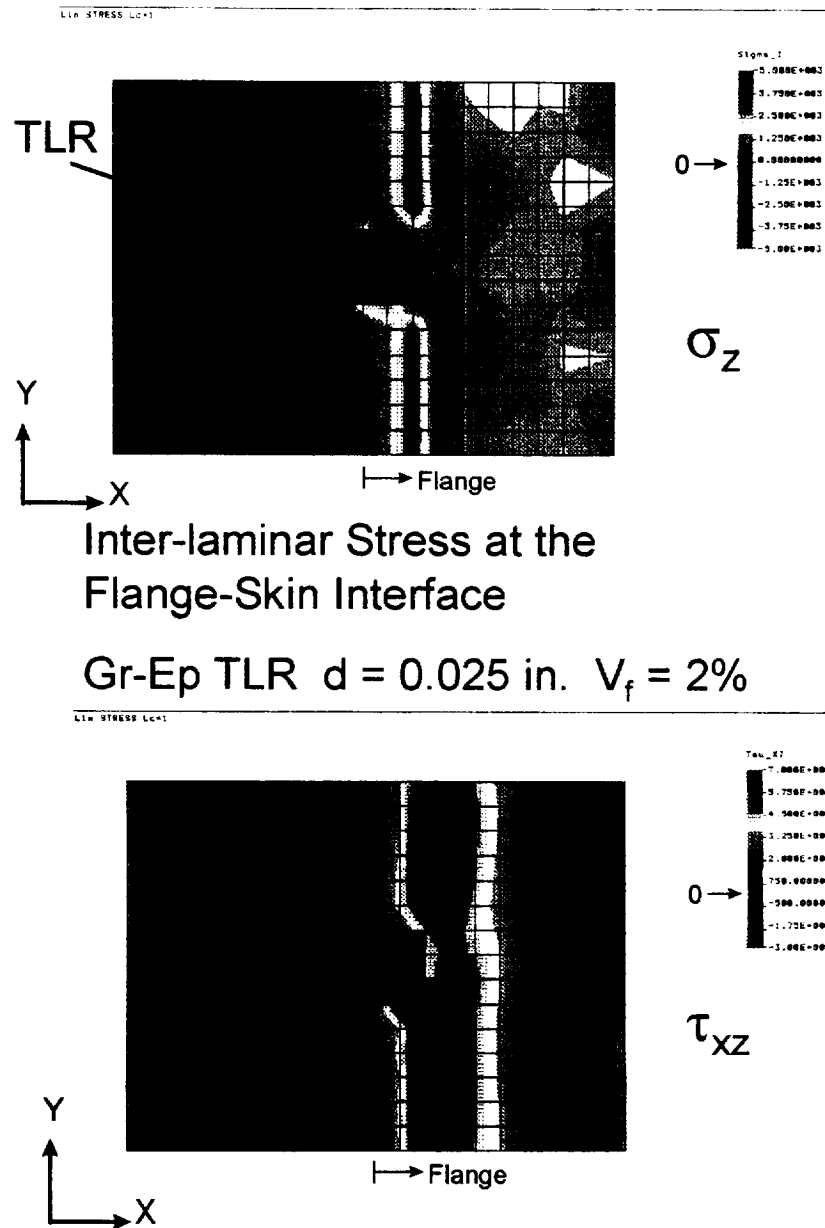
Figure 6-8 Inter-laminar normal and shear stresses at the flange-skin interface in the model with Gr-Ep TLR of diameter 0.025 inches at a volume fraction of two percent.
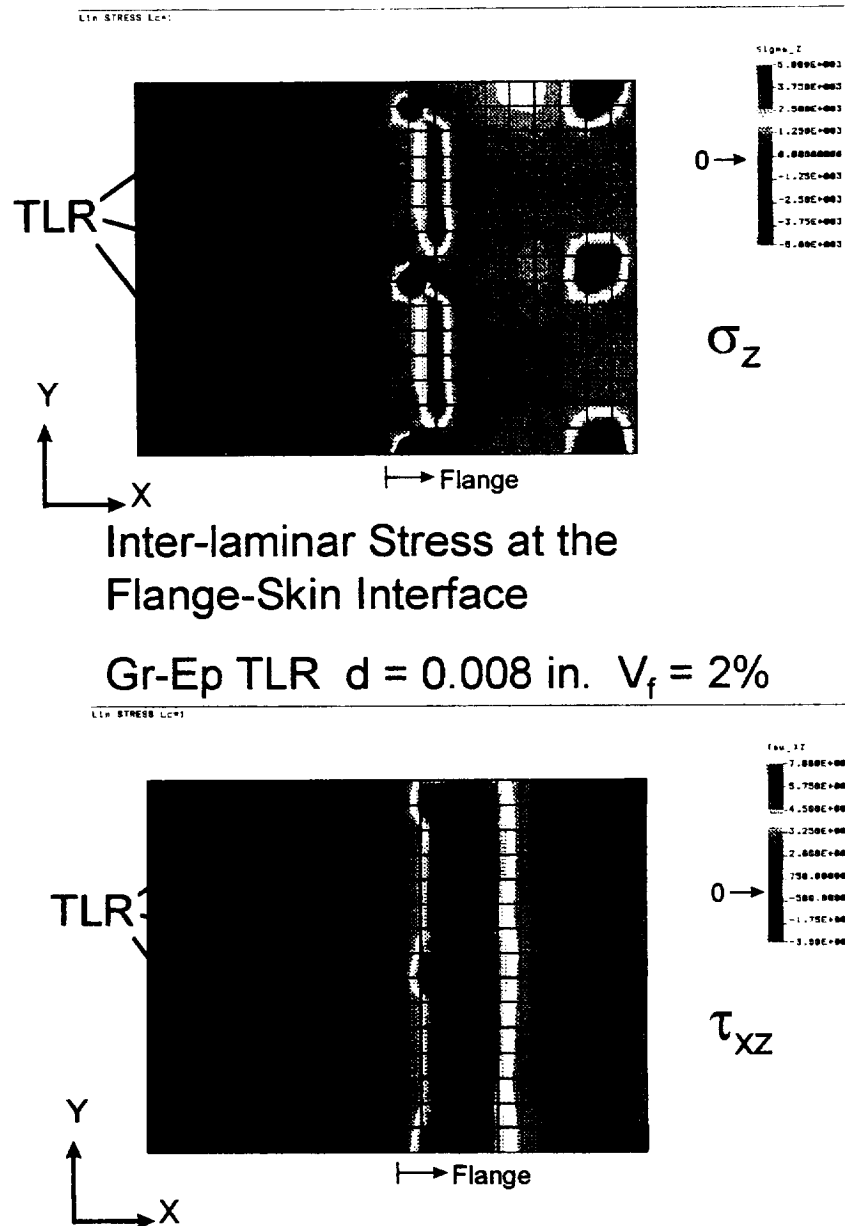
Figure 6-9 Inter-laminar normal and shear stresses at the flange-skin interface in the model with Gr-Ep TLR of diameter 0.008 inches at a volume fraction of two percent.
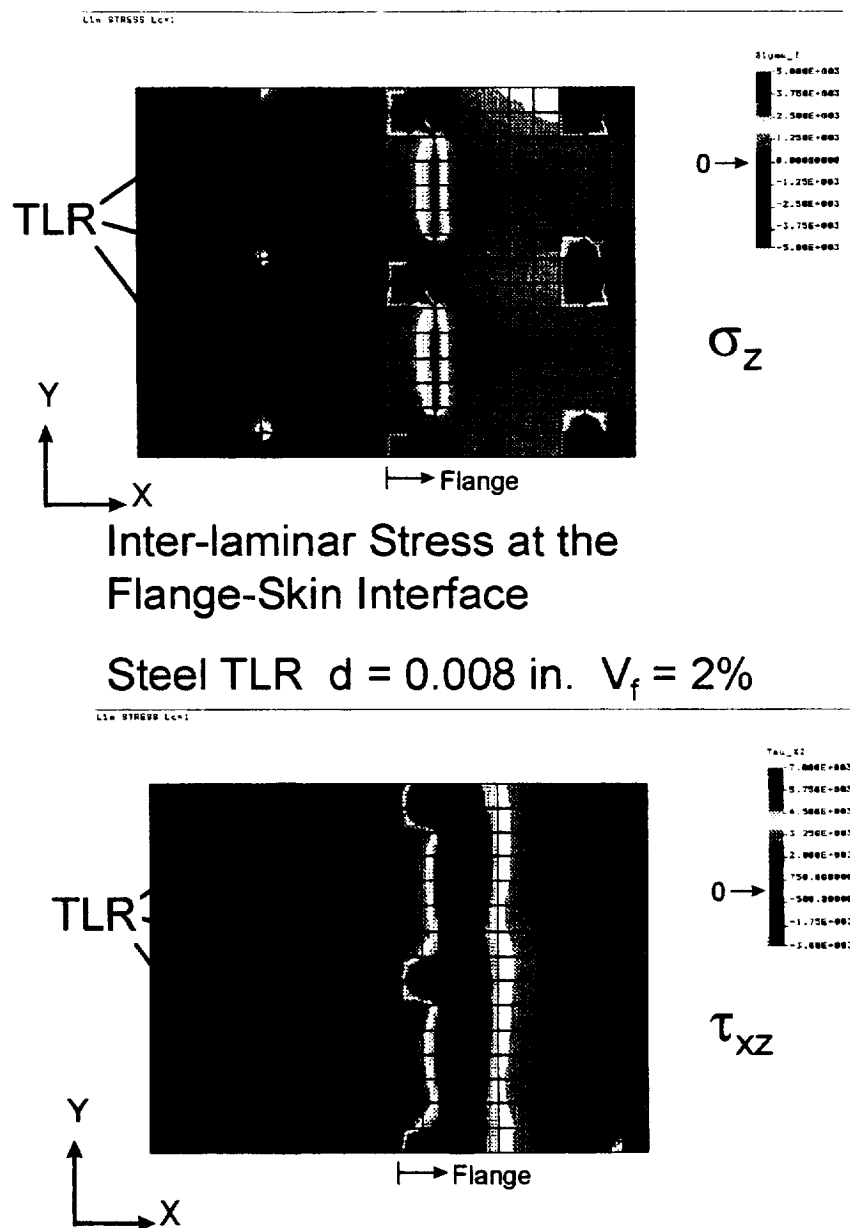
Figure 6-10 Inter-laminar normal and shear stresses at the flange-skin interface in the model with steel TLR of diameter 0.008 inches at a volume fraction of two percent.

σ_Z at the Flange-Skin Interface
Control Model Without TLR
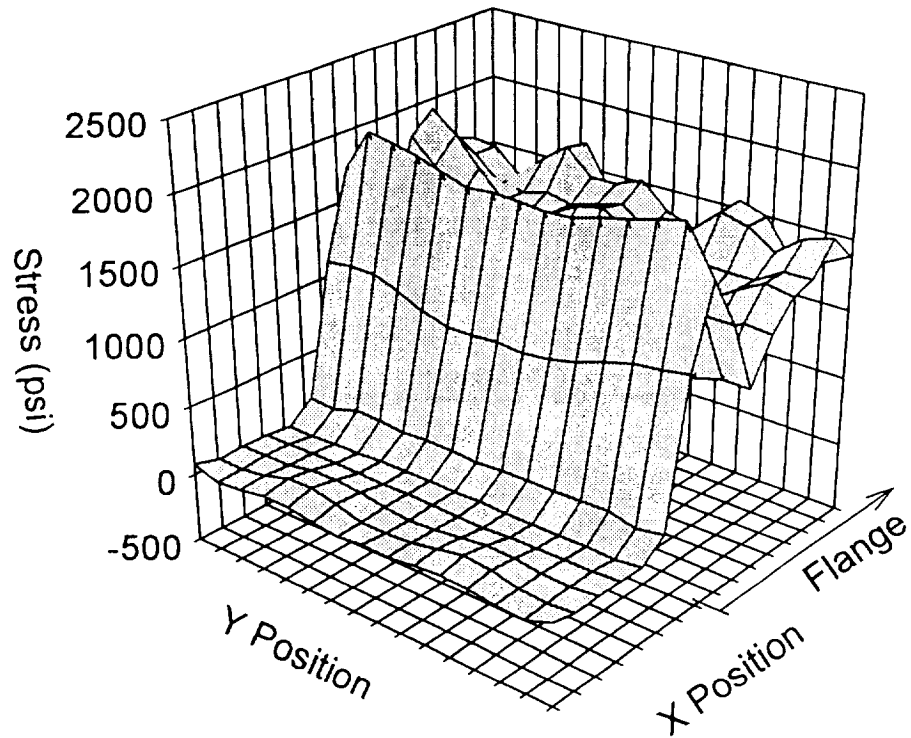
Figure 6-11 Inter-laminar normal stress at the flange-skin interface for the control model without TLR.

σ_Z at the Flange-Skin Interface
Steel TLR d = 0.008 in.
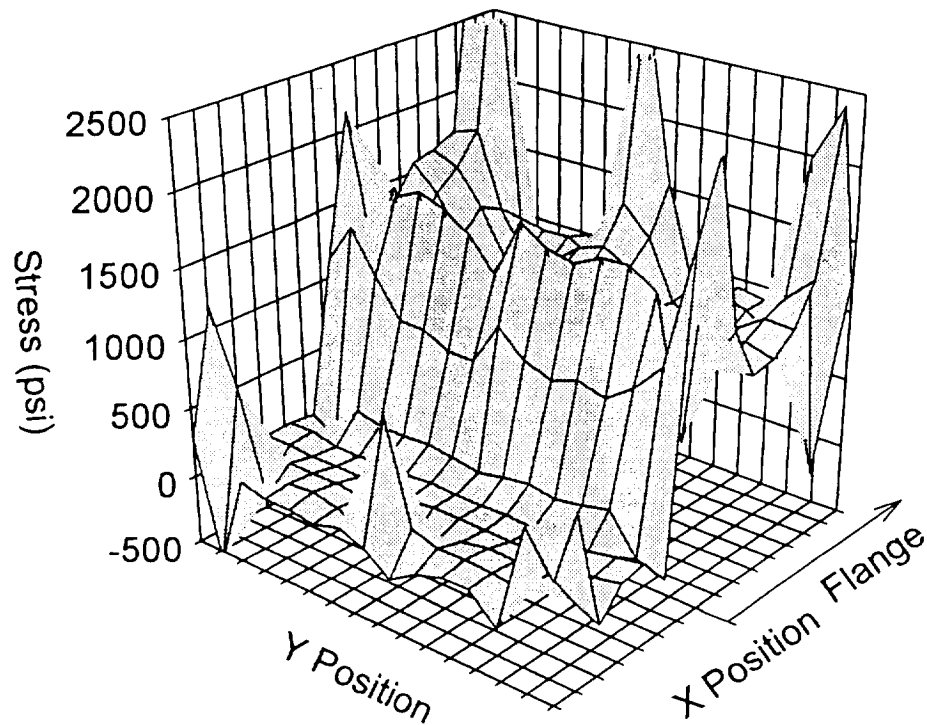
Figure 6-12 Inter-laminar normal stress at the flange-skin interface for the model with steel TLR of diameter 0.008 inches at a volume fraction of two percent.

σ_Z at the Flange-Skin Interface

Positon Across the Width

Legend:
- —○— Gr-Ep TLR d = 0.025 in.
- —▼— Gr-Ep TLR d = 0.008 in.
- —■— Steel TLR d = 0.008 in.
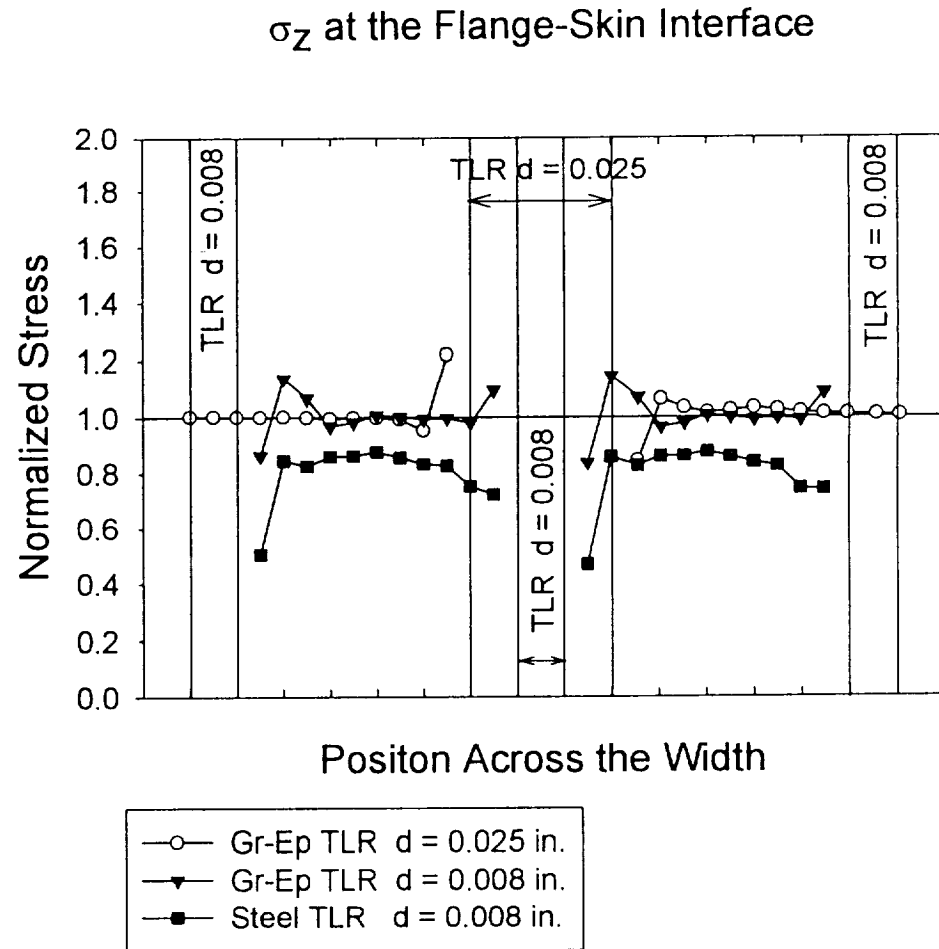
Figure 6-13 Normalized inter-laminar normal stress across the width of the model at the flange-skin interface just behind the flange tip.

τ_{XZ} at the Flange-Skin Interface
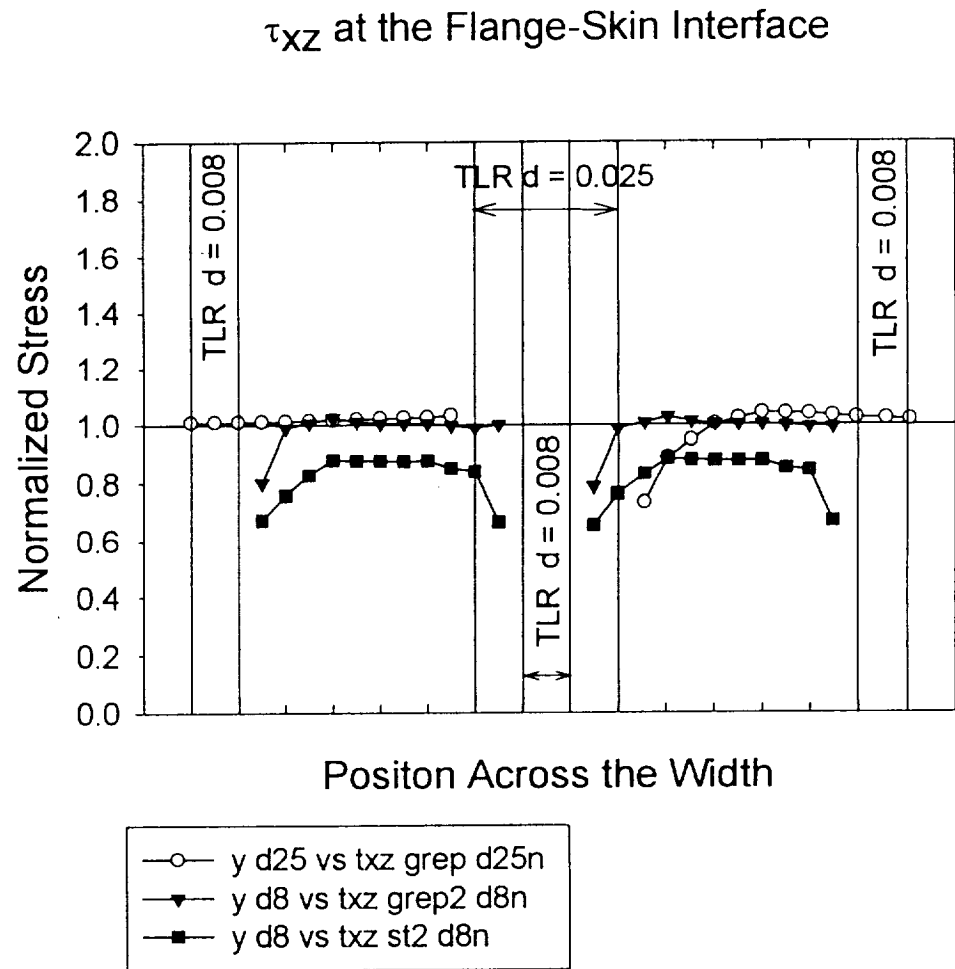
Figure 6-14 Normalized inter-laminar shear stress across the width of the model at the flange-skin interface just behind the flange tip.
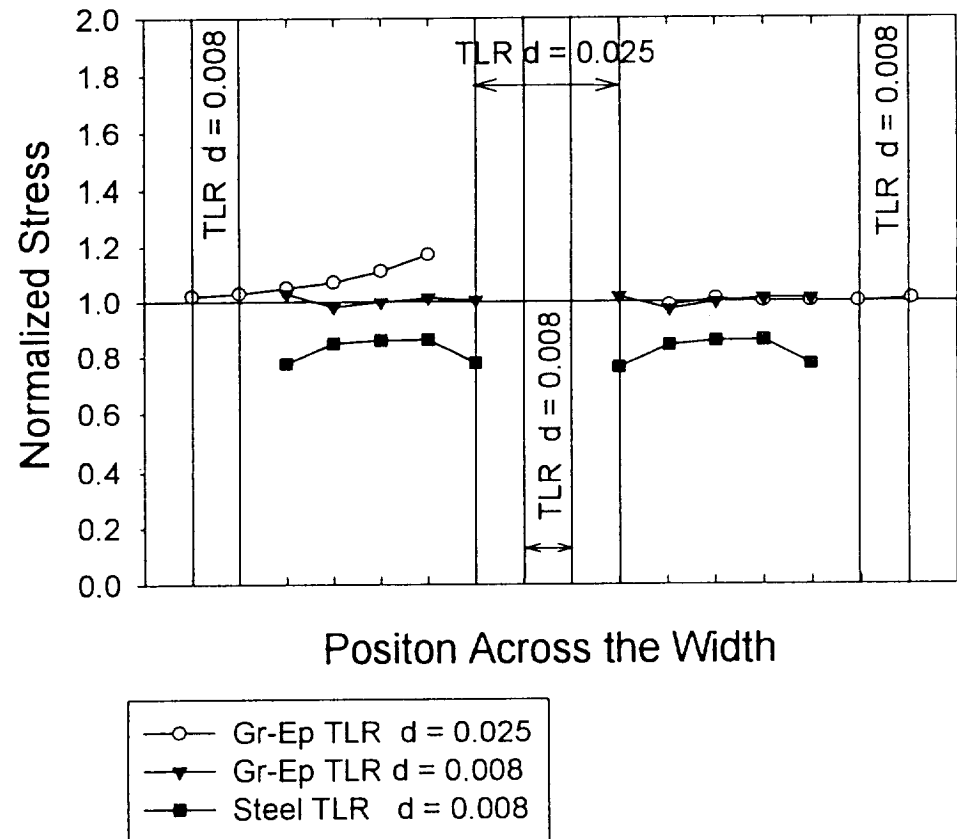
Figure 6-15 Normalized maximum transverse tensile stress within the top +45° ply of the skin, across the width of the model just behind the flange tip.

CHAPTER 7
SUMMARY AND CONCLUDING REMARKS

A Trans-Laminar-Reinforced (TLR) composite has been defined in this work as a composite laminate with up to five percent of its volume in the form of fibrous reinforcement oriented in a trans-laminar fashion in the through-thickness direction. The trans-laminar reinforcement can be in the form of continuous rovings or threads inserted by industrial stitching machines. TLR can also take the form of discontinuous rods or pins. Z-Fiber™ materials are a commercial example of discontinuous TLR. Both analytical and experimental work documented in the literature has consistently demonstrated that adding TLR to an otherwise two dimensional laminate results in the following advantages: significant increase in the load required for sublaminate buckling of delaminated plates; substantial improvements in the compression-after-impact response; considerable increase in the fracture toughness in mode I (double cantilever beam) and mode II (end notch flexure); and severely restricted size and growth of impact damage and edge delamination. TLR has also been shown to completely eliminate catastrophic stiffener disbonding as a failure mode in stiffened structures. Many of these benefits have been documented for both static and fatigue loading. By bridging cracks between lamina, even small amounts (order of one percent volume) of TLR significantly alter the mechanical response of the laminate and directly strengthen a severe weakness of laminated composites, that is delamination.

Considerable research is being conducted on crack bridging mechanisms and the restriction of damage growth offered by the addition of TLR. A primary objective of this work was to examine the issue of whether or not TLR is of benefit in delaying the onset of delamination initiation. To that end, detailed three dimensional finite element analyses of a "unit cell" or representative volume, were performed. The effects of various parameters were studied including TLR material, TLR volume fraction, TLR diameter, TLR through-thickness angle, ply stacking sequence, and the microstructural details of pure resin regions and curved in-plane fibers. The work was limited to the study of the linear response (undamaged) of a unit cell with a ply interface. The unit cell results were used to examine the effects of TLR on the elastic constants, in-plane tension and compression strength, and delamination initiation.

The calculation of the elastic constants, or engineering constants, was performed by applying a known stress to a unit cell constrained to deform in a shape consistent with the basic definitions of strain. The displacements were then used to calculate macrostrains. These macrostrains along with the known applied macrostress were used in constitutive relations resulting in the calculation of the full set of nine elastic constants for an orthotropic material. It was found that adding only a few percent of TLR had a small negative effect on the in-plane extensional and shear moduli, E_x, E_y and G_{xy}, but had a large positive effect (up to 60 percent) on the thickness direction extensional modulus, E_z. Although this positive change was significant, the actual values were still small relative to the in-plane extensional moduli. The volume fraction and the extensional modulus of the TLR were the controlling parameters in terms of overall thickness direction extensional modulus, E_z. The out-of-plane shear moduli, G_{xz} and G_{yz}, were significantly affected only

when steel or titanium TLR were used. The shear moduli of steel and titanium are an order of magnitude higher than the out-of-plane shear moduli of an unreinforced laminate.

The elastic constants were also calculated by using a stiffness averaging method documented in the literature. The two methods agreed to within ten percent for calculations of extensional moduli, E_x, E_y, and E_z, and in-plane shear modulus, G_{xy}. The out-of-plane shear moduli, G_{xz} and G_{yz}, varied by as much as 21 percent.

The stress results of the unit cell analyses were used to draw implications about the in-plane tension and compression strength of TLR materials. Adding TLR caused a stress concentration which was lessened by the presence of pure matrix regions and curved fiber next to the TLR. It was speculated that the reduction of in-plane properties would be inconsequential if the diameter of the TLR were sufficiently small or if the material's failure was dominated by other stress concentrations such as those found at open holes and bolted repairs.

The initiation of delamination was investigated using a strength of materials approach. In this approach, a maximum stress failure criterion was used to indicate the likelihood of delamination. A delamination was assumed to initiate when either 1) the inter-laminar stress at a ply interface exceeded the inter-laminar strength, or 2) the state of stress within a ply exceeded the transverse tension strength resulting in a transverse crack that could then grow into a delamination. Rather than predicting the exact stresses of failure, comparisons were made between models with and without TLR. This approach enabled a direct examination of the effect of adding TLR. This method of investigating delamination initiation was applied to the unit cell analyses and to an inter-laminar

dominated problem of practical interest. A flanged skin in bending was analyzed with a large finite element model. The flange-skin specimen has been proposed by other researchers as a simplified test capturing the important aspects of frame-skin disbonding failure in stiffened structure.

The results of both the unit cell and flange-skin modeling were used to conclude that the addition of TLR may delay the direct formation of a delamination due to high inter-laminar stress only when the TLR is composed of extremely stiff material such as steel. With such stiff TLR, the load path across the ply interface changes and the inter-laminar stress is directed away from the interface and into the TLR. For this to occur, both the extensional and shear moduli of the TLR must be an order of magnitude greater than that of the lamina in the transverse direction. Graphite-epoxy and Kevlar-epoxy TLR were not effective at delaying the onset of delamination. This finding was particularly evident in cases dominated by the inter-laminar shear stress. Since the positive benefits of TLR have been reported for materials with graphite and Kevlar® TLR, prevention of damage initiation must not be the key mechanism responsible for the performance changes associated with the addition of TLR. This conclusion was further substantiated when the tendency to form transverse cracks was examined. If the unavoidable microstructural features of pure resin regions and curved fibers are considered, the addition of TLR was found to increase the likelihood of transverse crack formation.

In total, these findings are consistent with the results of many experimental studies reported in the literature and they support the hypothesis that the addition of TLR has

little or no positive effect on the initiation of damage. The true benefit of TLR must then

be the increased resistance to damage growth or progression.

CHAPTER 8
RECOMMENDATIONS FOR FUTURE WORK

A. Experimental studies with detailed observations of failure initiation. The studies should include materials with and without TLR and encompass different TLR materials, including an extremely stiff material such as titanium or steel. Acoustic emission and other NDE techniques in conjunction with destructive cross sectioning and microscopy should be employed to make accurate determinations of the type and initiation of damage.

B. Application of detailed experimental observations in the ongoing investigation of using a rubber layer in the interface. This ongoing study discussed in Chapter 5 was outlined in [132]. The idea is to prevent damage initiation by inducing the redirection of inter-laminar stress away from the interface and into the TLR.

C. Studies of the thermal response of TLR materials with detailed FEA models of a similar nature to the ones used in this work.

D. Development of a method to automatically insert discontinuous TLR directly into prepreg or preforms at a very rapid rate.

E. Investigation of the stability of dry fiber preforms assembled using discontinuous TLR instead of stitching.

F. Both analytical and experimental investigations of the important parameters in the crack bridging mechanisms associated with TLR.

G. Continued development and verification of TLR design guidelines based on fracture mechanics and crack bridging phenomenon.

REFERENCES

1. Chan, W.S. *Design Approaches for Edge Delamination Resistance in Laminated Composites,* Journal of Composites Technology & Research, 1991, Vol. 14(No. 2).

2. Munjal, A.K. *Damage Tolerance Improvement Approaches for Composite Components,* in 44th Annual Forum of the American Helicopter Society, 1988.

3. Garg, A.C. *Delamination--A Damage Mode in Composite Structures,* Engineering Fracture Mechanics, 1988, Vol. 29, No.5.

4. Lu, T.-J. and Hutchinson, J.W. *Role of Fiber Stitching in Eliminating Transverse Fracture in Cross-ply Ceramic Composites,* American Ceramic Society, Journal, 1995, Vol. 78, No. 1(Jan.).

5. Ko, F., Koczak, M., and Layden, G. *Structural Toughening of Glass Matrix Composites by 3-D Fiber Architecture,* Ceramic Engineering and Science Proceedings, 1987, Vol. 8(July-Aug.).

6. Yamaki, Y.R., Ransone, P.O., and Maahs, H.G. *Investigation of Stitching as a Method of Interlaminar Reinforcement in Thin Carbon-Carbon Composites,* in *16th Conference on Metal Matrix, Carbon, and Ceramic Matrix Composites,* 1993, CASI HC A03/MF A04, Part 1.

7. Dransfield, K., Baillie, C., and Mai, Y.-W. *Improving the Delamination Resistance of CFRP by Stitching-A Review,* Composites Science and Technology, 1994, 50.

8. Dransfield, K., Baillie, C., and Mai, Y.-W. *On Stitching as a Method for Improving the Delamination Resistance of CFRPs,* in Advanced Composites '93, International Conference on Advanced Composite Materials, 1993, The Minerals, Metals & Materials Society.

9. Broslus, D. and Clarke, S. *Textile Preforming Techniques for Low Cost Structural Composites Conference Proceedings,* in Advanced Composite Materials: New Developments and Applications, 1991.

10. Schooneveld, G.V. *Potential of Knitting/Stitching and Resin Infusion for Cost Effective Composites,* in *Fibertex 1988,* 1988, NASA CP 3038, 1989.

11. Palmer, R. and Curzio, F. *Cost-Effective Damage-Tolerant Composites Using Multi-needle Stitching and RTM/VIM Processing,* in *Fibertex 1988,* 1988, NASA CP 3038, 1989.

12. Markus, A. *Resin Transfer Molding For Advanced Composite Primary Wing and Fuselage Structures,* in *Second NASA Advanced Composites Technology Conference,* 1991, NASA CP 3154, 1992.

13. Markus, A., Thrash, P. and Rohwer, K. *Progress in Manufacturing Large primary Aircraft Structures Using the Stitching/RTM Process*, in *Third NASA Advanced Composites Technology Conference*, 1992, NASA CP 3178, Vol. 1 Part 1, 1992.

14. Markus, A., Thrash, P., and Grossheim, B. *Manufacturing Development and Requirements for Stitched/RTM Wing Structure*, in *The Fourth NASA Advanced Composites Technology Conference*, 1993, NASA CP 3229, Vol 1 Part 1, 1993.

15. Harris, H., Schinske, N., Krueger, R., and Swanson, B. *Mulltiaxial Stitched Preform Reinforcements*, in 36th International SAMPE Symposium, 1991.

16. Rhodes, M.D. and Williams, J.G. *Concepts for Improving Damage Tolerance of Composite Compression Panels*, in 5th DOD/NASA Conference On Fibrous Composites in Structural Design, 1981.

17. Murphy, G.C. *Processing for an Improved Impact Resistant Composite Blade*, in AIAA-81-1356, AIAA/SAE/ASME 17th Joint Propulsion Conference, 1981, Colorado Springs.

18. Conrad, E.G. 3-D Reinforcement of Thin Composite Laminates for Improved Low-Velocity Impact Damage Tolerance, Masters Thesis, University of Texas at Arlington, 1983.

19. Murrin, L.J. and Erbacher, H. *Composite Center Fuselage-Phase I*, in 35th Annual conference on Reinforced Plastics/Composites, 1980.

20. Holt, D.J. *Future Composite Aircraft Structures May Be Sewn Together*, Automotive Engineering, 1982, Vol. 90, No. 7(July).

21. Cacho-Negrette, C. *Integral Composite Skin and Spar (ICSS) Study Program - Volume I*, AFWAL-TR-82-3053, 1982.

22. Green, A.K. and Bowyer, W.H. *The Development of Improved Attachement Methods for Stiffening Frames on Large GRP Panels*, Composites, 1981(Jan.).

23. Sawyer, J.W. *Effect of Stitching on the Strength of Bonded Composite Single Lap Joints*, AIAA Journal, 1985, Vol. 23(No. 1).

24. Lee, C. and Liu, D. *Stitching Joint in Woven Composite Material*, in Recent Advances in the Macro- and Micro-Mechanics of Composite Materials Structures, 1989, ASME.

25. Tada, Y. and Ishikawa, T. *Tentative Evaluation of Effects of Stitching on CFRP Laminate Specimens*, in Composites 86: Recent Advances in Japan and the United States, Japan US CCM-III, 1986.

26. Tada, Y. and Ishikawa, T. *Experimental Evaluation of Effects of Stitching on CFRP Laminate Specimens with Various Shapes and Loadings*, Key Engineering Materials, 1989, Vol. 37.

27. Garrett, R.A. *Effect of Defects on Aircraft Composite structures*, in *Characterization, Analysis and Significance of Defects in Composite Materials*, 1983, AGARD-CP 355.

28. Deaton, J.W., Kullerd, S.M., Madan, R.C., and Chen, V.L. *Test and Analysis Results for Composite Transport Fuselage and Wing Structures*, in *Second NASA Advanced Composites Technology Conference*, 1992, NASA CP 3154.

29. Madan, R.C. and Voldman, M. *Test Results From Large Wing and Fuselage Panels*, in *Third NASA Advanced Composites Technology Conference*, 1992, NASA CP 3178, Vol. 1 Part 1.

30. Hawley, A.V. and Sutton, J.O. *Design and Analysis Considerations for Stitched/RTM Composite Wing Structure*, in *Fourth NASA/DoD Advanced Composite Technology Conference*, 1993, NASA CP 3229, Vol. 1 Part 1, 1993.

31. Hawley, A.V. *Development of Stitched/RTM Primary Structures for Transport Aircraft*, NASA CR 191441, 1993.

32. Nishimura, A. and Aotani, H. *New Fabric Structures for Composite*, in Composites 86: Recent Advances in Japan and the United States, Japan US CCM-III, 1986.

33. Tsai, G.C. *Global/Local Stress Analysis of Stitched Composite Laminate*, in 23rd International SAMPE Technical Conference, 1991.

34. Jang, B.Z. and C., C.W. *Structure-Property Relationships in Three Dimensionally Reinforced Fibrous Composites*, in Advanced Composites: The Latest Developments, Second Conference on Advanced Composites, 1986, ASM International.

35. Chan, W.S. and Dan-Jumbo, E. *A Comparison of the Structural Behavior of Laminates Made of Knitted Nonwoven Fabric and Laminates Made of Conventional Unidirectional Tapes*, SAMPE Journal, 1986(Nov./Dec.).

36. Mignery, L.A., Tan, T.M., and Sun, C.T. *The Use of Stitching to Suppress Delamination in Laminated Composites*, Delamination and Debonding, ASTM STP 876, 1985.

37. Deaton, J.W., Kullerd, S.M., and Portanova, M.A. *Mechanical Characterization of 2-D, 2-D Stitched and 3-D Braided/RTM Materials*, in *Fourth NASA/DoD Advanced Composite Technology Conference*, 1993, NASA CP 3229, Vol. 1 Part 1, 1993.

38. Hasko, G.H. and Dexter, H.B. *Mechanical Properties and Damage Tolerance of Multiaxial Warp Knit Composites*, Submitted to Composite Science and Technology, 1994.

39. Dexter, H.B. and Hasko, G.H. *Performance of Resin Transfer Molded Multiaxial Warp Knit Composites*, in *Third NASA Advanced Composites Technology Conference*, 1992, NASA CP 3178, Vol. 1, 1992.

40. Dexter, H.B., Hasko, G.H., and Cano, R.J. *Characterization of Multiaxial Warp Knit Composites,* in *First NASA Advanced Composites Technology Conference,* 1990, NASA CP 3104, Part 2, 1991.

41. Dexter, H.B., Palmer, R.J., and Hasko, G.H. *Mechanical Properties and Damage Tolerance of Multiaxial Warp Knit Structural Elements,* in *Fourth NASA/DoD Advanced Composite Technology Conference,* 1993, NASA CP 3229, Volume 1 Part 2, 1993.

42. *First NASA Advanced Composites Technology Conference,* 1990, NASA CP 3104, 1991.

43. *Second NASA Advanced Composites Technology Conference,* 1991, NASA CP 3154, 1992.

44. *Third NASA Advanced Composites Technology Conference,* 1992, NASA CP 3178, 1992.

45. *Fourth NASA/DoD Advanced Composites Technology Conference,* 1993, NASA CP 3229, 1993.

46. *Fifth NASA/DoD Advanced Composites Technology Conference,* 1994, NASA CP 3294, 1995.

47. *Sixth NASA/DoD Advanced Composites Technology Conference,* 1995, NASA CP 3327, 1996.

48. Jang, B.Z. *Fracture Behavior of Fiber-Resin Composites Containing a Controlled Interlaminar Phase (CIP),* Science and Engineering of Composite Materials, 1991, Vol. 2(No. 1).

49. Dexter, H.B. and Funk, J.G. *Impact Resistance and Inter-laminar Fracture Toughness of Through-the-Thickness Reinforced Graphite/Epoxy,* in 27th Structures, Structural Dynamics and Materials Conference, 1986, AIAA.

50. Funk, J.G., Dexter, H.B., and Lubowinski, S.J. *Experimental Evaluation of Stitched Graphite/Epoxy Composites,* in *3-D Composite Materials,* 1986, NASA CP 2420.

51. Su, K.B. *Delamination Resistance of Stitched Thermoplastic Matrix Composite Laminates,* Advances in Thermoplastic Matrix Composite Materials, ASTM STP 1044, 1989.

52. Palmer, R.J., Dow, M.B., and Smith, D.L. *Development of Stitching Reinforcement for Transport Wing panels,* in *First NASA Advanced Composites Technology Conference,* 1990, NASA CP 3104, Part 1, 1991.

53. Dow, M.B. and Smith, D.L. *Damage-Tolerant Composite Materials Produced by Stitching Carbon Fabrics,* in 21st SAMPE Technical Conference, 1989.

54. Dow, M.B. and Smith, D.L. *An Evaluation of Stitching Concepts for Damage-Tolerant Composites,* in *Fibertex 1988,* 1989, NASA CP 3038.

55. Pelstring, R.M. and Madan, R.C. *Stitching to Improve Damage Tolerance of Composites*, in 34th International SAMPE Symposium, 1989.

56. Liu, D. *Delamination Resistance in Stitched and Unstitched Composite Plates Subjected to Impact Loading*, Journal of Reinforced Plastics and Composites, 1990, Vol. 9(Jan.).

57. Liu, D. *Delamination in Stitched and Nonstitched Composite Plates Subjected to Low-Velocity Impact*, in American Society for Composites 2nd Technical Conference, 1987.

58. Farley, G.L., Smith, B.T., and Maiden, J. *Compression Response of Stitched and Integrally Woven Through-the-Thickness Reinforced Composite Materials*, Journal of Reinforced Plastics and Composites, 1992, Vol. 11(No. 7).

59. Rossi, G.T. *Evaluation of 3-D Reinforcements in Commingled, Thermoplastic Structural Elements*, in American Helicopter Society 45th Annual Forum, 1989.

60. Kullerd, S.M. and Dow, M.B. *Development of Stitched/RTM Composite Primary Structures*, in Second NASA Advanced Composites Technology Conference, 1991, NASA CP 3154, 1992.

61. Portanova, M.A., Poe, C.C.J., and Whitcomb, J.D. *Open Hole and Post Impact Compression Fatigue of Stitched and Unstitched Carbon/Epoxy Composites*, NASA TM 102676, 1990.

62. Portanova, M.A., Poe, C.C.J., and Whitcomb, J.D. *Open Hole and Post Impact Compression Fatigue of Stitched and Unstitched Carbon/Epoxy Composites*, Composite Materials; Testing and Design, ASTM STP 1120, 1990.

63. Kullerd, S.M. *The Combined Effects of Glass Buffer Strips and Stitching on the Damage Tolerance of Composites*, in *Third NASA Advanced Composites Technology Conference*, 1992, NASA CP 3178, Vol. 1, 1992.

64. Madan, R.C. *Influence of Low-Velocity Impact on Composite Structures*, Composite Materials: Fatigue and Fracture, ASTM STP 1110, American Society for Testing and Materials, Philadelphia, 1991.

65. Dickinson, L.C. *A Designed Experiment in Stitched/RTM Composites*, in *Third NASA Advanced Composites Technology Conference*, 1992, NASA CP 3178, Vol. 1 Part 1.

66. Dickinson, L.C. *Effects of Stitching Parameters on Mechanical Properties and Damage Tolerance of Stitched/RTM Composites*, in *The Fourth NASA Advanced Composites Technology Conference*, 1993, NASA CP 3229, Vol. 1 Part 1, 1993.

67. Portanova, M. *Impact Testing of Textile Composite Materials*, in *The Mechanics of Textile Composites Conference*, 1994, NASA CP 3311, Part 2, 1995.

68. Sharma, S.K. and Sankar, B.V. *Effects of Through-the-Thickness Stitching on Impact and Interlaminar Fracture Properties of Textile Graphite/Epoxy Laminates*, NASA CR 195402, 1995.

69. Portanova, M.A. *Evaluation of the Impact Response of Textile Composites*, NASA CR 198265, 1995.

70. Jackson, W.C. and Portanova, M. *Out of Plane Properties*, in *The Mechanics of Textile Composites Conference*, 1994, NASA CP 3311, Part 2, 1995.

71. Kang, T.J. and Lee, S.H. *Effect of Stitching on the Mechanical and Impact Properties of Woven Laminate Composite*, Journal of Composite Materials, 1994, Vol. 28(No. 16).

72. Cholakara, M., Jang, B.Z., and Wang, C.Z. *Mechanical Properties of 3-D Composites*, in Society of Plastics Engineers 47th Technical Conference and Exhibits, 1989.

73. Ogo, Y. *The Effect of Stitching on In-Plane and Interlaminar Properties of Carbon- Epoxy Fabric Laminates*, Report Number CCM-87-17, 1987.

74. Morales, A. *Structural Stitching of Textile Preforms*, in 22nd SAMPE Technical Conference, 1990.

75. Sharma, S.K. and Sankar, B.V. *Effect of Stitching on Impact and Interlaminar Properties of Graphite/Epoxy Laminates*, in Ninth Technical Conference of the American Society for Composites, 1994.

76. Jain, L.K. and Mai, Y.-W. *On the Equivalence of Stress Intensity and Energy Approaches in Bridging Analysis*, Fatigue and Fracture of Engineering Materials and Structures, 1994, Vol. 17(No.3).

77. Shu, D. and Mai, Y.-W. *Effect of Stitching on Interlaminar Delamination Extension in Composite Laminates*, Composites Science and Technology, 1993, 49.

78. Jain, L.K. and Mai, Y.-W. *On the effect of Stitching on Mode I Delamination Toughness of Laminated Composites*, Composites Science and Technology, 1994, 51.

79. Chen, V.L., Wu, X.X., and Sun, C.T. *Effective Interlaminar Fracture Toughness in Stitched Laminates*, in 8th Annual Technical Meeting of the American Society of Composites, 1993.

80. Farley, G.L. *A Mechanism Responsible for Reducing Compression Strength of Through-the-Thickness Reinforced Composite Material*, Journal of Composite Materials, 1991, Vol. 26, No. 12.

81. Farley, G.L. and Dickinson, L.C. *Mechanical Response of Composite Materials With Through-the-Thickness Reinforcement*, in *Fiber-Tex 1991*, 1992, NASA CP 3179.

82. Farley, G.L. and Dickinson, L.C. *Removal of Surface Loop From Stitched Composites Can Improve Compression and Compression After Impact Strengths*, Journal of Reinforced Plastics and Composites, 1992, Vol. 11, No. 6(June).

83.   Reeder, J.R. *Stitching vs. A Toughened Matrix: Compression Strength Effects,* Journal of Composite Materials, 1995, Vol. 29, No. 18.

84.   Reeder, J.R. *Comparison of the Compressive Strengths for Stitched and Toughened Composite Systems,* NASA TM 109108, 1994.

85.   Jenq, S.T. and Sheu, S.L. *High Strain Rate Compressional Behavior of Stitched and Unstitched Composite Laminates With Radial Constraint,* Composite Structures, 1993, Vol. 25.

86.   Jang, B.Z., Suhling, J., Valoire, B., and Zee, R.H. *Optimization of Fracture Resistance in Composites,* Final Report to US Army, Contract Number DAA! 03-86-G-0211, 1989.

87.   Cholakara, M.T., Jang, B.Z., and Wang, C.Z. *Deformation and Failure Mechanisms in 3D Composites,* in 34th International SAMPE Symposium, 1989.

88.   Jang, B.Z., Shih, W.K., and Chung, W.C. *Mechanical Properties of Multidirectional Fiber Composites,* Journal of Reinforced Plastics and Composites, 1989, Vol 8, Nov.

89.   Chung, W.C., Jang, B.Z., Chang, T.C., Hwang, L.R., and Wilcox, R.C. *Fracture Behavior in Stitched Multidirectional Composites,* Materials Science and Engineering, 1989, A112.

90.   Jang, B.Z., Cholakara, M., Jang, B.P., and Shih, W.K. *Mechanical Properties in Multidimensional Composites, Mid-January,* Polymer Engineering and Science, 1991, Vol. 31, No. 1.

91.   Adanur, S. and Tsao, Y.P. *Stitch Bonded Textile Structural Composites,* in 25th International SAMPE Technical Conference, 1994.

92.   Billaut, F. *Mechancial Behavior of 3-D Graphite/Epoxy Composites,* in American Society for Composites Ninth Technical Conference, 1994.

93.   Du, X., Xue, F., and Gu, Z. *Experimental Study of the Effect of Stitching on Strength of a Composite Laminate,* in International Symposium on Composite Materials and Structures, 1986, Beijing, China.

94.   Minguet, P.J., Fedro, M.J., and Gunther, C.K. *Test Methods for Textile Composites,* NASA CR 4609, 1994.

95.   Wolterman, R.L., Kennedy, J.M., and Farley, G.L. *Fatigue Damage in Thick, Cross-Ply Laminates with a Center Hole,* Composite Materials: Fatigue and Fracture, Fourth Volume, ASTM STP 1156, 1993.

96.   Cox, B.N., Carter, W.C., Dadkhah, M.S., and Fleck, N.A. *A Failure Model for Textile Composites,* in The Fourth NASA Advanced Composites Technology Conference, 1993, NASA CP 3229, Vol. 1, Part 2.

97.   Moon, D.G. and Kennedy, J.M. *Predicting Post-Impact Damage Growth and Fatigue Failures in Stitched Composites,* in Ninth Technical Conference of the American Society for Composites, 1994.

98.   Lubowinski, S.J. and Poe, C.C.J. *Fatigue Characterization of Stitched Graphite/Epoxy Composites,* in *Fibertex 1987,* 1988, NASA CP 3001.

99.   Vandermey, N.E., Masters, J.E., Poe, C.C., and Morris, D.H. *Compression - Compression Fatigue of a Stitched Uniwoven Graphite/Epoxy Composite,* Compression Response of Composite Structures, ASTM STP 1185, 1994.

100.   Vandermey, N.E., Morris, D.H., and Masters, J.E. *Damage Development Under Compression - Compression Fatigue Loading in a Stitched Uniweave Graphite/Epoxy Composite Material,* CCMS-91-16, VPI-E-91-14, 1991.

101.   Cox, B.N., Dadkhah, M.S., and Inman, R.V. *Micromechanics of Fatigue in Woven and Stitched Composites,* in *First NASA Advanced Composites Technology Conference,* 1990, NASA CP 3104, Part 2, 1991.

102.   Whiteside, J.R., DeIasi, R.J., and Schulte, R.L. *Measurement of Preferential Moisture Ingress in Composite Wing/Spar Joints,* Composites Science and Technology, 1985, Vol 24.

103.   Cano, R.J. and Furrow, K.W. *Effects of Temperature and Humidity Cycling on the Strengths of Textile Reinforced Carbon/Epoxy Composite Materials,* in *Third NASA Advanced Composites Technology Conference,* 1992, NASA CP 3178, Vol. 1, 1992.

104.   Cano, R.J., Furrow, K.W., and Loos, A.C. *Environmental Effects on Textile Reinforced Carbon/Epoxy Composite Materials,* in *Fourth NASA/DoD Advanced Composite Technology Conference,* 1993, NASA CP 3229, Vol. 1, Part 2, 1993.

105.   Furrow, K.W., Loos, A.C., and Cano, R.J. *Environmental Effects on Stitched RTM Uniwoven Coomposites,* in 39th International SAMPE Symposium and Exhibition, 1994.

106.   Walker, J., Roundy, L., and]Goering, J. *Effects of thermal And Moisture Cycling on the Internal Structure of Stitiched RTM Laminates,* in *Third NASA Advanced Composites Technology Conference,* 1992, NASA CP 3178, Vol. 1, Part 1, 1992.

107.   Hipp, R.C., Renze, S.P., Saff, C.R., and Walker, J.V. *Effects of Environment on Textile Composites,* in *Fourth NASA/DoD Advanced Composite Technology Conference,* 1993, NASA CP 3229, Vol. 1, Part 1, 1993.

108.   Hyer, M.W., Lee, H.H., and Knott, T.W. *A Simple Evaluation of Thermally-Induced Stresses in the Vicinity of the Stitch in a Through-Thickness Reinforced Cross-Ply Laminate,* CCMS-94-05, VPI-E-94-05, NASA CR 196317, 1994.

109.   Shim, S.-B., Ahn, K., Seferis, C., J., Berg, A.J., and Hudson, W. *Cracks and Microcracks in Stitched Structural Composites Manufactured with Resin Film Infusion Process,* Journal of Advanced Materials, 1995, Vol. 26, No. 4(July).

110.   Barrett, D.J. *The Analysis of A Z-Fiber Reinforced Plate,* NAWCADWAR-95-12-TR, 1995.

111.   Long, E.R.J. *Enhancement of Ultrasonic Images of Defects in 3-D Composites,* Journal of Reinforced Plastics and Composites, 1994, Vol. 13(March).

112. Long, E.R.J., Kullerd, S.M., Johnston, P.H., and Madaras, E.I. *Ultrasonic Detection and Identification of Fabrication Defects in Composites,* in *First NASA Advanced Composites Technology Conference,* 1990, NASA CP 3104, Part 2, 1992.

113. Miller, J.G. *Physical Interpretation and Development of Ultrasonic Nondestructive Evaluation Techniques Applied to the Quantitative Characterization of Textile Composite Materials,* Semiannual Progress Report for NASA Grant Number NSG- 1601, 1993.

114. Smith, B.T. , Semi-Annual Report for NASA Grant NAG-1-1063, 1990.

115. Caneva, C., Olivieri, S., Santulli, C., and Bonifazi, G. *Impact Damage Evaluation on Advanced Stitched Composites by Means of Acoustic Emission and Image Analysis,* Composite Structures, 1993, Vol. 25.

116. Liu, D. *Photoelastic Study on Composite Stitching,* Experimental Techniques, 1990, Vol. 14(Feb.).

117. Hawley, A.V. *Preliminary Design of an Advanced Technology Composite Wing for a Transport Aircraft,* in *53rd Annual International Conference on Mass Properties Engineering,* 1994, SAWE Paper no. 2235, 1994.

118. Shu, D. and Mai, Y.-W. *Delamination Buckling with Bridging,* Composites Science and Technology, 1993, Vol. 47.

119. Flanagan, G. *Development of Design Guidelines for Stitching Skins to Substructure,* in *The Fourth NASA Advanced Composites Technology Conference,* 1993, NASA CP 3229, Vol. 1, Part 1, 1993.

120. Cox, B.N. *Fundamental Concepts in the Suppression of Delamination Buckling by Stitching,* in Ninth DoD/NASA/FAA Conference on Fibrous Composites in Structural Design, 1991.

121. Cox, B.N. *Delamination And Buckling in 3D Composites,* Journal of Composite Materials, 1994, Vol. 28, No. 12.

122. Drummond, T. and Krasnitz, R. *Advanced Stitching Technology, for the Composite Industry,* in *Fibertex 1989,* 1989, NASA CP 3089, 1989.

123. Cox, B.N. and Flanagan, G. *Handbook of Analytical Methods for Textile Composites; Version 1.0,* 1996.

124. Cox, B.N., Dadkhah, M.S., Inman, R.V., Morris, W.L., and Schroeder, S. *Mechanisms of Compressive Failure in Woven Composites and Stitched Laminates,* in Ninth DoD/NASA/FAA Conference on Fibrous Composites in Structural Design, 1991.

125. Cox, B.N., Dadkhah, M.S., Inman, R.V., Morris, W.L., and Zupon, J. *Mechanisms of Compressive Failure in 3D Composites,* Acta Metallurgica et Materialia, 1992, Vol. 40, No. 12.

126. Huang, S.L., Richey, R.J., and Deska, E.W. *Cross Reinforcement in a GR/EP Laminate,* in ASME Winter Annual Meeting,, 1978.

127. Krasnov, V.I., Kusnetsov, V.A., and Maksakov, A.Y. *Automated Method of Transverse Reinforcement of Composites by Short Fibers,* Translated from Mekhanika Kompozitnykh Materialov, 1987, No. 3(May-June).

128. Evans, D.A. and Boyce, J.S. *Transverse Reinforcement Methods for Improved Delamination Resistance,* in 34th International SAMPE Symposium, 1989.

129. Freitas, G., Magee, C., Boyce, J., and Bott, R. *Service Tough Composite Structures Using the Z-Direction Reinforcement Process,* in Ninth DoD/NASA/FAA Conference on Fibrous Composites in Structural Design, 1991.

130. Freitas, G. *Z-Fiber Insertion Process for Improved Damage Tolerance in Aircraft Laminates,* in 25th International SAMPE Technical Conference, 1993.

131. Freitas, G., Magee, C., Dardzinski, P., and Fusco, T. *Fiber Insertion Process for Improved Damage Tolerance in Aircraft Laminates,* Journal of Advanced Materials, 1994, Vol. 25, No. 24(July).

132. Freitas, G., Fuaco, T., Campbell, T., Harris, J., and Rosenberg, S. *Z-Fiber Technology and Products for Enhancing Composite Design,* in AGARD, 1996.

133. Tomashevskii, V.T., Sitnikov, S.Y., Shalygin, V.N., and Yakovlev, V.S. *A Method of Calculating Technological Regimes of Transversal Reinforcement of Composites with Short-Fiber Microparticles,* Translated from Mekhanika Kompozitnykh Materialov, 1989, No. 3(May-June).

134. Tomashevskii, V.T., Shalygin, V.N., Romanov, D.A., and Sitnikov, S.Y. *Transversal Reinforcement of Composite Materials using Ultrasonic Vibrations,* Translated from Mekhanika Kompozitnykh Materialov, 1987, No. 6(Nov.-Dec.).

135. Raju, I.S., Foye, F.L., and Avva, V.S. *A Review of Analytical Methods for Fabric and Textile Composites,* Composite Structures, Testing, Analysis and Design, J.N. Reddy and K.A.V. Murty, Editors, Narosa Publishing House, New Delhi, India, Bangalore, India, 1992.

136. Falzon, P.J., Herszberg, I., and Baker, A.A. *Stiffness Analysis of Textile Composites,* in 5th Australian Aeronautical Conference, 1993.

137. Gowayed, Y.A. and Pastore, C.M. *Analytical Techniques for Textile Structural Composites: A Comparative Study of US-USSR Research,* in *Fiber-Tex 1990,* 1990, NASA CP 3128, 1991.

138. Naik, R.A. *Analysis of Woven and Braided Fabric Reinforced Composites,* NASA CR 194930, 1994.

139. Naik, R.A. *Failure Analysis of Woven and Braided Fabric Reinforced Composites,* NASA CR 194981, 1994.

140. Cox, B. *Failure Models for Textile Composites,* NASA CR 4686, 1995.

141. Cox, B.N., Carter, W.C., and Fleck, N.A. *A Binary Model of Textile Composites--I Formulation*, Acta Metallurgica et Materialia, 1994, Vol. 42, No. 10.

142. Xu, J., Cox, B.N., McGlockton, M.A., and Carter, W.C. *A Binary Model of Textile Composites--I the Elastic Regime*, Acta Metallurgica et Materialia, 1995, Vol. 43, No. 9.

143. Flanagan, G. and Furrow, K. *Parametric Studies of Stitching Effectiveness for Preventing Substructure Disbond*, in *Fifth NASA Advanced Composites . Technology Conference*, 1994, In Press.

144. Bennett, G.R. A Parametric Study of the Global Stiffness and Stress Concentrations of Through-The-Thickness Reinforced Composite Laminae Using A Representative Volume Element Approach, M.S., Virginia Polytechnic Institute and State University, Draft.

145. Barrett, D.J. *A Micromechanical Model for the Analysis of Z-Fiber Reinforcement*, in 37th AIAA SDM Conference, 1996.

146. Cox, B.N. and Marshall, D.B. *Overview No. 111: Concepts for Bridged Cracks in Fracture and Fatigue*, Acta Metallurgica et Materialia, 1994, Vol. 42 No. 2.

147. Cox, B.N., Massabo, R., and Kedward, K.T. *The Suppression of Delaminations in Curved Structures by Stitching*, Composites, Submitted Oct. 1995, In Press.

148. Cox, B., He, M., Massabo, R., and Mumm, D. *Design Models for Through-Thickness Reinforcement of Laminated Composites (Extended Abstract)*, in ASME International Mechancial Engineering Congress and Exposition, Advanced Materials: Development, Characterization, Processing, and Mechanical Behavior (Book of Abstracts), 1996, Atlanta, GA.

149. Massabo, R. and Cox, B.N. *Concepts for Bridged Mode II Delamination Cracks*, Mechanics of Materials, Submitted April, 1996.

150. Ugural, A.C. and Fenster, S.K. *Advanced Strength and Applied Elasticity*. Second SI Edition ed. 1987, New York, NY: Elsevier Science Publishing Co. Inc.

151. Whitney, J.M. *Structural Analysis of Laminated Anisotropic Plates*. 1987, Lancaster, PA: Technomic Publishing Company, Inc.

152. Marrey, R.V. and Sankar, B.V. *Micromechancial Models for Textile Structural Composites*, NASA CR 198229, 1995.

153. Naik, R.A. *Micromechanical Combined Stress Analysis - Micstran, A User Manual*, NASA CR 189694, 1992.

154. Naik, R.A. and Crews, J.H.J. *Closed-Form Analysis of Fiber-Matrix Interface Stresses Under Thermo-Mechanical Loadings*, NASA TM 107575, 1992.

155. Naik, R.A. *TEXCAD--Textile Composite Analysis for Design; Version 1.0 User's Manual*, NASA CR 4639, 1994.

156. Minguet, P.J. and O'Brien, T.K. *Analysis of Test Methods for Characterizing Skin/Stringer Debonding Failures in Reinforced Composite Panels*, Composite

Materials: Testing and Design, ASTM STP 1274, R.B. Deo and C.R. Saff, Editors, American Society for testing and Materials, 1996.

VITA

Larry C. Dickinson was born in Hickory, North Carolina on June 3rd, 1966. He graduated Valedictorian from Fred T. Foard High School in June 1984. He then attended North Carolina State University, earning three degrees: B.S. in Textile Engineering (Summa Cum Laude) in May 1988, B.S. in Mechancial Engineering (Magna Cum Laude) in May 1990, M.S. co-major in Textile Engineeing and Mechanical Engineering in December 1990. From October 1990 through October 1994 he worked for Lockheed Martin Engineering and Sciences Company as a research engineer supporting three different branches of the Materials Division of NASA Langley Research Center, Hampton Virginia. In November 1994 he was accepted as a full time student in the Applied Science Department, College of William and Mary, Williamsburg, Virginia. Upon completion of the requirements for the degree of Doctor of Philosophy, he will assume a position of Project Engineer with Foster-Miller Inc., Waltham, Massachusetts.